Developmental Cell

A Fibroblast Growth Factor 20-expressing, Wnt-responsive progenitor populates the olfactory epithelium and regulates turbinate growth

--Manuscript Draft--

Manuscript Number:	DEVELOPMENTAL-CELL-D-18-00032R1
Full Title:	A Fibroblast Growth Factor 20-expressing, Wnt-responsive progenitor populates the olfactory epithelium and regulates turbinate growth
Article Type:	Research Article
Keywords:	FGF20; olfactory epithelium; progenitor cell; turbinate; Wnt/β-Catenin; tissue scaling; condensation
Corresponding Author:	David M Ornitz St. Louis, MO UNITED STATES
First Author:	Lu M Yang
Order of Authors:	Lu M Yang
	Sung-Ho Huh
	David M Ornitz
Abstract:	The olfactory epithelium (OE) is a neurosensory organ required for the sense of smell. Turbinates, bony projections from the nasal cavity wall, increase the surface area within the nasal cavity lined by the OE. Here, we use engineered Fibroblast Growth Factor 20 (Fgf20) knockin alleles to identify a population of OE progenitor cells that fill all layers of the embryonic and early postnatal OE, at specific locations. These cells expand horizontally during development to populate all lineages of the mature OE. We show that these Fgf20-positive, epithelium-spanning progenitor (FEP) cells are responsive to Wnt/β-Catenin signaling. Wnt signaling suppresses FEP cell differentiation into OE basal progenitors and their progeny, and positively regulates Fgf20 expression. We further show that FGF20 signals to the underlying mesenchyme to regulate the growth of turbinates. These studies thus identify a population of OE progenitor cells that function to scale OE surface area with the underlying turbinates.
Suggested Reviewers:	James Schwob Tufts University jim.schwob@tufts.edu
	Rashmi Bansal University of Connecticut bansal@neuron.uchc.edu
	Rachel Wong University of Washington wongr2@uw.edu
	Josh Sanes Harvard University sanesj@mcb.harvard.edu
	Roel Nusse Stanford University rnusse@stanford.edu
	Raj Ladher National Centre for Biological Sciences rajladher@ncbs.res.in
	Suzanne Mansour University of Utah suzi.mansour@genetics.utah.edu
Opposed Reviewers:	

Washington University in St. Louis
SCHOOL OF MEDICINE

The Department of Developmental Biology

David M. Ornitz, M.D.,Ph.D.
Alumni Endowed Professor
Developmental Biology

May 8, 2018

Masha Gelfand, Ph.D.
Scientific Editor
Developmental Cell

Dear Dr. Gelfand,

Please accept the accompanying revised manuscript, entitled "**A Fibroblast Growth Factor 20-expressing, Wnt-responsive progenitor populates the olfactory epithelium and regulates turbinate growth**", for consideration for publication in *Developmental Cell*. The corresponding author is David Ornitz, and the material presented is original research and has not been submitted for publication elsewhere. All authors have read the manuscript and have approved its submission.

In this revision we have responded to all reviewer comments. We have added a graphical abstract, STAR methods and highlights. In addition to modification to the results and discussion, we have added several new pieces of experimental data.

1. We have genetically activated FGF9 expression in the FGF20 lineage in the olfactory epithelium and showed a specific effect on proliferation of the underlying mesenchyme.
2. We have added in situ hybridization for the FGF responsive gene, *Dusp6*. We show decreased expression in *Fgf20*-null embryos and in βCatenin conditional knockouts. We also show increased expression in embryos in which we have activated FGF signaling from the olfactory epithelium.

These new experiments directly address the major critique of reviewers 2 and 3 and firmly establish that a primary target of olfactory epithelial FGF signaling is the underlying mesenchyme.

We hope that these additional experiments and our response to the reviewer comments addresses all major critiques of the manuscript. We thank you for your consideration of this manuscript for publication in *Developmental Cell.*

Sincerely,

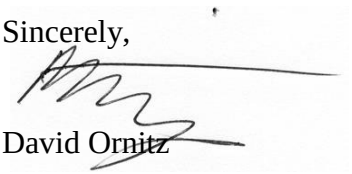

David Ornitz

Lu Yang

Washington University School of Medicine, Campus Box 8103, 660 South Euclid Avenue, St. Louis, MO 63110
Phone: 314.362.3908; Fax: 314.362.7058; Email: dornitz@wustl.edu; Web: http://ornitzlab.wustl.edu/

RE: DEVELOPMENTAL-CELL-D-18-00032
"A Fibroblast Growth Factor 20-expressing, Wnt-responsive progenitor populates the olfactory epithelium and regulates turbinate growth"

Reviewer comments:

Reviewer #1: In this study, the authors use olfactory epithelium (OE) to address the mechanism of horizontal expansion. The OE is a pseudostratified epithelium which acts as neurosensory organ and in which specialized skeletal projections called turbinates are instrumental in giving the animal an acute sense of smell. The OE is a polarized structure with neuronal cells and odorant receptors lined apically, and basal cells forming the inner lining, giving the organ its functionality. Much is known about how progenitor populations from the basal layers expand and differentiate to give rise to neuronal structures. However, the mechanism by which the epithelial layer expands horizontally and the identity of progenitor populations that mediate such an expansion have remained controversial. This manuscript dissects the role of Sox2+/Fgf20+ cells at unique regions in the developing epithelia which can act as a supply to support expansion of the epithelia not only during embryonic development but also during postnatal life.

The work presented is of very high quality, as is typical for this lab. However, my main concern is that the connection with Wnt signaling, while interesting, is unclear. Wnts have been found to regulate Fgf20 in other contexts, but it is unclear if FGFs and WNTs are working in the same or in a parallel pathway.

Response:
We show strong in vivo evidence supporting our argument that Wnt/βCat signaling is regulating Fgf20 expression. Fgf20 expression is gone in βCat loss-of-function mutants and upregulated in βCat-gain-of function mutants. Fgf20 is expressed in the OE, and Fgf20-null and OE-specific βCat deletion both result in smaller turbinates. Therefore, we conclude that Wnt/βCat and FGF20 signaling are acting in the same pathway to regulate turbinate development. Specifically, we conclude that OE-specific WNT signaling regulates turbinate development at least in part via FGF20. Consistent with this, we looked at Dusp6 expression, an FGF-regulated gene, and show that its expression in the mesenchyme is reduced in both Fgf20-null (Figure 3H) and βCat conditional knockout (Figure S5C) embryos.

We realize it might have been unclear whether the disappearance of Fgf20 expression is 1) directly due to loss of Wnt/βCat signaling, which leads to downregulation of Fgf20 expression or 2) indirectly due to loss of Wnt/βCat signaling, which leads to loss of FEP cells. In Figure S5A, we show that less severely affected βCat conditional knockout mice still have some FEP cells based on Sox2 expression and histology at P0. However, these cells do not express Fgf20. This strongly suggests that Wnt/βCat is required for both 1) direct regulation of Fgf20 expression and 2) FEP cell maintenance. To clarify, we have added to Figure S5A magnified images of these cells and indicate with arrows FEP cells that have lost Fgf20 expression.

Another general issue in the manuscript is that the Fgf20GFP-Cre lineage is cumulative, and to make definitive conclusions one really would need an inducible system.

Response:
We agree with the reviewer that our cumulative lineage experiments are not definitive. This issue is specifically addressed in the Discussion section, where we argue why we believe our cumulative lineage studies nevertheless strongly support our hypothesis. In Figures 2D-2G, we have compared real-time expression with lineage and show a clear expansion of lineage

compared to real time Fgf20 expression. Furthermore, Fgf20-lineage OE expands rapidly from E14.5 to P7, while non-lineage OE does not expand.

In regard to using $Fgf20^{GFP\text{-}Cre}$ for βCat deletion, we argue that because Wnt activity, as shown in Figure 4, overlaps with that of Fgf20 expression, using an inducible Cre would not necessarily be much more informative than a cumulative Cre. Importantly, Wnt activity was never detected in areas outside of Fgf20-lineage.

I have the following specific comments:

1. The data has been focused on negative folded regions or "neck" of the OE. These regions have a higher percentage of Sox2+Fgf10+ cells. The authors should determine using the ROS26AmTmG and ROSA26TdTomato reporters if these cells coincide with all the "neck" regions across the whole epithelia.

Response:
We showed via serial sections across the nasal cavity in Figures 1D-1F, S2C, and S2D that Fgf20+ cells are found at all “neck” regions across the whole epithelia. However, we did not specifically indicate all of these regions with arrows. We have added arrowheads in the figures for clarification.

Does the niche develop due to the specific shape of the cells at these "neck" regions?

Response:
We are not sure what the reviewer means by “shape of the cells”. Perhaps they mean shape of the epithelium (i.e. negatively curved). This is a very interesting question, and in the Discussion section we raise the idea that mechanical properties of the neck could contribute to the FEP niche, but we believe that investigating this idea is beyond the scope of our current study.

2. The functional role of Fgf20 in progenitor cell fate maintenance has not been discussed sufficiently. In the Fgf20 mutants, the mesenchyme derived structures (cartilage and bone) are reduced in size and features as opposed to the controls. As mentioned in the current version of the manuscript, FGF20 primarily appears to govern the growth of mesenchymal cells, but this needs to be further elaborated in the Discussion section.

Response:
We now address this important issue in the Discussion section. As stated below in response to Reviewer 2, we also have examined the expression patterns of an FGF20-regulated gene (Dusp6) in the developing turbinate mesenchyme in control, Fgf20-null (Figure 3H), and Fgf9 overactivation (Figure S4G) embryos. We show that Dusp6 is expressed in the diffuse mesenchymal layer during turbinate development at E14.5, and its expression is reduced in Fgf20-null embryos and increased in Fgf9 overactivation embryos. This suggests that FGF20 signals directly to diffuse mesenchymal cells to regulate proliferation.

3. Lef/TCF-H2B; Fgf20GFP-Cre experiments and BFF-CKO experiments demonstrate the importance of Wnt/beta-catenin signaling. However, activation of Wnt/beta-catenin leads to a highly disorganized epithelial layer. Higher magnification images should be provided.

Response:
We have added higher magnification images and outlined epithelial-mesenchymal boundaries.

If these cells lose tissue integrity and structure upon activation of Wnt/beta-catenin, they might exhibit hallmark properties of progenitors. The authors need to address this issue.

Response:
While it is an interesting idea, we do not necessarily argue that the irregular cells should exhibit hallmark properties of progenitors, as we do not believe that this argument is essential to our interpretation of the results. Our argument is that the greatly expanded population of irregular cells maintain high levels of Fgf20 and Sox2 expression, markers of OE progenitors (FEP cells), and do not acquire a neuronal fate (lack of expression of OMP+ ORNs). As discussed in Discussion section, these cells may exhibit dysplastic/tumorigenic properties.

Minor comments:

4. At times on some of the images the text occludes the features of the images.
5. Some of the low magnification images are difficult to interpret without arrowheads or some other kinds of markers as a key.

Response:
We provide high resolution images in this revision and have added arrows and labels.

Reviewer #2:
The authors show FGF20 expression in the early lateral nasal cavity epithelium and later in the "necks" of the turbinates (protuberances bearing the sensory epithelium). Their lineage labellng shows FGF20 descendants populating nearly the entire mature olfactory epithelium. Conditional FGF20 knockouts had reduced turbinate size. Knockout of canonical Wnt activity (roughly coincident with FGF20 expression) reduced FGF20 and more severely reduced turbinate size and epithelial proliferation, also giving premature differentiation. Canonical Wnt gain-of-function showed the opposite phenotype (excess FGF20-expressing progenitor cells, excess growth of the epithelium, enlarged, misshapen turbinates).

This is a fairly straightforward paper and an interesting investigation of major developmental signals in growth and lineage regulation in the nasal turbinates, a relatively under-studied set of structures. The writing is a bit careless and needs clarification at many points (the minor points listed below are for the first half of the paper - I gave up after that - detailed revision for the latter half is needed too).

Response:
We have incorporated appropriate changes suggested by the reviewer and clarified the writing in the second half of the paper as well.

The conclusions are broadly supported except that it is stated that FGF20 signals to underlying mesenchyme whereas the data are also consistent with indirect effects of FGF perturbation affecting mesenchyme (e.g. by mechanical effects rather than signaling as such).

Additional experiments that would improve the paper would be more direct demonstration of an FGF response in the mesenchyme (e.g. expression of validated direct targets in normal and mutant tissue) and FGF signaling gain-of-function to complement the loss-of-function.

Response:
To differentiate between direct effects of FGF20 on underlying mesenchyme and indirect effects, we have examined the expression of the FGF20 target gene, Dusp6, at E14.5, when a

mesenchymal phenotype first appears in Fgf20-null embryos. We now show that the expression level of Dusp6 is high in the mesenchyme in control embryos and reduced in Fgf20-null embryos (Figure 3H). Moreover, Dusp6 expression is completely gone from the mesenchyme in β-catenin conditional knockout embryos (Figure S5C).

In this revised manuscript we have added an in vivo overexpression model in which we overexpress FGF9 in the Fgf20-lineage OE. FGF9 is biochemically similar to FGF20. This resulted in expansion of the diffuse mesenchymal layer underlying the OE (Figure S4 F-L), similar to overactivation of Wnt/βCat signaling in the OE. We further show that Dusp6 expression is expanded in the mesenchyme at E14.5 in embryos overexpressing FGF9.

Minor points:

Title: "Wnt-responsive" should be "Wnt-expressing and -responsive"

Response:
We do not agree that the cell population should be labeled as “Wnt-expressing.” While we show that these cells respond to Wnt, we do not know whether they express Wnt-ligands. The possible sources of Wnt ligands are discussed in the Discussion section.

General: The coinage FEP should be "FP" or just FGF20-positive. The E for epithelial or epithelium-spanning is redundant given that all cells in this epithelium are, of couse, epithelial and all are epithelium-spanning because it is pseudostratified not stratified.

Response:
In the text, we have clarified that by “epithelium-spanning” we mean that the nuclei of these cells are located throughout the entire OE thickness, unlike basal progenitor cells, which are localized next to the basement membrane of the OE. We have further changed the text to refer to FEP region OE as “immature” OE to differentiate from the rest of the more “mature” OE, and explained this distinction at the end of the 2nd paragraph of the introduction.

p.4, para 2, last sentence "in real time" should be "over time"

Response:
We used the term “in real time” to differentiate the expression of the Fgf20 knock-in allele, GFP-Cre (real time), from the Cre activated lineage reporters. We have clarified this point.

p.4 and Fig.1C It is hard to see the non-stratification of the arrowhead-marked epithelium - the images themselves are a bit too highly pixellated. Could a higher-resolution image be provided?

Response:
Yes, we now provide a higher-resolution image.

p.4, penultimate para, "cells spanning the entire thickness of the OE"
There seems to be a confusion by the authors as to the meaning of the term "pseudo-stratified". In a pseudostratified epithelium ALL cells are epithelium-spanning. It is therefore confusing and misleading to distinguish the FGF20-positive cells as "epithelium-spanning". What they actually mean is that the FGF20-positive nuclei are at all apicobasal positions (just saying unstratified would be sufficient, although the additional clarification is fine).

Response:

We now provide additional clarification and use “immature” vs “mature” to differentiate between FEP regions and the rest of the OE.

p.5 "We term this cell population FEP (Fgf20-positive, epithelium-spanning progenitor) cells" Calling these progenitor cells is premature in the narrative - it pre-empts the testing of the just-stated hypothesis. At least the authors should say that their coinage is based on results below.

Response:
We now indicate that the FEP designation is based on the results presented in this manuscript.

p. 5, para.3 "we hypothesized that Fgf20 may be a marker for embryonic OE progenitors." Repeats the "hypothesis" statement in the previous paragraph. Pick one or the other.

Response:
We removed the hypothesis statement from the previous paragraph.

p.5, para 3, middle "The distribution of Fgf20+ cells and OMP+ ORNs in the c1 OE was linearly plotted" should be "The linear distribution of Fgf20+ cells and OMP+ ORNs in the c1 OE was plotted"

Response:
We have changed the text to make what we mean clearer.

p.5 para.3 "Pde2+ necklace ORNs". What is "necklace"? Should it be "neck"?

Response:
Necklace ORNs are a previously described subset of ORNs in the necklace olfactory system that express Pde2a, instead of OMP, as mentioned in the text and described in more detail in the publication we cited (Juilfs et al., 1997). The term “necklace” does not correspond to our term “neck.” We have clarified this.

p.5 para 4 "OE zones are described in Ressler et al., 1993; Vassar et al., 1993)" On the basis of what are these zones distinguished in the cited papers?

Response:
The cited publications distinguished OE zones based on olfactory receptor distribution. We cited these papers as basis for our identification of OE zones.

p.5, para.4 "Given that OE expansion occurs in a dorsomedial-to-ventrolateral direction, the Fgf20GFP-Cre lineage is consistent with the idea that FEP cells horizontally expand the OE." This is a non-sequitur, or at least extremely poorly explained. What has the progression (not really direction - the epithelium points in many different directions) of expansion got to do with the observed labeling or the hypothesis that FEP cells do the expansion? One could argue that the presence of FGF20-negative cells and regions is NOT consistent with the hypothesis (or at least not with the simplest version of it, which is all the reader has). Presumably the authors are saying something about the very initial lateral and ventral enrichment of FEP cells at E12.5. A better explanation is necessary.

Response:
We mean that the dorsomedial OE develops first (around E12), and then proceeds to expand ventro-laterally. The fact that the Fgf20 lineage contains the entire ventrolateral OE, but only

some of the dorsomedial OE is consistent with the hypothesis that FEP cells contribute to this expansion process. We have more clearly explained this in the revised manuscript (in the Discussion section).

p.6 "Fgf20-null mice have a deficit in turbinate development"
"Have a deficit" (could mean absence) should be "have reduced turbinate surface area".

Response:
We changed this to say “Fgf20-KO mice have reduced turbinate size and altered morphology.”

p.6, para 3 "Measurement of the surface of each turbinate to estimate size"
This is extremely unclear here and in the Methods. Points used to measure size could be better indicated in the figure (e.g. panels B')

Response:
We have explained this more clearly in the STAR methods section. We have also labeled this in Figure 3B’.

p.7, para 4 "H2B-GFP was detected…most brightly in negatively curved OE at E17.5 (Figure 4D)"
This statement is not supported by the data. The brightest GFP is sometimes at the curved regions but is as strong or stronger in the flat walls flanking these curved regions.

Response:
We agree that in certain “flat wall” regions of the OE, Tcf/Lef:H2b-Gfp was detected. As stated in the text, we attribute this to the very long half-life of the H2B-GFP protein (24 days, as described in Waghmare et al. The EMBO Journal. 2008;27:1309-20.), leading H2B-GFP to be detectable not only in negatively curved OE, but also in regions outside of the negatively curved OE. This also provides evidence further supporting our hypothesis that the expanding OE is derived from the cells residing in the negatively curved OE.

Etc.

Response:
We have clarified the remaining parts of the paper.

Reviewer #3:
In this study, Yang et al investigate the role of Fgf20 expressed by olfactory epithelium progenitors, which they call Fgf20-positive, epithelium-spanning progenitors or FEPS, in the horizontal expansion of the epithelium as well as the underlying cartilaginous turbinate structures. In principle this is an interesting story that has the potential to tie together signaling events responsible for epithelial development that also coordinate growth and morphogenesis of the epithelium's underlying structural scaffold. However, I have a several major concerns that lead me to question whether the experiments in their current form support the authors' main conclusions.

My main concerns center on the general question of whether the genetic tools and perturbations employed are as specific as the authors claim. For example, no validation is provided to demonstrate the fidelity of the Fgf20-GFPcre transgene in the olfactory epithelium (OE) itself.

Response:

We do not believe that this concern is well-founded. We have two Fgf20 knock-in reporters, one with GFP-Cre and one with β-galactosidase. Both reporters are driven by the endogenous Fgf20 promoter. As shown in Figures 1D, 1E, 1F, 4F and 4G, both reporters show the same pattern of expression, supporting our assertion that this expression pattern is reproducible and under the control of Fgf20 regulatory elements. No expression was detected in any other olfactory structure outside of the olfactory epithelia, the septal organ, and the vomeronasal organ.

There are also a number of known markers of OE progenitor cells that might have been used to produce a more complete characterization of these cells.

Response:
In the Discussion section, we discuss in depth four other relevant markers of OE progenitor cells and how none of them have been reported to show the same expression pattern as Fgf20.

Moreover, the undetectable levels of either the native mRNA/protein as well as the transgene reporter raises a serious question as to whether Fgf20 expressed by the OE progenitor cells could actually be active enough to serve as a developmental signal in the sub-mucosal tissue. It's certainly possible, but given these concerns a more careful analysis is warranted.

Response:
The reviewer might have mistaken our statement that "*Fgf20* expression was barely detectable without an antibody to GFP" to mean that we were unable to detect Fgf20 mRNA or protein. Instead, what we meant is that the native fluorescence from GFP in our *Fgf20*$^{GFP\text{-}Cre}$ allele is weak. Therefore, we used an anti-GFP antibody and a fluorescence secondary antibody to detect it. We have modified the text to make this clearer. Furthermore, while the GFP fluorescence in GFP-Cre is weak, the Cre recombinase is highly active, as is clearly shown in Figure 2. Therefore, the Fgf20 promoter is definitely active. Lastly, our experiment in response to reviewer 2, to examine downstream targets of FGF20 signaling in the mesenchyme also support the functional activity of endogenous FGF20. We show that the FGF20-target gene, Dusp6, is expressed in the mesenchyme underlying the OE, but its expression is reduced in Fgf20-knockouts (Figure 3H) and expanded in FGF overexpressing mice (Figure S4G).

The phenotypes of the various Fgf20 and beta-catenin knockouts also seem open to interpretation. For example, the Fgf20 knockout results in only a modest 15% reduction in overall surface area, a phenotype obtained with a germline knockout. Thus the contribution of Fgf20 to turbinate development seems modest at best,

Response:
We agree that the effect on turbinate size of Fgf20 knockout is modest (but not insignificant). This led us to hypothesize that other signals, perhaps other FGF molecules, could be compensating for the loss of FGF20. Furthermore, because the βCat loss of function mice have a much more severe turbinate size phenotype, we hypothesize that WNT/βCat signaling is regulating these other signals in addition to FGF20. This is supported by the incomplete loss of FGF-response gene Dusp6 in Fgf20-knockouts (Figure 3H) and complete loss in βCat knockouts (Figure S5C) We discuss this in detail in the Discussion section.

In addition, as stated in the Introduction and Discussion sections, no OE-to-turbinate signaling factor has been previously identified. The modest phenotype of mice lacking FGF20 signaling is, at the very least, proof-of-principle that the OE regulates the underlying turbinates via a signaling molecule.

and it's further difficult to rule out that the effect, however modest, may be due to loss of function outside the OE itself.

Response:
As stated above, we found no evidence that Fgf20 is expressed in any non-epithelial tissue in the olfactory system. We clearly show this in Figure 1. Moreover, we used the septal organ as an internal control (Figure 3F) and showed that there is no change in the surface area of the septal organ in Fgf20-null mice. This rules out contributions to the Fgf20 phenotype from factors such as skull size, and strongly suggests that the decrease in OE surface area in Fgf20-null mice can be specifically attributed to the smaller turbinate size.

Similarly, the authors argue that canonical wnt signaling lies upstream of Fgf20, yet both beta-catenin knockouts demonstrate more severe phenotypes than the Fgf20 mutant.

Response:
We reason that Wnt signaling is upstream of Fgf20 because in Wnt loss-of-function, Fgf20 expression is absent (Figure S5), while in Wnt gain-of-function, Fgf20 expression is increased (both in level and in number of cells expressing Fgf20, as shown in Figures 7 and S7). Furthermore, OE-specific deletion of βCat leads to reduced turbinate sizes, suggesting that OE Wnt signaling regulates an epithelial-to-mesenchymal signaling factor important for turbinate development. FGF20 is one such factor, as Fgf20-null mice also have decreased turbinate size and decreased expression of the FGF-responsive gene, Dusp6, in the underlying mesenchyme. Therefore, Wnt lies upstream of Fgf20 and regulates turbinate development via FGF20 and likely other signals, as discussed in the Discussion section. We interpret the βCat loss of function turbinate phenotypes being more severe than that of Fgf20-null mice to mean that other OE-to-turbinate signals, potentially other FGFs, are also regulated by Wnt/βCat signaling. Consistent with this, Dusp6 is completely absent in βCat loss of function embryos (Figure S5C) while it is decreased but not completely gone in Fgf20-null mice (Figure 3H).

These observations indicate to me that the genetic perturbations employed here are not restricted to the OE progenitor cells in the way that the authors are presenting.

Response:
We do not claim that $Fgf20^{GFP\text{-}Cre}$ is only targeting and deleting βCat in FEP cells. Our argument is that the role of Wnt/βCat signaling in the developing OE is to maintain FEP cells in an undifferentiated state and regulate turbinate development via FGF20 and potentially other signaling factors. According to the Tcf/Lef:H2b-Gfp reporter, Wnt activity in the OE has a similar expression pattern as Fgf20 expression *throughout* development (Figure 4), showing that OE Wnt activity is at least mostly restricted to the $Fgf20^{+}$ progenitor cells. We further argue, based on our data and on previous publications, that Fgf20 expression itself is a reporter for Wnt activity in the OE. We agree with the reviewer that we cannot completely rule out that there might be some contribution from Wnt activity in the OE outside of $Fgf20^{+}$ progenitors to the phenotype of βCat knockout mice, and we acknowledge this possibility in the Discussion. However, we do not believe this possibility challenges the conclusion that Wnt signaling in FEP cells regulates turbinate development via FGF20.

From Figure 6, the authors contend that beta-catenin knockout leads to premature differentiation and progenitor cell depletion. However the data shown, while suggestive, in fact are inconsistent with this conclusion, as no significant difference is found in the number of EdU+ progenitors at E14.5

Response:
The reviewer argues that in βCat LOF, the OE phenotype at P0 is NOT due to premature differentiation and progenitor depletion because at E14.5, progenitor proliferation is unchanged. We do not agree with this reasoning. Our logic is that depletion of progenitors at P0 could be explained by: 1) premature differentiation or 2) decreased progenitor proliferation at an earlier stage. We showed that at an earlier stage, there is 1) premature differentiation (increased number of differentiated cells), but 2) no change in progenitor proliferation. This is very much consistent with the hypothesis that the phenotype is due to premature differentiation and not decreased progenitor proliferation. The reviewer seems to be arguing the opposite.

nor were other known markers of OE progenitors tested.

Response:
Sox2 is widely accepted as the marker of the most undifferentiated basal progenitors, which is the cell population we are interested in. We further found that Sox2 also marks the $Fgf20^{+}$ progenitors. We do not believe that examining other known markers will add much meaningful information.

Similarly, the expression of the constitutively active beta-catenin seems to cause loss of mature cells in OE and other effects in underlying mesenchyme, but the phenotypes are too incompletely characterized to allow any meaningful conclusions to be drawn.

Response:
We disagree with this statement. We believe that the images showing a full complement of mature ORNs in control mice and virtually no mature ORNs in the βCat gain-of-function mice (Figure 7C) convincingly shows that activation of Wnt signaling dramatically expands an Fgf20-expressing immature epithelial cell population at the expense of differentiated cell types, such as ORNs. In the mesenchyme, we showed that there is an increase in diffuse cell proliferation, but no sign of condensation formation (leading to lack of chondrocytes at later stages). As stated in the discussion, the overexpression experiments complement the knockout experiments in supporting our conclusions. The reviewer did not elaborate on how else we should characterize the phenotype.

TITLE

A Fibroblast Growth Factor 20-expressing, Wnt-responsive progenitor populates the olfactory epithelium and regulates turbinate growth

Lu M. Yang[1], Sung-Ho Huh[1,2], David M. Ornitz[1,3,*]

[1]Department of Developmental Biology; Washington University School of Medicine; St. Louis, Missouri, 63110; USA

[2]Current address: Holland Regenerative Medicine Program, and the Department of Developmental Neuroscience, Munroe-Meyer Institute; University of Nebraska Medical Center; Omaha, Nebraska, 68198; USA

[3]Lead Contact

*Correspondence: dornitz@wustl.edu

SUMMARY

The olfactory epithelium (OE) is a neurosensory organ required for the sense of smell. Turbinates, bony projections from the nasal cavity wall, increase the surface area within the nasal cavity lined by the OE. Here, we use engineered Fibroblast Growth Factor 20 (*Fgf20*) knockin alleles to identify a population of OE progenitor cells that fill all layers of the embryonic and early postnatal OE, at specific locations. These cells expand horizontally during development to populate all lineages of the mature OE. We show that these *Fgf20*-positive, epithelium-spanning progenitor (FEP) cells are responsive to Wnt/β-Catenin signaling. Wnt signaling suppresses FEP cell differentiation into OE basal progenitors and their progeny, and positively regulates *Fgf20* expression. We further show that FGF20 signals to the underlying mesenchyme to regulate the growth of turbinates. These studies thus identify a population of OE progenitor cells that function to scale OE surface area with the underlying turbinates.

Keywords: FGF20, olfactory epithelium, progenitor cell, turbinate, Wnt/β-Catenin, tissue scaling, condensation

INTRODUCTION

The mammalian nose serves two main functions: respiration/air-conditioning and olfaction (Van Valkenburgh et al., 2014). Bony plates projecting from the nasal cavity wall, called turbinates, greatly increase the surface area within the nasal cavity, which is lined by respiratory epithelia and olfactory epithelia (OE). Turbinates in the posterior nasal cavity are mainly lined by OE, which houses specialized receptor cells called olfactory receptor neurons (ORNs) that detect chemical odorants and transmit electrical signals to the olfactory bulb and the brain (Albert Farbman, 1992). In mammals, turbinate size and complexity varies dramatically among species. It has been hypothesized that such interspecies differences in turbinate complexity, and therefore surface area within the nasal cavity, correlates with interspecies differences in olfactory ability (Negus, 1959; Van Valkenburgh et al., 2014). For example, terrestrial carnivorous caniforms have increased olfactory surface area relative to body size compared to omnivorous caniforms, correlating with their need to detect far-away prey due to their more specialized diet (Green et al., 2012). Despite the importance of the OE and turbinates, the developmental mechanisms that regulate their size and complexity are unknown.

The mature mouse OE is a pseudostratified epithelium consisting of three main cell types with nuclei located in different layers of the epithelium: sustentacular cell (Sus, a supporting cell population) nuclei in the apical layer, ORN nuclei in the middle layers, and basal cell (BC, progenitors that give rise to Sus cells and ORNs) nuclei in the basal layer (Murdoch and Roskams, 2007; Schwob et al., 2017). Other OE cell types include Bowman's duct cells and microvillar cells (Weng et al., 2016). OE development and neurogenesis can be divided into two main phases: embryonic day 10 (E10) to E13, and E13 to adult (Beites et al., 2005; Ikeda et al., 2007; Smart, 1971). Neurogenesis begins at around E10 with the invagination of the olfactory placode to form the nasal pit (Treloar et al., 2010). From this stage to E13, nuclei of Sox2-expressing ($Sox2^+$) progenitors are found throughout the thickness of the OE, particularly apically. However, from E13 to adult, progenitor nuclei are found in the basal layer, and are referred to as BCs (Cau et al., 1997; Cuschieri and Bannister, 1975a, 1975b; Smart, 1971). This shift in progenitor location is associated with the pseudostratification of the OE, as ORN and Sus cell nuclei localize to their respective locations in the mature OE. BCs continue to divide and differentiate into the overlying ORNs and Sus cells throughout life, a process termed "established neurogenesis." It has been suggested that during early development prior to E13, the pool of OE progenitors mainly expand, while after E13, these progenitors fill the OE with ORNs (Beites et al., 2005). In this article, we use the term "immature" to refer to OE in which progenitor nuclei are located throughout the thickness of the OE, and the term "mature" to refer to OE containing progenitor (BC) nuclei in the basal layer, ORN nuclei in the middle layers, and Sus cell nuclei in the apical layer.

Established neurogenesis during development, adult homeostasis, and regeneration in the OE is well understood. We refer to this process as vertical development, as it involves the differentiation of BCs into cells that fill the upper layers of the OE. Horizontal development, or OE surface area expansion, is less well understood. Despite the importance of OE surface area to many mammals, the mechanism and a progenitor population regulating OE scaling has not been found (Murdoch et al., 2010). Moreover, despite the evolutionary importance of nasal turbinates and their large size relative to the rest of the skull, they are the least well studied craniofacial structure (Van Valkenburgh et al., 2014). The only mechanistic study investigating turbinate morphogenesis in the mouse showed that mechanical forces from airflow affect the postnatal development of the anterior (respiratory) turbinates (Coppola et al., 2014). The molecular and genetic factors that regulate turbinate development are unknown.

A particularly interesting question is how OE expansion is scaled with turbinate growth. Crosstalk between the OE and the underlying turbinates has been predicted but not identified (Adameyko and Fried, 2016). Notably, genetic manipulations resulting in early failure of OE development seem to also lead to disrupted formation of turbinates and other nasal structures, highlighting the importance of the OE to the growth of the nasal cavity (Duggan et al., 2008; Kawauchi et al., 2009; Kersigo et al., 2011; Laclef et al., 2003). Here, we propose that throughout embryonic and early postnatal development, there are regions of the OE that remain immature and facilitate horizontal expansion of the OE, rather than vertical development. We identify the cells that make up these regions as an OE progenitor population that regulates turbinate growth via Fibroblast Growth Factor 20 (FGF20), a member of the FGF family of signaling molecules (Ornitz and Itoh, 2015). We further show that Wnt/β-Catenin (βCat, also Ctnnb1) signaling is required for the maintenance of these *Fgf20*-positive, epithelium-spanning progenitor (FEP) cells and their expression of *Fgf20*. These mechanisms regulate the overall size of the olfactory system and ensure that the OE and underlying turbinates scale proportionally.

RESULTS

In adult mice, the OE lines the nasal septum, the ethmo- (olfactory) turbinates, and the superior and lateral nasal cavity walls of the olfactory recess (Barrios et al., 2014). A layer of mesenchyme, called the lamina propria in the adult, separates the OE from the underlying cartilaginous or bony structures (Figure S1H). Throughout development and in the adult, the six olfactory turbinates have highly conserved branching, scrolling, and folding morphology (Figures S1I and S1I'). In order of most anterodorsal to posteroventral, they are: endoturbinate I (n1), ectoturbinate 1 (c1), endoturbinate II (n2), ectoturbinate 2 (c2), endoturbinate III (n3), and endoturbinate IV (n4). Anteriorly, n2 separates into two branches, n2' and n2". In this study, we focus mainly on c1. All images of turbinates presented are frontal sections through the posterior nasal cavity. We refer to "neck" (site of attachment of turbinate to nasal cavity wall) and "tip" regions of the turbinate as shown in Figure S1H, inset. We refer to "neck" OE as the negatively-curved OE directly overlying the "neck" region of the turbinate. In the adult, "neck" regions have sometimes been referred to as the cul-de-sac of the turbinate (Greer et al., 2016).

Fgf20 is expressed in a subset of $Sox2^+$ cells in the developing OE

Initial studies of the $Fgf20^{\beta gal}$ knockin allele showed *Fgf20* expression in progenitor-like cells in several developmental systems, including the inner ear (Huh et al., 2012), kidney cap mesenchyme (Barak et al., 2012), hair follicle (Huh et al., 2013), mammary buds (Elo et al., 2017), taste buds (unpublished data), and OE (unpublished data). To further investigate the cell type marked by *Fgf20* expression in the developing OE, we used the $Fgf20^{GFP\text{-}Cre}$ allele (Huh et al., 2015). Native GFP fluorescence from this allele is mostly undetectable; however, allele expression can be readily detected using an anti-GFP antibody.

$Fgf20^{GFP\text{-}Cre}$ expression was found in the developing OE as early as E10.5, albeit very weakly, in the lateral nasal pit (Figures 1A and S1A). Throughout its expression in the OE, *Fgf20* co-localized with a subset of $Sox2^+$ cells, a marker expressed by progenitors that fill the immature OE, and by BCs and Sus cells in the mature OE (Kawauchi et al., 2005). At E12.5, the shapes of turbinates n1, n2, and n3 can be observed, composed of mesenchyme surrounded by OE and respiratory epithelia (Figure S1B, n3 not shown). At this stage, *Fgf20* was still mainly expressed throughout the lateral OE (Figure 1B). Importantly, *Fgf20* was expressed in the OE overlying the site of future c1 development (Figure 1B, asterisk).

Turbinates develop through endochondral ossification initiated via epithelial budding and followed by proliferation of the underlying mesenchymal cells (Dieulafé, 1906; Martineau-Doizé et al., 1992). At E14.5, turbinates c1, c2, and n4 began to appear as mesenchymal condensations protruding from the nasal cavity wall (Figures S1C and S1C', c2 and n4 not shown). At this stage, most of the OE was mature, with an apical and a basal layer of $Sox2^+$ cells separated by a $Sox2^-$ middle layer of ORNs. In mature OE, *Fgf20* was expressed in a subset of apical $Sox2^+$ cells (Figure 1C, arrows). *Fgf20* was also expressed in regions of negatively-curved OE. These regions of the OE mostly retained an immature histology, where $Fgf20^+/Sox2^+$ cell nuclei were found throughout all layers of the OE (Figure 1C, white arrowheads). The negative curvature of the OE appeared to be formed by the protruding turbinates. *Fgf20* expression was still found in the OE overlying c1 at this stage (Figure 1C, asterisk).

By E17.5, in all six turbinates, cells of the mesenchymal condensations have differentiated into chondrocytes (Figures S1D-S1F, and S1E'). At this stage, intense *Fgf20* expression remained localized to areas of negatively-curved OE, which surround the "neck" of each of the six turbinates (Figures 1D-1F, arrowheads). Importantly, for turbinates n1, c1, c2, n3, and n4, these areas remained immature, with $Fgf20^+/Sox2^+$ cell nuclei spanning the entire thickness of the OE. For turbinate n2, the earliest turbinate to develop, "neck" OE has become more mature by E17.5 and only retained $Fgf20^+/Sox2^+$ cell

nuclei towards the apical layers of the OE (Figure 1E, blue arrowheads). The medial "neck" OE of turbinate n1, formed by the nasal septum and n1, has likewise become more mature by E17.5 (Figure 1E, blue arrowheads).

Turbinate chondrocytes undergo hypertrophy at early postnatal stages and by postnatal day 7 (P7) most of the cartilage has been replaced by ossified bone (Figures S1G and S1G'). At this stage, *Fgf20* expression was still primarily found in negatively-curved "neck" OE, but at the apical surface (Figure 1G, arrowheads). The concentrated expression seen at earlier stages has mostly dissipated, as the "neck" OE of every turbinate became almost completely mature by P7. After complete ossification, turbinates continue to grow, fold, and scroll until at least P30 (Figure S1I). At P30, *Fgf20* expression was undetectable (data not shown).

Interestingly, at E17.5, just outside of *Fgf20* expression hotspots in negatively-curved, immature OE, low GFP fluorescence was detected in the $Sox2^+$ basal and apical cells of the mature OE (Figure 1E', arrowheads). We suspect that this represents the capture of the transient $Fgf20^{GFP\text{-}Cre}$ lineage, due to GFP-Cre perdurance, suggesting that $Fgf20^+$ cells give rise to adjacent $Sox2^+$ BCs and Sus cells. These cells likely no longer actively transcribed *Fgf20*, but still retained some undegraded GFP-Cre protein.

Overall in development, intense *Fgf20* expression was found in immature regions of the OE, in a pattern associated with the growing turbinates. Upon maturation of a region of OE, *Fgf20* expression was initially shifted towards the basal and particularly apical layers before disappearing completely. Together, these observations led to the hypothesis that $Fgf20^+$ cells are a progenitor population in the developing OE. Based on results from experiments described below, we term this population FEP (*Fgf20*-positive, epithelium-spanning progenitor) cells, as their nuclei are found throughout all layers of the immature OE.

Fgf20 lineage includes all major OE cell types and responds to cues for expansion

OE surface area expansion is not well understood. A recent study showed that proliferation and neurogenesis shifts from dorsomedial zones of the OE to ventrolateral zones between E12.5 and E15.5 (Eerdunfu et al., 2017). This suggests that expansion of the OE occurs in a dorsomedial-to-ventrolateral direction. Interestingly, this wave of neurogenesis does not reach the OE at "neck" regions of turbinates, where FEP cells are localized, until perinatal stages, when FEP cells begin to disappear.

"Neck" OE housing FEP cells at E14.5 and E17.5 resemble immature OE at E12.5. Based on this and the overall *Fgf20* expression pattern, we hypothesized that *Fgf20* may be a marker for OE progenitors. To test this and to confirm findings by Eerdunfu et al. (2017), we first looked at proliferation and neurogenesis rates in negatively-curved "neck" OE, where FEP cells are located. At E17.5, these regions incorporated EdU at a higher rate than the OE at the turbinate "tip" (Figures S2A and S2B). This difference could be partially explained by a relative lack of post-mitotic ORNs in "neck" regions. Confirming this explanation, "neck" OE contained far fewer olfactory marker protein (OMP) positive cells (Figures S2C and S2D, arrowheads), a marker for mature ORNs (Hartman and Margolis, 1975). The only exception was the medial "neck" OE of n1, the most mature "neck" OE at E17.5. The distribution of $Fgf20^+$ cells and OMP^+ ORNs along the length of the c1 OE, when plotted along a straight line, showed low OMP^+ ORN density in areas of high $Fgf20^+$ cell density (Figure S2E). No cells were found to co-express *Fgf20* and OMP.

In the adult, OE at "recesses of olfactory turbinates" have been shown to contain $Pde2a^+$ ORNs belonging to the "necklace" olfactory system, rather than OMP^+ ORNs (Figure S2F; Juilfs et al., 1997). To rule out the possibility that "neck" OE contained these OMP^- ORNs during embryonic stages, we

examined Pde2a expression at E17.5. Pde2a^{+} ORNs were not found in “neck” OE or anywhere else at this stage (Figure S2G). Note: the term “necklace” refers to the spatial organization of the glomeruli that receive projections from ORNs of the necklace olfactory system. It is not to be confused with the term “neck,” which in this study refers to a specific part of the turbinate. Altogether, these results suggest that immature, “neck” OE have increased rates of proliferation and decreased rates of neurogenesis. This supports the idea that these regions host embryonic progenitors involved in horizontal, as opposed to vertical, development.

Next, we combined *Fgf20*$^{GFP\text{-}Cre}$ with Cre reporter alleles *ROSA*^{mTmG} (Muzumdar et al., 2007) or *ROSA*^{tdTomato} (Madisen et al., 2010) to trace the lineage of *Fgf20*$^{GFP\text{-}Cre}$-expressing cells. The *ROSA*^{mTmG} allele, in which Cre-expressing cells and their progeny express membrane-localized eGFP (mG), while all other cells express membrane-localized tdTomato (mT), showed that the *Fgf20*$^{GFP\text{-}Cre}$ lineage includes most of the postnatal OE, and the entire ventrolateral OE containing zones 2-4 (Figures 2A-2C; OE zones are described in Ressler et al., 1993; Vassar et al., 1993). Only a few spots associated with the dorsomedial zone 1 were outside of the lineage (Figures 2A-2C, arrowheads). This pattern was consistent across individuals. The other olfactory structures with *Fgf20*$^{GFP\text{-}Cre}$-lineage cells were the vomeronasal organ (VNO; Figure S2H) and septal organ (SO; Figure S2I).

Importantly, in *Fgf20*$^{GFP\text{-}Cre}$-lineage OE, the entire thickness of the OE (the BC, ORN, and Sus cell layers, as well as the brightly fluorescent cilia layer apical to the Sus cell layer) expressed mG, and not mT (Figure 2B’). mG expression was restricted to the OE, except for two accessory OE structures found in the lamina propria (mesenchymal layer): axon bundles (Ax) projected by ORNs, and Bowman’s glands (BG), which associate with Bowman’s ducts that traverse the OE. These structures can be readily identified based on their morphology.

We then examined the *Fgf20*$^{GFP\text{-}Cre}$ “real-time” expression, identified with an antibody to GFP-Cre, compared to its lineage with the *ROSA*^{tdTomato} reporter at various stages of OE development. At E11.5, the lineage almost completely overlapped with real-time *Fgf20* expression (Figure 2D). However, as the OE expands (E14.5 and E17.5), the lineage increasingly exceeded the domain of real-time *Fgf20* expression (Figures 2E and 2F). Furthermore, quantification of surface area within and outside of the *Fgf20*$^{GFP\text{-}Cre}$ lineage showed that growth of the *Fgf20*$^{GFP\text{-}Cre}$-lineage OE far outpaced that of non-lineage OE (Figure 2G). In fact, surface area of the non-lineage OE did not significantly change from E14.5 to P7: 0.38 ± 0.02 mm^2 at E14.5, 0.46 ± 0.18 mm^2 at E17.5, and 0.53 ± 0.25 mm^2 at P7 (n = 3, mean ± SD, p = 0.6, one-way ANOVA). The *Fgf20*$^{GFP\text{-}Cre}$-lineage OE, on the other hand, grew significantly in surface area during this period: 1.39 ± 0.21 mm^2 at E14.5, 5.21 ± 0.06 mm^2 at E17.5, and 16.5 ± 1.1 mm^2 at P7 ($p < 0.001$, one-way ANOVA). Therefore, the *Fgf20*$^{GFP\text{-}Cre}$ lineage accounted for nearly all the expanding OE from E14.5 to P7. Together with *Fgf20*$^{GFP\text{-}Cre}$ immunostaining showing transient *Fgf20* expression in BCs and Sus cells (Figure 1E’ arrowheads), *Fgf20*$^{GFP\text{-}Cre}$ lineage tracing supports the hypothesis that FEP cells are multipotent progenitors of the OE contributing to horizontal expansion.

<u>*Fgf20*-KO mice have reduced turbinate size and altered morphology</u>

Next, we investigated the function of FGF20 signaling in olfactory system development. Because *Fgf20* was expressed in a pattern associated with the developing turbinates (overlying sites of future turbinate development at early stages and occupying “neck” regions at later stages), we compared the morphology of turbinates in *Fgf20*-KO (*Fgf20*$^{GFP\text{-}Cre/\beta gal}$) mice to those in heterozygous littermate controls (*Fgf20*$^{GFP\text{-}Cre/+}$). Gross overview of serial frontal sections of the nasal cavity at P30 showed that most of the olfactory turbinates were smaller and/or differed in shape in *Fgf20*-KO mice compared to control (Figures 3A-3D). These changes were consistent across individuals. Measurement of the surface of each turbinate to estimate size (Figure 3B’, outline) showed that of the six turbinates, c1, c2, and n4 were the most reduced in size in *Fgf20*-KO mice, by 35%, 28%, and 34%, respectively (Figure

3E). Most strikingly, c1 showed reduced folding and was missing its dorsal branch (Figure 3B'). n1, n2, and n3, the earliest turbinates to appear developmentally, were the least reduced in size, by 15%, 3.7%, and 7.0%, respectively (Figure 3E). In total, *Fgf20*-KO mice had a 17% average decrease in OE surface area within the nasal cavity, due to smaller turbinates, while septal organ surface area was not changed (Figure 3F). The septal organ is made up of olfactory epithelia, some of which is in the *Fgf20*$^{GFP\text{-}Cre}$ lineage (Figure S2I) and is only found overlying the nasal septum and not turbinates. This makes it a good internal control for turbinate surface area. The nasal cavity wall and septum did not appear to be affected by loss of FGF20 signaling.

We then examined *Fgf20*-KO mice at P0, when turbinates are still made up of chondrocytes. Many of the turbinates in *Fgf20*-KO mice appeared smaller than those in control (Figure S3A and S3B). Focusing on c1, there was a measurable decrease in the size of the turbinate cartilage ($p = 0.009$) and in the OE surface area overlying the turbinate ($p < 0.001$; Figures S3A', S3C, and S3D). Therefore, the turbinate deformity seen in the adult can at least be partially attributed to a defect prior to osteogenesis.

Fgf20 is required for mesenchymal proliferation early in turbinate development

In the initial stages of endochondral bone development, mesenchymal cells condense to form a mesenchymal condensation, and subsequently differentiate into chondrocytes (Long and Ornitz, 2013). To determine the cause of the decrease in c1 cartilage size at P0, we looked at these initial stages in *Fgf20*-KO embryos. Development of turbinate c1 began at around E14.5, as mesenchymal cells between the OE and the nasal cavity wall started to form a mesenchymal condensation. The condensed mesenchymal cells were proliferative and had high Sox9 expression (Sox9^{hi}; Figure 3G). Chondrocytes of the nasal cavity wall were also Sox9^{hi} but were distinguished from the condensed mesenchymal cells by their round nuclei and large soma. Mesenchymal cells that remained diffuse (uncondensed) were found between the condensation and the OE. These cells had weak or almost undetectable Sox9 expression (Sox9^{low}).

In *Fgf20*-KO embryos at E14.5, the number of condensed cells and diffuse cells were not significantly changed compared to control, although there was a trend towards fewer condensed cells (Figures 3G, 3I, and 3J). Consistent with this, the ratio of condensed cells to diffuse cells was slightly decreased compared to control ($p = 0.05$; Figure 3K), suggesting a defect in formation of the condensation. Analysis of EdU incorporation showed a decrease in proliferation rate in condensed cells ($p = 0.007$; Figures 3G and 3L) and diffuse cells ($p = 0.06$; Figure 3M) in *Fgf20*-KO embryos, although the latter was not statistically significant. To identify the cell type directly responding to FGF20, we examined *Dusp6* expression by in situ hybridization. *Dusp6* is a downstream target of FGF signaling (Ekerot et al., 2008; Kawakami et al., 2003; Li et al., 2005, 2007; Ornitz and Itoh, 2015) and is a target of FGF20 signaling in the cochlea (unpublished data). At E14.5, *Dusp6* was expressed in the c1 mesenchyme directly underneath the OE in control embryos (Figure 3H) and was markedly reduced in *Fgf20*-KO embryos (arrows). This suggests that FGF20 is signaling to diffuse cells directly underneath the OE to regulate proliferation and condensation. However, *Dusp6* expression was not completely absent in *Fgf20*-KO embryos (Figure 3H, arrow), suggesting that another FGF ligand may be compensating for the loss of FGF20.

At E17.5, Sox9^{hi} condensations were no longer observed in the turbinates. In *Fgf20*-KO mice, the rate of proliferation was decreased in "neck" region mesenchymal cells compared to control (Figures S4A, S4A', and S4B), but not in "tip" region mesenchymal cells (Figure S4C). There was no change in proliferation in turbinate chondrocytes at E17.5 (Figure S4D). Together, these data suggest that *Fgf20* regulates the proliferation of chondrocyte progenitors and potentially the formation of the mesenchymal condensation.

We also investigated whether *Fgf20*-KO mice have a defect in OE development. At P30, there was no measurable difference in OE thickness between control and *Fgf20*-KO mice (data not shown). Interestingly, at E14.5, there was a slight but statistically significant increase in both OE thickness ($p = 0.04$; Figures S3J and S3K) and the density of $Sox2^+$ basal cells ($p = 0.02$; Figure S3L). The proliferation rate of $Sox2^+$ BCs was unchanged (Figure S3M). This increase in thickness and $Sox2^+$ BC density may be an effect of the constriction in OE surface area due to a smaller turbinate. By P0, *Fgf20*-KO pups had normal OE thickness (Figure S3F), likely having adjusted to the constriction. Importantly, at P0, the OE of *Fgf20*-KO mice had a normal complement of OMP^+ ORNs, Sus cells, and $Sox2^+$ BCs (Figures S3G-S3I). In addition, neither *Fgf20* expression (Figure S3G) nor FEP cell proliferation (Figures S4A' and S4E) was affected in *Fgf20*-KO mice. Together, these data suggest that loss of FGF20 signaling does not affect OE vertical development.

Ectopic activation of FGF ligand expression in the OE drives mesenchymal growth

To determine whether overactivation of FGF signaling will increase proliferation in turbinate mesenchyme, we combined $Fgf20^{GFP\text{-}Cre}$ with the $ROSA^{rtTA}$ (Belteki et al., 2005) and TRE-Fgf9-IRES-eGfp (White et al., 2006) alleles. We generated Fgf9-OA ($Fgf20^{GFP\text{-}Cre/+}$; $ROSA^{rtTA}$; TRE-Fgf9-IRES-eGfp) mice along with littermate controls ($Fgf20^{GFP\text{-}Cre/+}$; $ROSA^{rtTA}$). The Fgf9-OA mouse expresses the reverse tetracycline transactivator (rtTA) in the $Fgf20^{GFP\text{-}Cre}$ lineage, which drives the expression of TRE-Fgf9-IRES-eGfp upon doxycycline (Dox) induction. FGF9 is biochemically similar to FGF20 (Ornitz and Itoh, 2015), and is able to rescue and compensate for the loss of FGF20 signaling in the cochlea (Huh et al., 2012, 2015).
Pregnant dams were fed a Dox diet starting at E11.5 and embryos were collected at E14.5. Fgf9-OA embryos showed a markedly thickened c1 mesenchymal layer (Figure S4F) and expansion and increased intensity of *Dusp6* expression (Figure S4G). Compared to control, Fgf9-OA embryos had a slight but non-significant decrease in the number of condensed mesenchymal cells ($p = 0.1$) and a two- to three-fold increase in the number of diffuse cells ($p = 0.01$; Figures S4F, S4H, and S4I). Correspondingly, the ratio of condensed to diffuse cells was significantly decreased ($p = 0.002$; Figure S4J). However, there was no significant change in either condensed or diffuse cell proliferation (Figures S4F, S4K, and S4L).

The lack of a measurable increase in diffuse cell proliferation in Fgf9-OA embryos may be due to increased mesenchyme thickness, causing cells further away from the OE to receive less FGF signaling. Consistent with this, high levels of *Dusp6* expression in Fgf9-OA embryos was only found in the mesenchyme within 58 μm of the OE (average of four samples). Therefore, we hypothesized that only diffuse cells close to the OE had an increase in proliferation in Fgf9-OA embryos. In control embryos, the diffuse mesenchymal layer averaged 69 μm thick. Quantification of proliferation of diffuse cells within 69 μm of the OE ("OE adjacent cells") in Fgf9-OA embryos showed a significant increase compared to the total diffuse cell population in controls (Figures S4F, brackets and S4L). These data suggest that the increase in diffuse cell number in Fgf9-OA embryos likely had contributions from decreased condensation as well as increased proliferation. Unfortunately, the Fgf9-OA pups die at birth, precluding us from examining the postnatal phenotype.

Wnt activity in the developing OE coincides with *Fgf20* expression

Given the interesting expression pattern of *Fgf20* in the OE, the properties of *Fgf20*-expressing cells, and the function of FGF20 signaling, we sought to understand the regulation of *Fgf20* expression and FEP cell maintenance. We turned to the canonical Wnt/βCat signaling pathway, which is a known direct transcriptional regulator of *Fgf20* (Chamorro et al., 2005) and commonly involved in progenitor and stem cell maintenance (Clevers and Nusse, 2012; Nusse and Clevers, 2017).

We used the Tcf/Lef:H2b-Gfp mouse, a well-described Wnt/βCat signaling reporter (Ferrer-Vaquer et al., 2010), to study Wnt/βCat activity in the developing OE. Interestingly, the Tcf/Lef:H2b-Gfp expression pattern was similar to that of *Fgf20* throughout the developing OE. H2B-GFP was detected in the lateral nasal pit at E10.5 (Figure 4A), consistent with previous reports of Wnt/βCat activity at this stage (Brugmann et al., 2007; Zhu et al., 2016). H2B-GFP was detected in the OE overlying the site of c1 development at E12.5 and E14.5 (Figures 4B, asterisk and 4C), and in negatively-curved "neck" OE at E17.5 (Figure 4D). At E17.5, H2B-GFP expression was found in FEP cell nuclei, which span all layers of the "neck" OE (Figure 4D', arrowheads). By P7, H2B-GFP expression was less concentrated, mainly found in the apical layer at and surrounding "neck" OE (Figure 4E). Unlike *Fgf20*, Tcf/Lef:H2b-Gfp was also highly expressed in the nasal pit rim at E10.5 (Figure 4A, arrowhead) and in the respiratory epithelium (RE) at later stages (Figures 4B and 4C). In addition, H2B-GFP has a long half-life, likely much longer than that of GFP-Cre (Waghmare et al., 2008), resulting in a larger expression domain for Tcf/Lef:H2b-Gfp compared to $Fgf20^{GFP\text{-}Cre}$. Consistent with this, the size of the Tcf/Lef:H2b-Gfp expression domain lies in between that of $Fgf20^{GFP\text{-}Cre}$ real-time expression and that of $Fgf20^{GFP\text{-}Cre}$-lineage. Importantly, Tcf/Lef:H2b-Gfp expression was not found in non-$Fgf20^{GFP\text{-}Cre}$-lineage OE. Furthermore, products of the Tcf/Lef:H2b-Gfp and $Fgf20^{\beta gal}$ reporters appeared to have similar half-lives. Expression patterns of these two reporters more closely overlapped (Figures 4F and 4G).

βCat conditional deletion results in a severe deficit in turbinate development

To determine the role of Wnt/βCat signaling in the OE, we combined $Fgf20^{GFP\text{-}Cre}$ with the $\beta Cat^{fl(ex2\text{-}6)}$ allele (Brault et al., 2001) to conditionally delete *βCat*. We generated βFF-CKO ($Fgf20^{GFP\text{-}Cre/+}$; $\beta Cat^{fl(ex2\text{-}6)/fl(ex2\text{-}6)}$) mice along with littermate controls ($Fgf20^{GFP\text{-}Cre/+}$; $\beta Cat^{fl(ex2\text{-}6)/+}$). Notably, since *Fgf20* is a downstream target of Wnt/βCat signaling, Wnt/βCat signaling is predicted to activate prior to the onset of $Fgf20^{GFP\text{-}Cre}$ expression, leading to delayed disruption of Wnt/βCat signaling. βFF-CKO pups appeared grossly normal at birth but most died by P1, with only a few surviving to adulthood. The surviving mice appeared smaller than littermate controls.

At P0, *Fgf20* expression was almost completely absent from the OE in βFF-CKO pups, as expected (Figure S5A). Therefore, a defect in turbinate development was predicted, as observed in *Fgf20*-KO mice. Examination of a few adult βFF-CKO mice that survived to P30 showed dramatically stunted turbinate growth of all six turbinates (Figure S5B). We focused our quantitative analysis on P0 pups, since the surviving P30 cohort was a biased sample. In addition, quantitation of turbinate size could be affected by the decreased overall size of βFF-CKO adult mice.

At P0, very noticeably, βFF-CKO mice had a more severe defect in turbinate development than *Fgf20*-KO mice (Figure 5A). This turbinate phenotype exhibited variability across individuals. A few pups had almost no detectable structural defect compared to control, while pups with the most severe phenotype had a complete lack of c1, c2, and n4 turbinates (Figure 5A, shape 3). This variability is likely attributable to residual Wnt/βCat signaling from delayed or inefficient *βCat* deletion, as well as to variability in $Fgf20^{GFP\text{-}Cre}$ expression. Therefore, we believe mice with the most severe phenotypes represented the most complete *βCat* deletion. Focusing on c1 (Figure 5A'), we classified the varying P0 βFF-CKO phenotypes into 3 categories based on turbinate shape: shape 1 resembles control, shape 2 has a reduction in size, and shape 3 lacks c1. Shape 1 was relatively rare and not found in every experiment.

To quantify the size of c1, we measured cartilage volume and overlying surface area. Cartilage volume was significantly decreased in βFF-CKO mice compared to control ($p < 0.001$; Figure 5B), as was surface area ($p < 0.001$; Figure 5C). Mesenchyme thickness was noticeably decreased but only in the most severe (shape 3) βFF-CKO mice (Figure 5D). This phenotype was not observed in *Fgf20*-KO mice

(Figure S3E). OE thickness was decreased in βFF-CKO mice, also a phenotype not observed in *Fgf20*-KO mice (see below).

Specific disruption of βCat signaling also results in a severe deficit in turbinate development

βCat serves two major functions in epithelial cells: Wnt/βCat signaling and cell adhesion. To rule out the contribution of disrupted cell adhesion to the βFF-CKO phenotype, we used the βCat^{DM} allele (Valenta et al., 2011) to generate a second *βCat* conditional deletion mouse: βDF-CKO ($Fgf20^{GFP\text{-}Cre/+}$; $\beta Cat^{DM/fl(ex2\text{-}6)}$), along with littermate controls ($Fgf20^{GFP\text{-}Cre/+}$; $\beta Cat^{+/+}$, $Fgf20^{GFP\text{-}Cre/+}$; $\beta Cat^{DM/+}$, and $Fgf20^{GFP\text{-}Cre/+}$; $\beta Cat^{fl(ex2\text{-}6)/+}$). When not specified, "control" refers to $Fgf20^{GFP\text{-}Cre/+}$; $\beta Cat^{fl(ex2\text{-}6)/+}$. βDF-CKO pups appeared grossly normal at birth but almost all died by P1.

Like βFF-CKO mice, *Fgf20* expression was absent from βDF-CKO pups at P0 (Figure S5A). The βDF-CKO turbinate phenotype was similar to that of βFF-CKO mice. However, the most severe βDF-CKO mice still had some observable c1, c2, and n4 development, unlike the most severe βFF-CKO mice (Figures S5D and S5D'). Despite this, βDF-CKO mice (40% reduction in cartilage volume, compared to control; Figure S5E) had a worse phenotype than *Fgf20*-KO mice (21% reduction) at P0 (Figure S3C). Like βFF-CKO mice, βDF-CKO mice also had decreased turbinate surface area and mesenchyme thickness, compared to littermate controls (Figures S5D', S5F, and S5G). Also, like βFF-CKO mice, examination of a few adult βDF-CKO mice that survived to P30 showed dramatically stunted turbinate growth of all six turbinates (Figure S5B).

βCat conditional deletion causes decreased mesenchymal proliferation in developing turbinates

To explain the decreased c1 turbinate size in βFF-CKO mice, we looked at proliferation in and around the mesenchymal condensation. The earliest phenotype in βFF-CKO mice was observed at E14.5. At this stage, there was a decrease in the number of $Sox9^{hi}$ condensed mesenchymal cells in βFF-CKO mice compared to control (Figures 5E and 5F), but no difference in the number of diffuse cells (Figure 5G), leading to a decreased ratio of condensed cells to diffuse cells (Figure 5H). Like at P0, the phenotype at E14.5 was also variable, with the most severe having almost no condensation. We did not categorize the E14.5 phenotype into shapes.

Proliferation in condensed cells was decreased in βFF-CKO mice (Figures 5E and 5I). This proliferation defect was more severe than that of *Fgf20*-KO mice. There was also a decrease in proliferation of diffuse cells at E14.5 (Figure 5J). The lack of a decrease in diffuse cell number at E14.5, despite the decrease in proliferation, suggests a defect in the formation of the condensation.

To directly assess effects on FGF signaling, *Dusp6* expression was examined by in situ hybridization. In the c1 mesenchymal layer in βFF-CKO mice at E14.5, *Dusp6* expression was absent (Figure S5C, arrows), unlike in *Fgf20*-KO mice at the same stage, where some *Dusp6* expression remained. This suggests that other OE signals regulating mesenchymal *Dusp6* expression could also be downregulated in βFF-CKO mice, in addition to FGF20. Also, *Dusp6* expression appeared to be slightly, yet consistently decreased in $Fgf20^{GFP\text{-}Cre/+}$; $\beta Cat^{flox/+}$ controls compared to $Fgf20^{GFP\text{-}Cre/+}$; $\beta Cat^{+/+}$ (compare Figures S5C and 3H). This may be attributable to heterozygosity of *βCat* in the OE. Overall, the βFF-CKO phenotype was similar to that of *Fgf20*-KO embryos, but more severe.

βCat conditional deletion leads to premature differentiation and progenitor depletion in the OE

Interestingly, βFF-CKO mice had significantly thinner OE compared to control at P0 ($p < 0.001$; Figures 5A', 6A, and 6B). In the most severe βFF-CKO mice at P0, OE at the tip of c1 was only 2-3 cell layers thick, whereas control OE was 7-9 cell layers thick in the same region (Figures 5A' and 6A).

Surprisingly, however, βFF-CKO OE contained a normal complement of Sus cells and OMP^+ ORNs (Figures 6A, 6C, and 6D). Even the most severely thinned βFF-CKO OE had a normal complement of these cells, which comprised nearly the entire OE. The presence of these differentiated OE cell types suggest that vertical development is intact in βFF-CKO mice.

Notably, there was a lack of FEP cells in the more severe βFF-CKO mice at P0, as evidenced by an absence of $Sox2^+$ epithelium-spanning cells and maturation of negatively-curved "neck" OE, where $Sox2^+$ cells were found only in the apical and basal layers (Figure 6A, arrowheads). In less severe βFF-CKO mice, some $Sox2^+$ epithelium-spanning cells were observed, resembling FEP cells in control mice (Figures S5A and 6A, arrows). However, these cells did not express *Fgf20* (Figure S5A, arrows). This shows that βCat is required for the maintenance of both *Fgf20* expression and FEP cells. There was also a decrease in the density of $Sox2^+$ BCs in βFF-CKO mice, with just a few cells remaining in the most severe cases (Figures 6A and 6D). Given that the severely thinned βFF-CKO OE contained a normal complement of the most differentiated cell types, this decrease in progenitor number suggests that FEP cells and $Sox2^+$ BCs were not maintained in an undifferentiated state.

Next, we examined differentiation at an earlier stage. At E14.5, the OE was only slightly thinner in βFF-CKO embryos ($p = 0.05$; Figures 6E and 6F). There was also a detectable decrease in the number of $Sox2^+$ BCs ($p = 0.05$; Figures 6E and 6G). Proliferation levels of $Sox2^+$ BCs did not appear to be dramatically changed ($p = 0.2$; Figures 6E and 6H). There was also a noticeable decrease in the number of, or absence of, FEP cells in the c1 OE of βFF-CKO embryos, based on a lack of epithelium-spanning $Sox2^+$ cells (Figure 6E, asterisk indicates "neck" region). At this stage, there was some residual $Fgf20^{GFP\text{-}Cre}$ expression in the n1 and n2 OE of βFF-CKO embryos (Figure 6I, arrowheads), likely attributable to GFP perdurance. However, there was no *Fgf20* expression in the c1 OE (Figure 6I, asterisk indicates "neck" region).

Remarkably, there was an increase in the number of OMP^+ ORNs in βFF-CKO mice at E14.5 compared to control (Figures 6I and 6J), despite a slight decrease in OE thickness. This supports the hypothesis that the P0 βFF-CKO phenotype was a result of premature differentiation, leading to a depletion of progenitors. At an earlier stage of development (E13.5), no obvious differences between βFF-CKO and control mice were observed (data not shown).

Examination of a few βFF-CKO mice that survived to P30 showed a lack of OE in some areas, as indicated by absence of OMP expression. This was particularly noticeable in areas overlying and surrounding "neck" regions of turbinates (Figure S5B, arrowhead). This suggests a defect in OE expansion or maintenance in the surviving adult βFF-CKO mice.

Specific disruption of βCat signaling leads to premature OE differentiation

βDF-CKO mice also exhibited decreased OE thickness at P0 (Figures S5D', S6A, and S6B), with a normal complement of Sus cells and OMP^+ ORNs (Figures S6A, S6C, and S6D). Similar to severe βFF-CKO mice, βDF-CKO mice also lacked FEP cells and showed early maturation of negatively-curved "neck" OE (Figure S6A, arrowheads). Interestingly, there was a small, but statistically significant increase in $Sox2^+$ BC density in βDF-CKO mice ($p = 0.03$; Figure S6D), opposite of the βFF-CKO phenotype.

At E17.5 in βDF-CKO mice, the OE was only slightly thinner compared to control (Figures S6E and S6F), with no change in $Sox2^+$ BC density (Figure S6G). $Sox2^+$ BCs were less proliferative compared to control ($p = 0.01$; Figures S6E and S6H), suggesting that the increase in $Sox2^+$ BCs at P0 was not due to increased proliferation. Unlike at P0, at E17.5 some FEP cells were still found in the c1 OE of βDF-

CKO mice (Figure S6E, arrow), along with *Fgf20* expression (Figure S6I, arrows). The increase in $Sox2^+$ BCs at P0 likely can be explained by premature differentiation of FEP cells.

At E17.5, in control mice, regions of "neck" OE were filled with FEP cells, with a dearth of OMP^+ ORNs. However, in βDF-CKO mice, these regions were prematurely filled with OMP^+ ORNs (Figure S6I, arrowheads). A distribution plot of OMP^+ and $Fgf20^+$ cells showed that in control mice, OMP^+ ORN density was lowest where $Fgf20^+$ cell density was highest ("neck" regions). In βDF-CKO mice, OMP^+ ORNs were much more evenly distributed across the turbinate.

Like βFF-CKO mice, examination of a few βDF-CKO mice that survived to P30 also showed a lack of OE in some areas, as indicated by absence of OMP expression (Figure S5B, arrowhead).

<u>βCat stabilization prevents differentiation of FEP cells</u>

To determine whether over-activation of Wnt/βCat signaling (gain-of-function) will produce the opposite phenotype as inactivation (loss-of-function), we combined $Fgf20^{GFP\text{-}Cre}$ with the $\beta Cat^{fl(ex3)}$ allele (Harada et al., 1999) to activate a dominant stable version of βCat. βEX3-OA ($Fgf20^{GFP\text{-}Cre/+}$; $\beta Cat^{fl(ex3)/+}$) pups had pronounced growth retardation post-partum, compared to littermate controls ($Fgf20^{GFP\text{-}Cre/+}$; $\beta Cat^{+/+}$) and died within a few days of birth. Some had notable abdominal distension and died at birth.

At E17.5, βEX3-OA mice had increased *Fgf20* expression in the OE compared to controls. In control mice, native GFP fluorescence from the $Fgf20^{GFP\text{-}Cre}$ allele was barely detectable without using an antibody to GFP (Figure S7A, arrowheads). However, in βEX3-OA mice, native GFP expression was broad and intense throughout the OE.

One of the most salient phenotypes in βEX3-OA mice at E17.5 was disrupted OE development (Figure 7A). The c1 OE of βEX3-OA mice was very thin and contained almost exclusively $Fgf20^+$/$Sox2^+$ FEP cells (Figures 7A' and 7B) and very few OMP^+ ORNs or Sox2 single-positive (BC or Sus) cells (Figures 7B and 7C). This cell composition resembles that of "neck" OE at E17.5 and the lateral OE at E12.5 in wildtype mice. Interestingly, the FEP cells at E17.5 were mostly non-proliferative (Figure S7B), suggesting that the increase in the number of FEP cells was due to lack of differentiation, and not an increase in proliferation. Areas of the OE not targeted by $Fgf20^{GFP\text{-}Cre}$ (for example, overlying dorsomedial regions of n2) still showed comparatively normal appearing OE, with $Sox2^+$ cells in apical and basal layers, and OMP^+ ORNs in between (Figures S7C and S7D).

In βEX3-OA mice, extra blebs of OE and mesenchyme were found throughout the nasal cavity (Figure 7A, asterisk). There were also clumps of very densely packed and highly $Fgf20^+$ FEP cells (Figure 7B, arrowheads). These FEP cells appeared dysplastic, with irregularly shaped nuclei and a high nuclear-cytoplasmic ratio (Figure S7A, inset). The epithelial-mesenchymal boundary was difficult to identify in βEX3-OA mice. In fact, the OE seemed to be invading into the mesenchyme, as highlighted by the presence of OMP^+ cells (Figure 7C, arrows) and duct structures (Figure S7A, arrows) in the mesenchyme.

Given the dense packing of cells, distorted cell morphology, and potentially disrupted basement membrane, it was difficult to quantify OE cells at E17.5. Therefore, we examined E13.5, the earliest stage that a phenotype was detectable. At this stage, the OE was already thinner in βEX3-OA mice (Figures S7E and S7F). In addition, there were clumps of FEP cells (Figure S7E, arrowheads) and a measurable increase in the density of FEP cells in the OE (Figure S7G). At this stage, there was no change in FEP cell proliferation (Figures S7E and S7H), again suggesting that the increase in FEP cell number was due to inhibition of differentiation, rather than increased proliferation.

βCat stabilization results in mesenchyme expansion without condensation in turbinates

Examination of turbinate development showed a vast expansion of the mesenchymal layer in βEX3-OA mice at E17.5, at the expense of the turbinate chondrocytes (Figure 7A'). At this stage, the nasal cavity wall in βEX3-OA mice appeared relatively normal, containing $Sox9^{hi}$ chondrocytes (Figure 7C). However, turbinate c1 was made up entirely of $Sox9^{low}$ mesenchymal cells, suggesting a defect in formation of the mesenchymal condensation (Figures 7C). Chondrocytes of n2 and n3, the least affected turbinates in *Fgf20*-KO and βCat loss-of-function mice, were also the least affected in βEX3-OA mice (Figure S7D). However, the shapes of these turbinates were affected along with notable expansion of the mesenchymal layer (Figure 7A).

At E13.5, control embryos showed no sign of c1 protrusion from the lateral wall (Figure 7D), which does not occur until E14.5. However, in βEX3-OA mice, a large protrusion made up of $Sox9^{low}$ mesenchyme could be seen in some embryos (Figure 7D). These $Sox9^{low}$ cells formed the shape of a turbinate, increasing the thickness of the mesenchyme (Figures 7D and 7E). Similarly to E17.5, the mesenchymal cells in βEX3-OA embryos at E13.5 were more proliferative than in control embryos (Figures 7D and 7F), accounting for the mesenchymal expansion seen at E17.5. However, these mesenchymal cells remained $Sox9^{low}$ without showing any signs of condensation formation. Overall, the turbinate phenotype in βEX3-OA mice was similar to that of Fgf9-OA embryos, but much more severe.

DISCUSSION

The results presented here identify an *Fgf20*-expressing, Wnt-responsive OE progenitor population, termed FEP cells. These cells horizontally expand the OE and scale its growth with that of the underlying turbinates. We find that within these cells, Wnt/βCat signaling is required to maintain an undifferentiated progenitor state and regulate the expression of *Fgf20,* while FGF20 directly promotes turbinate growth.

FEP cells are an embryonic OE progenitor population that expands the OE

A definitive embryonic progenitor population has not been identified in the OE, although a few have been proposed. These include nestin^{+} radial glia-like progenitors (RGLPs) and Pax7^{+} cells. RGLPs only give rise to ORNs, and their lineage is restricted to zone 1 of the OE (Murdoch and Roskams, 2008). Pax7^{+} cells give rise to ORNs, Sus cells, BCs, and Bowman's glands and ducts (Murdoch et al., 2010). However, the *Pax7*^{Cre}-lineage contribution to the OE is minimal, accounting for only ~16% of the OE at E11.5, ~7% at P5, and ~1% in the adult. This pattern is opposite to that of the *Fgf20*$^{GFP\text{-}Cre}$ lineage, which increases in percentage of total OE with age. Murdoch et al. (2010) predicted that another progenitor population exists, which responds to cues for OE expansion and gives rise to the rest of the OE. We propose that FEP cells could be this complementary population. Other proposed embryonic OE progenitors include Meis1^{+} cells and Foxg1^{+} cells, both of which may overlap with FEP cells at different stages. Meis1^{+} cells are found in the lateral OE at E11.5, and are slow-dividing, self-renewing, and less neurogenic relative to more medial progenitors (Tucker et al., 2010). These properties are reminiscent of FEP cells. It is likely that *Fgf20* and *Meis1* expression overlap at E11.5. However, the expression pattern of Meis1 post E11.5 has not been reported. *Foxg1* expression is found early in the olfactory placode, and its lineage therefore includes the entire OE (Duggan et al., 2008; Hébert and McConnell, 2000). At E10.5, *Foxg1* is expressed mainly in the medial and central nasal pit, unlike *Fgf20*, which is expressed laterally (Duggan et al., 2008; Kawauchi et al., 2009). From E12.5 to E17.5, Foxg1^{+} cells are found in the ventrolateral OE, in a pattern somewhat similar to that of the *Fgf20*$^{GFP\text{-}Cre}$ lineage. However, Foxg1^{+} cells are located in the BC layer and co-express BC markers, unlike FEP cells. This suggests that Foxg1^{+} BCs could be derived from FEP cells.

We propose that FEP cells are an embryonic OE progenitor population. FEP cells were identified in the early embryonic (E10.5 and E12.5) lateral OE, which is less developed than the medial OE (Eerdunfu et al., 2017; Tucker et al., 2010). Even after the OE begins to mature and undergo established neurogenesis at E13 (Cau et al., 1997; Cuschieri and Bannister, 1975a, 1975b; Smart, 1971), FEP cells continued to be localized laterally in immature and undifferentiated OE, which resembled early-stage embryonic OE. This suggests that FEP cells define parts of the developing OE focused on progenitor expansion (horizontal development), rather than established neurogenesis (vertical development). Moreover, given that the OE expands in a ventrolateral direction, at around E12.5 to E15.5, after initial development of the dorsomedial region (Eerdunfu et al., 2017), FEP cells occupy the correct location to account for this lateral expansion. Consistent with this, the *Fgf20*$^{GFP\text{-}Cre}$ lineage included the entire ventrolateral OE (zones 2-4) but spared some of the dorsomedial OE (zone 1).

The total lineage of FEP cells included all the major cell types of the OE, including Sus cells, ORNs, BCs, as well as Bowman's glands and ducts. Transient *Fgf20* lineage labeling, taking advantage of GFP-Cre perdurance, suggests that FEP cells give rise immediately to Sox2^{+} BCs. Sox2^{+} BCs, in turn, differentiate in a well-described, step-wise manner into ORNs in established neurogenesis (reviewed in Calof et al., 2002; Maier et al., 2014). Transient *Fgf20* lineage tracing also suggests that FEP cells can differentiate directly to Sus cells. In addition, it has been recently shown that *Ascl3*$^{+}$ cells found in the apical layer of the embryonic OE are progenitors for both Bowman's gland and duct cells, and microvillar cells (Weng et al., 2016). We predict that FEP cells give rise to these *Ascl3*$^{+}$ progenitors.

A caveat in analyzing *Fgf20*$^{GFP\text{-}Cre}$ lineage tracing data is that the lineage is cumulative. To definitively show that FEP cells give rise to the expanding OE will require an inducible system to target the FEP population at a specific time point. Nevertheless, results from the cumulative lineage strongly suggest that FEP cells contribute to OE expansion. The *Fgf20*$^{GFP\text{-}Cre}$ lineage accounted for nearly all of the OE expansion that occurred from E14.5 to P7, during which the OE surface area increased by eleven-fold. This high rate of expansion coincided with FGF20-regulated cartilaginous growth of turbinates beginning at E14.5 with the formation of a mesenchymal condensation and ending around P7 with ossification of the turbinates. From P7 to P30, the OE surface area continued to expand by roughly three-fold, as turbinates grow by what has been hypothesized as secondary membranous bone extensions (Martineau-Doizé et al., 1992). During these stages, *Fgf20*$^{GFP\text{-}Cre}$-lineage OE and non-lineage OE grew proportionally, which is expected, given the absence of FEP cells at these stages. This suggests a different method of OE expansion accompanying a different method of turbinate growth. Furthermore, while the *Fgf20*$^{GFP\text{-}Cre}$ lineage did not extend beyond the FEP domain at the start of OE development (E11.5), it quickly and increasingly exceeded the FEP domain horizontally during the stages of rapid OE expansion (E14.5 and E17.5). These lineage trace data, together with results showing increased proliferation and decreased neurogenesis in FEP regions of the OE, strongly support a role for FEP cells in horizontal OE development.

Wnt/βCat signaling maintains FEP stemness

The “neck” OE where FEP cell were found may define a niche environment to maintain these embryonic progenitors into perinatal stages. Wnt/βCat signaling is often an important component of stem cell and progenitor niches (Clevers and Nusse, 2012; Nusse and Clevers, 2017). This ubiquitous signaling pathway has been studied in the OE at the nasal pit stage in the context of facial development (Brugmann et al., 2007; Mani et al., 2010; Reid et al., 2011; Zhu et al., 2016) and at the postnatal and adult stage in the context of OE stem cell maintenance (Chen et al., 2014; Wang et al., 2011). However, it has not been studied at the stages in between, except for an ectopic activation study (see below; Engel et al., 2016). Here, we report Wnt/βCat activity at various stages throughout the embryonic and early postnatal OE using the Tcf/Lef:H2b-Gfp mouse (Ferrer-Vaquer et al., 2010) in addition to *Fgf20*$^{GFP\text{-}Cre}$ expression, an established transcriptional target of Wnt signaling (Chamorro et al., 2005).

βCat loss- and gain-of-function experiments show that Wnt/βCat signaling is necessary and sufficient for the maintenance of FEP cells. Loss-of-function led to loss of FEP cells due to premature differentiation into Sox2^{+} BCs, and in turn, ORNs, while gain-of-function led to sustained FEP cell maintenance without differentiation into other cell types. Notably, in βEX3-OA mice at E17.5, almost the entire OE resembled early-stage immature OE. Loss-of-function experiments also suggest that Wnt/βCat signaling is necessary for the maintenance of Sox2^{+} BCs, perhaps secondary to defects in the FEP cells that give rise to them.

Other signals may also be important for FEP niche maintenance. Mechanical forces from negative curvature generation and signals from the turbinates or nasal cavity wall could be important, since negatively-curved OE is formed by the developing turbinates. These signals could be Wnt ligands or other factors upstream of Wnt/βCat signaling. This possibility suggests an interesting feedback loop in which developing turbinates help shape the niche to maintain expansive OE progenitors that, in turn, secrete signals to promote turbinate growth. It is further conceivable that the loss of FEP cells in βCat loss-of-function mice is secondary to defects in turbinate growth affecting OE negative curvature formation. However, we believe that Wnt/βCat signaling most likely acts directly to maintain FEP cells, since Wnt/βCat activity has the same pattern of expression as *Fgf20*. Furthermore, overactivation of Wnt/βCat signaling was sufficient to maintain FEP cells outside of negatively-curved “neck” OE.

FEP cells have potential for dysplasia

In βCat gain-of-function mice, FEP cells became dysplastic, densely packed clumps of undifferentiated cells. A similar tumorigenic phenotype has been recently studied, in which *Sox2:CreER^{T2}* was used to activate the *βCat$^{fl(ex3)}$* allele (Engel et al., 2016), presumably targeting FEP cells along with Sox2^{+} BCs and Sus cells. Notably, the strongest tumorigenic phenotype occurred when tamoxifen was given at E14.5. The phenotype was markedly and progressively less severe when tamoxifen was given at P7, P14, and P21 (no phenotype). This strongly suggests that FEP cells, which are present early in development and disappear after P7, were the cells responding to Wnt/βCat overactivation in their experiment. Therefore, our βEX3-OA experiment most likely targets the more specific cell type. Engel et al. also discuss the similarity and differences between this tumorigenic phenotype and human tumors, including olfactory neuroblastoma and sinonasal haemangiopericytoma. The results from Engel et al. indicated a turbinate phenotype, but it was not described.

Disruptions to signaling, not cell adhesion, accounts for most of the βCat loss-of-function phenotype

βFF-CKO mice have disruptions in both the signaling and cell adhesion functions of βCat. However, evidences suggest that defects in cell adhesion were not responsible for the βFF-CKO phenotype. Importantly, βDF-CKO mice, in which only signaling was affected, had similar phenotypes to the complete knockout. Furthermore, a recent study found no defects in the total number of ORNs and Sus cells in the P0 OE in mice lacking functional αN-catenin, an important component of cell adhesion that is highly expressed in ORNs (Katsunuma et al., 2016). However, in these mice, there was abnormal adhesion between ORNs and Sus cells, resulting in abnormal apical patterning of the OE.

The *βCat^{DM}* allele is hypomorphic, and βDF-CKO mice had similar but less severe phenotypes compared to βFF-CKO mice. One difference between the two knockouts is that Sox2^{+} BC density was increased in βDF-CKO mice at P0 but decreased in βFF-CKO mice. We hypothesize that this difference was due to a later onset of premature differentiation in βDF-CKO mice. Supporting this idea, FEP cells could still be found at E17.5 in βDF-CKO mice, while they were almost completely gone in the most severe βFF-CKO mice as early as E14.5. The increase in Sox2^{+} BC density at P0, therefore, was likely the result of premature differentiation of the FEP cells remaining at E17.5.

Importantly, βDF-CKO mice are not equivalent to the less severe βFF-CKO mice (shape 2). We observed that in some βFF-CKO mice, turbinates on the left and right sides of the nasal cavity showed different phenotype severity, suggesting that the phenotype variability was due to differences in Cre activation and efficiency. This is supported by the lack of high variability in the βDF-CKO phenotype, as the βCat^{DM} allele is not dependent on Cre for activation. Furthermore, because the βCat^{DM} allele is constitutive, βDF-CKO mice had decreased Wnt/βCat signaling levels prior to the onset of *Fgf20$^{GFP-Cre}$* expression, further distinguishing them from βFF-CKO mice.

Wnt/βCat signaling in FEP cells regulates turbinate development via epithelial-mesenchymal signaling

Mice lacking *Fgf20* had decreased total OE surface area, but normal OE cellular composition and organization. Based on these findings, we conclude that the OE is not directly affected by loss of FGF20 signaling. Rather, FGF20 appears to be signaling directly to the underlying mesenchyme to regulate turbinate growth. Consistent with this, in the absence of FGF20, expression of the FGF target gene *Dusp6* is markedly decreased in diffuse mesenchymal cells directly beneath the OE. Conversely, ectopic activation of FGF signaling led to increased *Dusp6* expression in the diffuse cells. However, we cannot completely rule out the possibility that FGF20 may be signaling to both the mesenchyme and the OE, which is the case during cochlea development (Huh et al., 2012, 2015).

The βCat loss- and gain-of-function experiments strongly suggest that *Fgf20* is a downstream target of Wnt/βCat signaling. Wnt/βCat activity and *Fgf20* expression were detected in a pattern associated with turbinate development prior to their complete calcification at around P7. Consistent with this, loss of Wnt/βCat-FGF20 signaling affected the cartilaginous growth of turbinates. Prior to and during the initiation of turbinate c1 development at E14.5, Wnt/βCat activity and *Fgf20* expression were detected in the OE overlying the site of c1 development. This suggests that the OE has a role in the initiation of turbinate development, as hypothesized previously (Adameyko and Fried, 2016; Dieulafé, 1906). In both *Fgf20*-KO and βFF-CKO mice, the ratio of c1 condensed mesenchymal cells to diffuse cells at E14.5 was decreased. Both also showed decreased proliferation of diffuse cells as well as the normally highly proliferative condensed cells. *Dusp6* expression showed that diffuse cells are likely the direct targets of FGF20 signaling. Together, these results suggest that Wnt/βCat-FGF20 signaling is required for chondrocyte progenitor proliferation and potentially mesenchymal condensation. The reason for reduced proliferation of condensed cells is not clear at this point. Fgf9-OA and βEX3-OA mice, which had dramatically increased *Fgf20* expression, had increased proliferation of diffuse mesenchymal cells, but decreased or a lack of condensed cells. In βEX3-OA mice, this led to an expansion of the mesenchymal layer at the expense of turbinate cartilage. Together, these results show that an appropriate level of Wnt/βCat-FGF20 signaling is required for normal chondrocyte progenitor proliferation and formation of the mesenchymal condensation.

Strikingly, in both βFF-CKO and βDF-CKO mice, turbinate phenotypes were more severe than that of *Fgf20*-KO mice. In the most severe βFF-CKO mice, there was no formation of the mesenchymal condensation. This indicates that other Wnt/βCat-regulated epithelial-mesenchymal signals may complement FGF20 and compensate for its loss during turbinate development. We hypothesize that these signals are also expressed by FEP cells; however, we cannot rule out the possibility that they are expressed by other parts of the OE within the FEP-lineage. These signals could be other members of the FGF family, which often have complementary and redundant functions with each other (Ornitz and Itoh, 2015). Consistent with this, some residual expression of the FGF target gene *Dusp6* was found in the turbinate mesenchyme in *Fgf20*-KO embryos, but not in βFF-CKO embryos.

FGFs shown to be expressed in or around the embryonic nasal pit and OE include *Fgf3, 4, 7, 8*, *9*, *10*, *15*, and *17* (Bachler and Neubüser, 2001; Kawauchi et al., 2004, 2005; Zhu et al., 2016). Among these, only *Fgf8* has been shown *in vivo* to be necessary for olfactory development, although whether it is directly or indirectly required is a topic of debate. *Fgf8* is expressed at the rim of the nasal pit, and its conditional deletion leads to death of cells required for OE neurogenesis (Kawauchi et al., 2005). This causes loss of almost all OE cells and other olfactory structures in the nasal cavity very early in development. Interestingly, *Fgf8* expression in the nasal pit is partly regulated by Wnt/βCat signaling (Reid et al., 2011). However, it has been shown that *Fgf8* expression and lineage is restricted to the respiratory epithelium, and loss of *Fgf8* leads to olfactory defects secondary to defects in craniofacial development (Forni et al., 2013).

Other candidate FGFs that potentially work together with FGF20 include FGF9, which is a part of the same FGF subfamily as FGF20, and has been shown to work with FGF20 in kidney (Barak et al., 2012) and cochlea (Huh et al., 2015) development. FGF10, which is essential for the initiation of limb bud formation (Min et al., 1998; Sekine et al., 1999), is also a candidate. However, neither *Fgf9*; *Fgf20* nor *Fgf10*; *Fgf20* double-knockout mice exhibited a more severe phenotype than *Fgf20*-KO (unpublished data). Future experiments targeting *Fgfrs* for deletion in turbinate chondrocyte progenitors can help address FGF redundancy.

Bone morphogenetic proteins (BMPs) are another class of Wnt/βCat-regulated signaling factors that have well described roles in chondrogenesis (Lin et al., 2016) and could promote turbinate growth.

Bmp2, *4*, *6*, and *7* expression have been detected in the embryonic OE, particularly in ORNs (Peretto et al., 2002; Shou et al., 2000). These genes have not been studied in the context of *in vivo* turbinate development, although there is *in vitro* evidence that they function in feedback inhibition of ORN differentiation (Shou et al., 1999, 2000), similarly to other members of the TGFβ superfamily (Gokoffski et al., 2011; Kawauchi et al., 2004, 2009; Wu et al., 2003). Unlike FGF20, other epithelial-mesenchymal signals may not necessarily be directly regulated by Wnt/βCat signaling. In the absence of Wnt/βCat signaling, FEP cells are not maintained, resulting in the loss of signals produced by FEP cells.

The decrease in OE surface area and turbinate size and complexity in *Fgf20*-KO mice makes them a potentially useful model for understanding olfaction, particularly from an evolutionary perspective. Turbinate complexity is highly variable among mammals, and this variability has been hypothesized to be correlated with, and evolutionarily driven by, the importance of olfaction (Negus, 1959). However, the idea that increased OE surface area results in increased olfactory ability has not been directly tested (Van Valkenburgh et al., 2014). *Fgf20*-KO mice are useful for testing this hypothesis. Olfactory receptors in the OE are zonally distributed (Ressler et al., 1993; Vassar et al., 1993). *Fgf20*-KO mice may therefore have a deficiency in specific zones of the OE, resulting in a decrease of a specific subset of olfactory receptors. This could be studied by examining distribution patterns of various olfactory receptors in the *Fgf20*-KO OE and testing for ability to detect a range of different odorants.

Overall, this study addresses several important gaps in knowledge in olfactory system development, including the identity of an expansive pool of OE progenitors, mechanisms regulating OE expansion, genetic regulation of turbinate development, role of Wnt/βCat signaling in olfactory development, and mechanisms linking scaling of the OE and the underlying turbinates. We do not know whether FEP cells exist in other mammalian species, but our findings have implications for mammalian evolution. Evolutionarily-driven factors acting on FEP cell number and function are a potential mechanism accounting for the diversity of OE surface area and turbinate complexity seen across mammals. Furthermore, dysregulation of FEP cells or their equivalent in humans may contribute to human diseases such as anosmia and olfactory tumors. Finally, this study provides an interesting model for tissue-scaling and progenitor niche maintenance with potential relevance to other developmental systems.

ACKNOWLEDGEMENTS

We thank Y. Yin and A. Hagan for critically reading the manuscript. This work was funded by a grant from the March of Dimes Foundation, NIH grant HL111190 (D.M.O.), the Department of Developmental Biology, and DC012825 (S.H.). Hamamatsu NanoZoomer slide scanning system use was supported by the HOPE Center Alafi Neuroimaging Laboratory (NCRR 1S10RR027552). Zeiss Axio Imager Z2 use was supported by the Washington University Center for Cellular Imaging (The Children's Discovery Institute CDI-CORE-2015-505; NS086741).

AUTHOR CONTRIBUTIONS

Conceptualization, L.M.Y., S.H., and D.M.O.; Methodology, L.M.Y. and D.M.O.; Formal Analysis, L.M.Y.; Investigation: L.M.Y. and D.M.O.; Resources: D.M.O.; Writing – Original Draft: L.M.Y. and D.M.O.; Writing – Review & Editing: L.M.Y., S.H., and D.M.O.; Supervision: D.M.O.; Funding Acquisition: S.H. and D.M.O.

DECLARATION OF INTERESTS

The authors declare no competing interests.

REFERENCES

Adameyko, I., and Fried, K. (2016). The Nervous System Orchestrates and Integrates Craniofacial Development: A Review. Front. Physiol. *7*, 49.

Albert Farbman (1992). Cell Biology of Olfaction (Cambridge University Press).

Bachler, M., and Neubüser, A. (2001). Expression of members of the Fgf family and their receptors during midfacial development. Mech. Dev. *100*, 313–316.

Barak, H., Huh, S.-H., Chen, S., Jeanpierre, C., Martinovic, J., Parisot, M., Bole-Feysot, C., Nitschké, P., Salomon, R., Antignac, C., et al. (2012). FGF9 and FGF20 Maintain the Stemness of Nephron Progenitors in Mice and Man. Dev. Cell *22*, 1191–1207.

Barrios, A.W., Núñez, G., Sánchez Quinteiro, P., and Salazar, I. (2014). Anatomy, histochemistry, and immunohistochemistry of the olfactory subsystems in mice. Front. Neuroanat. *8*, 63.

Beites, C.L., Kawauchi, S., Crocker, C.E., and Calof, A.L. (2005). Identification and molecular regulation of neural stem cells in the olfactory epithelium. Exp. Cell Res. *306*, 309–316.

Belteki, G., Haigh, J., Kabacs, N., Haigh, K., Sison, K., Costantini, F., Whitsett, J., Quaggin, S.E., and Nagy, A. (2005). Conditional and inducible transgene expression in mice through the combinatorial use of Cre-mediated recombination and tetracycline induction. Nucleic Acids Res. *33*, e51–e51.

Brault, V., Moore, R., Kutsch, S., Ishibashi, M., Rowitch, D.H., McMahon, A.P., Sommer, L., Boussadia, O., and Kemler, R. (2001). Inactivation of the (β)-catenin gene by Wnt1-Cre-mediated deletion results in dramatic brain malformation and failure of craniofacial development. Development *128*, 1253–1264.

Brugmann, S.A., Goodnough, L.H., Gregorieff, A., Leucht, P., Berge, D. ten, Fuerer, C., Clevers, H., Nusse, R., and Helms, J.A. (2007). Wnt signaling mediates regional specification in the vertebrate face. Development *134*, 3283–3295.

Calof, A.L., Bonnin, A., Crocker, C., Kawauchi, S., Murray, R.C., Shou, J., and Wu, H.-H. (2002). Progenitor cells of the olfactory receptor neuron lineage. Microsc. Res. Tech. *58*, 176.

Cau, E., Gradwohl, G., Fode, C., and Guillemot, F. (1997). Mash1 activates a cascade of bHLH regulators in olfactory neuron progenitors. Development *124*, 1611–1621.

Chamorro, M.N., Schwartz, D.R., Vonica, A., Brivanlou, A.H., Cho, K.R., and Varmus, H.E. (2005). FGF-20 and DKK1 are transcriptional targets of beta-catenin and FGF-20 is implicated in cancer and development. EMBO J. *24*, 73–84.

Chen, M., Tian, S., Yang, X., Lane, A.P., Reed, R.R., and Liu, H. (2014). Wnt-Responsive Lgr5+ Globose Basal Cells Function as Multipotent Olfactory Epithelium Progenitor Cells. J. Neurosci. *34*, 8268–8276.

Clevers, H., and Nusse, R. (2012). Wnt/β-Catenin Signaling and Disease. Cell *149*, 1192–1205.

Coppola, D.M., Craven, B.A., Seeger, J., and Weiler, E. (2014). The effects of naris occlusion on mouse nasal turbinate development. J. Exp. Biol. *217*, 2044–2052.

Cuschieri, A., and Bannister, L.H. (1975a). The development of the olfactory mucosa in the mouse: electron microscopy. J. Anat. *119*, 471–498.

Cuschieri, A., and Bannister, L.H. (1975b). The development of the olfactory mucosa in the mouse: light microscopy. J. Anat. *119*, 277–286.

Dieulafé, L. (1906). Morphology and Embryology of the Nasal Fossae of Vertebrates. Ann. Otol. Rhinol. Laryngol. *15*, 1–584.

Duggan, C.D., DeMaria, S., Baudhuin, A., Stafford, D., and Ngai, J. (2008). Foxg1 Is Required for Development of the Vertebrate Olfactory System. J. Neurosci. *28*, 5229–5239.

Eerdunfu, Ihara, N., Ligao, B., Ikegaya, Y., and Takeuchi, H. (2017). Differential timing of neurogenesis underlies dorsal-ventral topographic projection of olfactory sensory neurons. Neural Develop. *12*, 2.

Ekerot, M., Stavridis, M.P., Delavaine, L., Mitchell, M.P., Staples, C., Owens, D.M., Keenan, I.D., Dickinson, R.J., Storey, K.G., and Keyse, S.M. (2008). Negative-feedback regulation of FGF signalling by DUSP6/MKP-3 is driven by ERK1/2 and mediated by Ets factor binding to a conserved site within the DUSP6/MKP-3 gene promoter. Biochem. J. *412*, 287–298.

Elo, T., Lindfors, P.H., Lan, Q., Voutilainen, M., Trela, E., Ohlsson, C., Huh, S.-H., Ornitz, D.M., Poutanen, M., Howard, B.A., et al. (2017). Ectodysplasin target gene Fgf20 regulates mammary bud growth and ductal invasion and branching during puberty. Sci. Rep. *7*, 5049.

Engel, N.W., Neumann, J.E., Ahlfeld, J., Wefers, A.K., Merk, D.J., Ohli, J., and Schüller, U. (2016). Canonical Wnt Signaling Drives Tumor-Like Lesions from Sox2-Positive Precursors of the Murine Olfactory Epithelium. PLoS ONE *11*, e0166690.

Ferrer-Vaquer, A., Piliszek, A., Tian, G., Aho, R.J., Dufort, D., and Hadjantonakis, A.-K. (2010). A sensitive and bright single-cell resolution live imaging reporter of Wnt/ß-catenin signaling in the mouse. BMC Dev. Biol. *10*, 121.

Forni, P.E., Bharti, K., Flannery, E.M., Shimogori, T., and Wray, S. (2013). The Indirect Role of Fibroblast Growth Factor-8 in Defining Neurogenic Niches of the Olfactory/GnRH Systems. J. Neurosci. *33*, 19620–19634.

Gokoffski, K.K., Wu, H.-H., Beites, C.L., Kim, J., Kim, E.J., Matzuk, M.M., Johnson, J.E., Lander, A.D., and Calof, A.L. (2011). Activin and GDF11 collaborate in feedback control of neuroepithelial stem cell proliferation and fate. Development *138*, 4131–4142.

Green, P.A., Van Valkenburgh, B., Pang, B., Bird, D., Rowe, T., and Curtis, A. (2012). Respiratory and olfactory turbinal size in canid and arctoid carnivorans. J. Anat. *221*, 609–621.

Greer, P.L., Bear, D.M., Lassance, J.-M., Bloom, M.L., Tsukahara, T., Pashkovski, S.L., Masuda, F.K., Nowlan, A.C., Kirchner, R., Hoekstra, H.E., et al. (2016). A Family of non-GPCR Chemosensors Defines an Alternative Logic for Mammalian Olfaction. Cell *165*, 1–15.

Harada, N., Tamai, Y., Ishikawa, T., Sauer, B., Takaku, K., Oshima, M., and Taketo, M.M. (1999). Intestinal polyposis in mice with a dominant stable mutation of the β-catenin gene. EMBO J. *18*, 5931–5942.

Hartman, B.K., and Margolis, F.L. (1975). Immunofluorescence localization of the olfactory marker protein. Brain Res. *96*, 176–180.

Hébert, J.M., and McConnell, S.K. (2000). Targeting of cre to the Foxg1 (BF-1) Locus Mediates loxP Recombination in the Telencephalon and Other Developing Head Structures. Dev. Biol. *222*, 296–306.

Huh, S.-H., Jones, J., Warchol, M.E., and Ornitz, D.M. (2012). Differentiation of the Lateral Compartment of the Cochlea Requires a Temporally Restricted FGF20 Signal. PLoS Biol. *10*, e1001231.

Huh, S.-H., Narhi, K., Lindfors, P.H., Haara, O., Yang, L., Ornitz, D.M., and Mikkola, M.L. (2013). Fgf20 governs formation of primary and secondary dermal condensations in developing hair follicles. Genes Dev. *27*, 450–458.

Huh, S.-H., Warchol, M.E., and Ornitz, D.M. (2015). Cochlear progenitor number is controlled through mesenchymal FGF receptor signaling. ELife *4*.

Ikeda, K., Ookawara, S., Sato, S., Ando, Z., Kageyama, R., and Kawakami, K. (2007). Six1 is essential for early neurogenesis in the development of olfactory epithelium. Dev. Biol. *311*, 53–68.

Juilfs, D.M., Fülle, H.J., Zhao, A.Z., Houslay, M.D., Garbers, D.L., and Beavo, J.A. (1997). A subset of olfactory neurons that selectively express cGMP-stimulated phosphodiesterase (PDE2) and guanylyl cyclase-D define a unique olfactory signal transduction pathway. Proc. Natl. Acad. Sci. U. S. A. *94*, 3388–3395.

Katsunuma, S., Honda, H., Shinoda, T., Ishimoto, Y., Miyata, T., Kiyonari, H., Abe, T., Nibu, K., Takai, Y., and Togashi, H. (2016). Synergistic action of nectins and cadherins generates the mosaic cellular pattern of the olfactory epithelium. J Cell Biol *212*, 561–575.

Kawakami, Y., Rodríguez-León, J., Koth, C.M., Büscher, D., Itoh, T., Raya, Á., Ng, J.K., Esteban, C.R., Takahashi, S., Henrique, D., et al. (2003). MKP3 mediates the cellular response to FGF8 signalling in the vertebrate limb. Nat. Cell Biol. *5*, 513–519.

Kawauchi, S., Beites, C.L., Crocker, C.E., Wu, H.-H., Bonnin, A., Murray, R., and Calof, A.L. (2004). Molecular Signals Regulating Proliferation of Stem and Progenitor Cells in Mouse Olfactory Epithelium. Dev. Neurosci. *26*, 166–180.

Kawauchi, S., Shou, J., Santos, R., Hébert, J.M., McConnell, S.K., Mason, I., and Calof, A.L. (2005). Fgf8 expression defines a morphogenetic center required for olfactory neurogenesis and nasal cavity development in the mouse. Development *132*, 5211–5223.

Kawauchi, S., Kim, J., Santos, R., Wu, H.-H., Lander, A.D., and Calof, A.L. (2009). Foxg1 promotes olfactory neurogenesis by antagonizing Gdf11. Development *136*, 1453–1464.

Kersigo, J., D'Angelo, A., Gray, B.D., Soukup, G.A., and Fritzsch, B. (2011). The role of sensory organs and the forebrain for the development of the craniofacial shape as revealed by Foxg1-cre-mediated microRNA loss. Genesis *49*, 326–341.

Laclef, C., Souil, E., Demignon, J., and Maire, P. (2003). Thymus, kidney and craniofacial abnormalities in Six1 deficient mice. Mech. Dev. *120*, 669–679.

Li, C., Xu, X., Nelson, D.K., Williams, T., Kuehn, M.R., and Deng, C.-X. (2005). FGFR1 function at the earliest stages of mouse limb development plays an indispensable role in subsequent autopod morphogenesis. Development *132*, 4755–4764.

Li, C., Scott, D.A., Hatch, E., Tian, X., and Mansour, S.L. (2007). Dusp6 (Mkp3) is a negative feedback regulator of FGF-stimulated ERK signaling during mouse development. Development *134*, 167–176.

Lin, S., Svoboda, K.K.H., Feng, J.Q., and Jiang, X. (2016). The biological function of type I receptors of bone morphogenetic protein in bone. Bone Res. *4*, 16005.

Long, F., and Ornitz, D.M. (2013). Development of the endochondral skeleton. Cold Spring Harb. Perspect. Biol. *5*, a008334.

Madisen, L., Zwingman, T.A., Sunkin, S.M., Oh, S.W., Zariwala, H.A., Gu, H., Ng, L.L., Palmiter, R.D., Hawrylycz, M.J., Jones, A.R., et al. (2010). A robust and high-throughput Cre reporting and characterization system for the whole mouse brain. Nat. Neurosci. *13*, 133.

Maier, E.C., Saxena, A., Alsina, B., Bronner, M.E., and Whitfield, T.T. (2014). Sensational placodes: Neurogenesis in the otic and olfactory systems. Dev. Biol. *389*, 50–67.

Mani, P., Jarrell, A., Myers, J., and Atit, R. (2010). Visualizing canonical Wnt signaling during mouse craniofacial development. Dev. Dyn. *239*, 354–363.

Martineau-Doizé, B., Caya, I., and Martineau, G.P. (1992). Osteogenesis and growth of the nasal ventral conchae of the piglet. J. Comp. Pathol. *106*, 323–331.

Min, H., Danilenko, D.M., Scully, S.A., Bolon, B., Ring, B.D., Tarpley, J.E., DeRose, M., and Simonet, W.S. (1998). Fgf-10 is required for both limb and lung development and exhibits striking functional similarity to Drosophila branchless. Genes Dev. *12*, 3156–3161.

Murdoch, B., and Roskams, A.J. (2007). Olfactory epithelium progenitors: insights from transgenic mice and in vitro biology. J. Mol. Histol. *38*, 581–599.

Murdoch, B., and Roskams, A.J. (2008). A Novel Embryonic Nestin-Expressing Radial Glia-Like Progenitor Gives Rise to Zonally Restricted Olfactory and Vomeronasal Neurons. J. Neurosci. *28*, 4271–4282.

Murdoch, B., DelConte, C., and Garcia-Castro, M.I. (2010). Embryonic Pax7-Expressing Progenitors Contribute Multiple Cell Types to the Postnatal Olfactory Epithelium. J. Neurosci. *30*, 9523–9532.

Muzumdar, M.D., Tasic, B., Miyamichi, K., Li, L., and Luo, L. (2007). A global double-fluorescent Cre reporter mouse. Genesis *45*, 593–605.

Negus, V. (1959). Comparative Anatomy and Physiology of the Nose and Paranasal Sinuses. Proc. R. Soc. Med. *52*, 147–148.

Nusse, R., and Clevers, H. (2017). Wnt/β-Catenin Signaling, Disease, and Emerging Therapeutic Modalities. Cell *169*, 985–999.

Ornitz, D.M., and Itoh, N. (2015). The Fibroblast Growth Factor signaling pathway. Wiley Interdiscip. Rev. Dev. Biol. *4*, 215–266.

Packard, A., Schnittke, N., Romano, R.-A., Sinha, S., and Schwob, J.E. (2011). Np63 Regulates Stem Cell Dynamics in the Mammalian Olfactory Epithelium. J. Neurosci. *31*, 8748–8759.

Peretto, P., Cummings, D., Modena, C., Behrens, M., Venkatraman, G., Fasolo, A., and Margolis, F.L. (2002). BMP mRNA and protein expression in the developing mouse olfactory system. J. Comp. Neurol. *451*, 267–278.

Reid, B.S., Yang, H., Melvin, V.S., Taketo, M.M., and Williams, T. (2011). Ectodermal WNT/β-catenin signaling shapes the mouse face. Dev. Biol. *349*, 261–269.

Ressler, K.J., Sullivan, S.L., and Buck, L.B. (1993). A zonal organization of odorant receptor gene expression in the olfactory epithelium. Cell *73*, 597–609.

Schwob, J.E., Jang, W., Holbrook, E.H., Lin, B., Herrick, D.B., Peterson, J.N., and Coleman, J.H. (2017). The stem and progenitor cells of the mammalian olfactory epithelium: Taking poietic license. J. Comp. Neurol. *525*, 1034–1054.

Sekine, K., Ohuchi, H., Fujiwara, M., Yamasaki, M., Yoshizawa, T., Sato, T., Yagishita, N., Matsui, D., Koga, Y., Itoh, N., et al. (1999). Fgf10 is essential for limb and lung formation. Nat. Genet. *21*, 138–141.

Shou, J., Rim, P.C., and Calof, A.L. (1999). BMPs inhibit neurogenesis by a mechanism involving degradation of a transcription factor. Nat. Neurosci. *2*, 339–345.

Shou, J., Murray, R.C., Rim, P.C., and Calof, A.L. (2000). Opposing effects of bone morphogenetic proteins on neuron production and survival in the olfactory receptor neuron lineage. Development *127*, 5403–5413.

Smart, I.H. (1971). Location and orientation of mitotic figures in the developing mouse olfactory epithelium. J. Anat. *109*, 243–251.

Treloar, H.B., Miller, A.M., Ray, A., and Greer, C.A. (2010). Development of the Olfactory System. In The Neurobiology of Olfaction, A. Menini, ed. (Boca Raton (FL): CRC Press), p. Chapter 5.

Tucker, E.S., Lehtinen, M.K., Maynard, T., Zirlinger, M., Dulac, C., Rawson, N., Pevny, L., and LaMantia, A.-S. (2010). Proliferative and transcriptional identity of distinct classes of neural precursors in the mammalian olfactory epithelium. Development *137*, 2471–2481.

Valenta, T., Gay, M., Steiner, S., Draganova, K., Zemke, M., Hoffmans, R., Cinelli, P., Aguet, M., Sommer, L., and Basler, K. (2011). Probing transcription-specific outputs of β-catenin in vivo. Genes Dev. *25*, 2631–2643.

Van Valkenburgh, B., Smith, T.D., and Craven, B.A. (2014). Tour of a labyrinth: exploring the vertebrate nose. Anat. Rec. *297*, 1975–1984.

Vassar, R., Ngai, J., and Axel, R. (1993). Spatial segregation of odorant receptor expression in the mammalian olfactory epithelium. Cell *74*, 309–318.

Waghmare, S.K., Bansal, R., Lee, J., Zhang, Y.V., McDermitt, D.J., and Tumbar, T. (2008). Quantitative proliferation dynamics and random chromosome segregation of hair follicle stem cells. EMBO J. *27*, 1309–1320.

Wang, Y.-Z., Yamagami, T., Gan, Q., Wang, Y., Zhao, T., Hamad, S., Lott, P., Schnittke, N., Schwob, J.E., and Zhou, C.J. (2011). Canonical Wnt signaling promotes the proliferation and neurogenesis of peripheral olfactory stem cells during postnatal development and adult regeneration. J. Cell Sci. *124*, 1553–1563.

Weng, P.-L., Vinjamuri, M., and Ovitt, C.E. (2016). Ascl3 transcription factor marks a distinct progenitor lineage for non-neuronal support cells in the olfactory epithelium. Sci. Rep. *6*, 38199.

White, A.C., Xu, J., Yin, Y., Smith, C., Schmid, G., and Ornitz, D.M. (2006). FGF9 and SHH signaling coordinate lung growth and development through regulation of distinct mesenchymal domains. Development *133*, 1507–1517.

Wu, H.-H., Ivkovic, S., Murray, R.C., Jaramillo, S., Lyons, K.M., Johnson, J.E., and Calof, A.L. (2003). Autoregulation of neurogenesis by GDF11. Neuron *37*, 197–207.

Zhu, X.-J., Liu, Y., Yuan, X., Wang, M., Zhao, W., Yang, X., Zhang, X., Hsu, W., Qiu, M., Zhang, Z., et al. (2016). Ectodermal Wnt controls nasal pit morphogenesis through modulation of the BMP/FGF/JNK signaling axis. Dev. Dyn. *245*, 414–426.

FIGURE TITLES AND LEGENDS

Figure 1. *Fgf20* is expressed in a subset of Sox2^{+} cells in the developing OE

(A-G) *Fgf20* expression detected via an anti-GFP antibody in *Fgf20*$^{GFP\text{-}Cre/+}$ mice (green). The OE is identified via an anti-Sox2 antibody (red). Sox2 is expressed throughout the OE at E10.5 (A) and E12.5 (B), and mainly in the basal and apical layers at E14.5 (C), E17.5 (D-F), and P7 (G).

(A) Faint *Fgf20*$^{GFP\text{-}Cre}$ expression in the nasal pit at E10.5. Arrowheads indicate extent of the expression. Arrow indicates autofluorescence from red blood cells outside of the nasal pit.

(B) *Fgf20*$^{GFP\text{-}Cre}$ expression in the OE at E12.5. * indicates site of future c1 development. VNO, vomeronasal organ.

(C) *Fgf20*$^{GFP\text{-}Cre}$ expression in the OE at E14.5. White arrowheads indicate immature negatively-curved OE. Blue arrowheads indicate mature negatively-curved OE. Arrows indicate apical *Fgf20* expression in OE outside of regions of negative curvature. * indicates expression in OE overlying c1.

(D-F) *Fgf20*$^{GFP\text{-}Cre}$ expression in anterior (D), mid (E), and posterior (F) sections at E17.5. White arrowheads indicate immature negatively-curved OE. Blue arrowheads indicate mature negatively-curved OE.

(E') Magnification of the c1 neck region, boxed in (E). Arrowheads indicate fainter *Fgf20*$^{GFP\text{-}Cre}$ expression in Sox2^{+} basal and apical cells adjacent to negatively-curved OE (*). A, apical layer; B, basal layer indicated in the merged image.

(G) *Fgf20*$^{GFP\text{-}Cre}$ expression at P7. Arrowheads indicate apical *Fgf20*$^{GFP\text{-}Cre}$ expression at negatively-curved OE. Inset, 2.5x magnification of boxed region.

(H) Diagram of a mid-sagittal mouse nasal cavity showing locations of the three sections in (D-F). A, anterior; M, mid; P, posterior.

RE, respiratory epithelium. S, nasal septum. D, dorsal; M, medial. Dashed line, epithelial-mesenchymal boundary. DAPI, nuclei (blue). Scale bars, 100 μm (A-C, E'), 500 μm (D-G). See also Figure S1.

Figure 2. *Fgf20* lineage includes all major OE cell types and responds to cues for expansion

(A-C) mG expression in the *Fgf20*$^{GFP\text{-}Cre}$ lineage and mT expression (arrowheads) in non-*Fgf20*$^{GFP\text{-}Cre}$ lineage in anterior (A), mid (B), and posterior (C) frontal sections of *Fgf20*$^{GFP\text{-}Cre/+}$; *ROSA*^{mTmG} mice at P15. S, nasal septum. Dotted line, zone 1 and zones 2-4 demarcation.

(B') Magnification of boxed region in (B). mG expression in the basal cell (BC), olfactory receptor neuron (ORN), sustentacular cell (Sus), and cilia layers of the OE, as well as in axon bundles (Ax) and Bowman's glands (BG) found in the lamina propria.

(D-F) Real-time *Fgf20* expression (GFP-Cre) and *Fgf20*$^{GFP\text{-}Cre}$ lineage (tdTomato) in *Fgf20*$^{GFP\text{-}Cre/+}$; *ROSA*^{tdTomato} mice at E11.5 (D), E14.5 (E), and E17.5 (F). Dashed line, epithelial-mesenchymal boundary.

(G) Quantification of total *Fgf20*$^{GFP\text{-}Cre}$ lineage and non-*Fgf20*$^{GFP\text{-}Cre}$ lineage OE surface area at E11.5, E14.5, E17.5, P7, and P30. Error bars, mean ± SD; n = 3 at each stage; each bar represents one mouse

DAPI, nuclei. Scale bars, 500 μm (A-C, D-F), 100 μm (B'). See also Figure S2.

Figure 3. *Fgf20*-KO mice have reduced turbinate size and altered morphology

(A-D) H&E staining in anterior (A), mid-anterior (B), mid-posterior (C), and posterior (D) sections through the nasal cavity in control (*Fgf20*$^{GFP\text{-}Cre/+}$) and *Fgf20*-KO (*Fgf20*$^{GFP\text{-}Cre/\beta gal}$) mice at P30. S, nasal septum.

(B') Magnification of boxed region in (B). Dashed outline used to estimate relative turbinate size.

(E) Quantification of turbinate size for each turbinate at P30. * indicates $p < 0.05$. $p = 0.03$ (n1), $p < 0.001$ (c1), $p = 0.02$ (n2), $p = 0.02$ (c2), $p = 0.05$ (n3), $p < 0.001$ (n4), n = 4, Student's t-test.

(F) Quantification of OE surface area and septal organ (SO) surface area at P30. n = 4, Student's t-test

(G) EdU incorporation in c1 condensed and diffuse mesenchymal cells at E14.5. Dashed outline, c1 mesenchyme (M), including both condensed ($Sox9^{hi}$) and diffuse cells. N, nasal cavity wall.

(H) In situ hybridization at E14.5 showing c1 mesenchymal *Dusp6* expression in control (arrows) and reduced expression in *Fgf20*-KO embryos (arrow). Data is representative of 7 control and 7 *Fgf20*-KO embryos. N, nasal cavity wall.

(I-M) Quantification of c1 normalized condensed cell number (I), normalized diffuse cell number (J), ratio of condensed cells to diffuse cells (K), and percent of EdU-incorporating condensed cells (L) and EdU-incorporating diffuse cells (M) at E14.5. n = 7, Student's t-test.

DAPI, nuclei. Scale bars, 1 mm (A-D), 500 μm (B'), 100 μm (G, H). Error bars, mean ± SD. See also Figures S3 and S4.

Figure 4. Wnt activity in the developing OE coincides with *Fgf20* expression

(A-E) Tcf/Lef:H2b-Gfp expression at E10.5 (A), E12.5 (B), E14.5 (C), E17.5 (D), and P7 (E). Arrowhead indicates rim of the nasal pit (NP). Arrow indicates epithelium outside of the nasal pit. * indicates site of future c1 development. RE, respiratory epithelium.

(D') Magnification of boxed region in (D). Arrowheads indicate immature, negatively-curved OE.

(F,G) Tcf/Lef:H2b-Gfp and $Fgf20^{\beta gal}$ expression in Tcf/Lef:H2b-Gfp; $Fgf20^{\beta gal/+}$ mice at E17.5.

Dashed line, epithelial-mesenchymal boundary. DAPI, nuclei. Scale bar, 100 μm (A-C), 500 μm (D-G, D').

Figure 5. *βCat* conditional deletion results in a severe deficit in turbinate development

(A) H&E staining in control ($Fgf20^{GFP\text{-}Cre/+}$; $\beta Cat^{fl(ex2\text{-}6)/+}$) and βFF-CKO ($Fgf20^{GFP\text{-}Cre/+}$; $\beta Cat^{fl(ex2\text{-}6)/fl(ex2\text{-}6)}$) mice, with two phenotype examples (shapes 2 and 3) at P0. S, nasal septum.

(A') Magnification of boxed region in (A). N, nasal cavity wall; T, turbinate cartilage; M, mesenchyme. Inset, 2x magnification of the OE at the turbinate tip. Dashed line, epithelial-mesenchymal boundary.

(B-D) Quantification of c1 cartilage volume (B), OE surface area (C), and mesenchyme thickness (D) at P0. βFF-CKO phenotype categorized into three shapes (1, 2, and 3). n = 9 control, 14 βFF-CKO, Welch's t-test.

(E) EdU incorporation in c1 condensed and diffuse mesenchymal cells at E14.5, with two βFF-CKO phenotype examples. Dashed outline, c1 mesenchyme (M), including both condensed ($Sox9^{hi}$) and diffuse cells. N, nasal cavity wall.

(F-J) Quantification of c1 normalized condensed cell number (F), normalized diffuse cell number (G), ratio of condensed cells to diffuse cells (H), and percent of EdU-incorporating condensed cells (I) and EdU-incorporating diffuse cells (J) in control and βFF-CKO at E14.5. n = 8 control, 10 βFF-CKO, Welch's t-test.

DAPI, nuclei. Scale bars, 500 μm (A), 100 μm (A', E). Error bars, mean ± SD. See also Figure S5.

Figure 6. *βCat* conditional deletion leads to premature differentiation and progenitor depletion in the OE

(A) Sox2 expression in c1 of control ($Fgf20^{GFP\text{-}Cre/+}$; $\beta Cat^{fl(ex2\text{-}6)/+}$) and βFF-CKO ($Fgf20^{GFP\text{-}Cre/+}$; $\beta Cat^{fl(ex2\text{-}6)/fl(ex2\text{-}6)}$) mice at P0, with two phenotype examples (shapes 2 and 3). Arrows indicate presence of FEP cells in control and the less severe βFF-CKO phenotype. Arrowheads indicate absence of FEP cells in the severe βFF-CKO phenotype. BC, basal cells; Sus, sustentacular cells.

(B) Quantification of c1 OE thickness at P0. βFF-CKO phenotype categorized into three shapes (1, 2, and 3). n = 9 control, 14 βFF-CKO, Welch's t-test.

(C) OMP expression in c1 at P0.

(D) Quantification of c1 OMP^+ ORNs (n = 4 control, 5 βFF-CKO), Sus cells (n = 6 control, 8 βFF-CKO), and $Sox2^+$ BCs (n = 6 control, 8 βFF-CKO) per 100 μm OE at P0. βFF-CKO phenotype categorized into two shapes (2 and 3). Welch's t-test.
(E) EdU incorporation in c1 $Sox2^+$ cells at E14.5. * indicates "neck" region. M, mesenchyme.
(F-H) Quantification of c1 OE thickness (H), $Sox2^+$ BCs per 100 μm OE (F), and percent of EdU-incorporating $Sox2^+$ BCs (G) at E14.5. n = 8 control, 10 βFF-CKO, Welch's t-test.
(I) *Fgf20*$^{GFP\text{-}Cre}$ and OMP expression in c1 at E14.5, with two βFF-CKO phenotype examples. * indicates "neck" region. Arrowheads indicate *Fgf20* expression in n1 and n2 OE. M, mesenchyme.
(J) Quantification of c1 OMP^+ ORNs per 100 μm OE at E14.5. n = 3 control, 6 βFF-CKO, Welch's t-test.
Dashed line, epithelial-mesenchymal boundary. Solid line, OE apical surface. DAPI, nuclei. Scale bars, 100 μm. Error bars, mean ± SD. See also Figure S6.

Figure 7. βCat stabilization prevents differentiation of FEP cells and results in mesenchyme expansion without condensation in turbinates
(A) H&E staining in control (*Fgf20*$^{GFP\text{-}Cre/+}$; *βCat*$^{+/+}$) and βEX3-OA (*Fgf20*$^{GFP\text{-}Cre/+}$; *βCat*$^{fl(ex3)/+}$) mice at E17.5. * indicate extra blebs of OE and mesenchyme. S, nasal septum.
(A') Magnification of boxed region in (A). N, nasal cavity wall; T, turbinate cartilage; M, mesenchyme.
(B) *Fgf20*$^{GFP\text{-}Cre}$ and Sox2 expression in c1 at E17.5. Arrowheads indicate dense clumps of FEP cells. Solid line, OE apical surface.
(C) Sox9 and OMP expression in c1 at E17.5. Dashed line, epithelial-mesenchymal boundary. Solid line, OE apical surface. * indicates $Sox9^{low}$ mesenchyme. Arrows indicate OMP^+ ORNs in the mesenchyme. Arrowheads indicate OMP^+ ORNs in the n2 OE (see Figure S7D). N, nasal cavity wall; T, turbinate cartilage.
(D) EdU incorporation and Sox9 expression in c1 at E13.5. Dashed line, epithelial-mesenchymal boundary. Solid line, nasal cavity wall (N)-mesenchymal (M) boundary. Green fluorescence in the βEX3-OA OE is from *Fgf20*$^{GFP\text{-}Cre}$.
(E,F) Quantification of c1 mesenchyme thickness (E) and percent of EdU-incorporating mesenchymal cells
(F) at E13.5. n = 4, Student's t-test.
DAPI, nuclei. Scale bars, 500 μm (A), 100 μm (A', B-D). Error bars, mean ± SD. See also Figure S7.

STAR Methods

CONTACT FOR REAGENT AND RESOURCE SHARING

Further information and requests for resources and reagents should be directed to and will be fulfilled by the Lead Contact, David M. Ornitz (dornitz@wustl.edu). Mouse models will require an MTA issued by Washington University in St. Louis.

EXPERIMENTAL MODEL AND SUBJECT DETAILS

Mice

Mice were group housed with littermates, in breeding pairs, or in a breeding harem (2 females to 1 male), with food and water provided ad libitum.

For timed-pregnancy experiments, embryonic day 0.5 (E0.5) was assigned as noon of the day the vaginal plug was found. For postnatal experiments, postnatal day 0 (P0) was determined as the day of birth.

Mice were of mixed sexes and maintained on a mixed C57BL/6J x 129X1/SvJ genetic background. All mouse lines were previously reported:

- *Fgf20*$^{GFP\text{-}Cre}$: knockin allele containing a sequence encoding a GFP-Cre fusion protein replacing exon 1 of *Fgf20*, resulting in a null mutation (Huh et al., 2015).
- *Fgf20*$^{\beta gal}$: knockin allele containing a sequence encoding β-galactosidase (βgal) replacing exon 1 of *Fgf20*, resulting in a null mutation (Huh et al., 2012).
- *ROSA*^{mTmG}: knockin allele containing a sequence encoding a membrane-localized tdTomato (mT) flanked by loxP sequences, followed by a sequence encoding a membrane-localized eGFP (mG), targeted to the ubiquitously expressed *ROSA26* locus. In the absence of Cre-mediated recombination, mT is expressed; upon Cre-mediated recombination, mG is alternatively expressed (Muzumdar et al., 2007).
- *ROSA*^{tdTomato}: Ai9 knockin allele containing a loxP-Stop-loxP sequence followed by a sequence encoding tdTomato, targeted to the ubiquitously expressed *ROSA26* locus. Upon Cre-mediated recombination, tdTomato is expressed (Madisen et al., 2010).
- *ROSA*^{rtTA}: knockin allele containing a loxP-Stop-loxP sequence followed by a sequence encoding rtTA-IRES-eGFP, targeted to the ubiquitously expressed *ROSA26* locus. Upon Cre-mediated recombination, reverse tetracycline transactivator (rtTA) and eGFP are expressed (Belteki et al., 2005).
- TRE-Fgf9-IRES-eGfp: transgene containing seven tetracycline-inducible regulatory elements driving the expression of FGF9-IRES-eGFP (White et al., 2006).
- Tcf/Lef:H2b-Gfp: transgene containing a sequence encoding a histone 2B-eGFP (H2B-GFP) fusion protein, expressed under the control of six copies of a TCF/LEF responsive element (Ferrer-Vaquer et al., 2010). TCF/LEFs are transcription co-factors that bind β-Catenin to activate Wnt/β-Catenin regulated genes (Clevers and Nusse, 2012; Nusse and Clevers, 2017).
- *βCat*$^{fl(ex2\text{-}6)}$: allele containing loxP sequences flanking exons 2 (containing ATG) through 6 of *β-Catenin*. Upon Cre-mediated recombination, produces a null mutation (Brault et al., 2001).
- *βCat*^{DM}: allele containing a constitutive double mutation that partially blocks the signaling capacity of β-Catenin, while preserving its function in adherens junctions (Valenta et al., 2011).

- *βCat*$^{fl(ex3)}$: allele containing loxP sequences flanking exon 3 (containing all regulatory phosphorylation sites) of *β-Catenin*. Upon Cre-mediated recombination, produces a dominant stabilized β-Catenin to activate Wnt/β-Catenin signaling (Harada et al., 1999).

All studies performed were in accordance with the Institutional Animal Care and Use Committee at Washington University in St. Louis.

METHOD DETAILS

Doxycycline induction

For the Fgf9-OA experiment, pregnant dams were fed Dox Diet, Grain-Based Doxycycline, 200 mg/kg (Bio-Serv, S3888) ad libitum starting at noon on E11.5 until sample harvest at E14.5.

Sample preparation

Heads from mice younger than five days old were fixed in 4% PFA in PBS overnight at 4°C with gentle agitation. Samples were then washed x3 in PBS and cryoprotected in 15% sucrose in PBS overnight and then in 30% sucrose in PBS overnight. Samples were embedded in Tissue-Tek O.C.T. compound (VWR International, 4583) and frozen on dry ice. Serial frontal sections through the nasal cavity were cut at 12 μm with a cryostat, dried at room temperature, and stored at -80°C until use. Mice that were five days old or older were perfused with PBS and 4% PFA in PBS prior to post-fixation in 4% PFA in PBS overnight at 4°C with gentle agitation. After PBS wash, parts of the head posterior to the maxilla and frontal bone were cut and removed, along with the mandible, hard palate, and most of the remaining exposed soft tissue, except for the olfactory bulb. Front incisors and molars, if any, were removed with rongeurs. The remaining skulls with intact nasal cavity were then decalcified by incubation in 0.5 M EDTA, pH 8 at 4°C with gentle agitation for two days, or three days for mice two weeks old or older, with daily EDTA solution replacement. Cryoprotection, embedding, and sectioning were performed as above, except prior to embedding, samples were submerged in O.C.T. and placed in a vacuum chamber to remove air bubbles from inside the nasal cavity.

RNA in situ hybridization

Probe preparation: plasmid containing 413 bp of *Dusp6* 5'-UTR was a gift from Suzanne Mansour (Li et al., 2007). To make antisense probe, the plasmid was linearized with restriction enzyme Acc65I (New England Biolabs, R0599S) and transcribed with T7 RNA polymerase (New England Biolabs, M0251S) according to manufacturer's instructions, with DIG RNA Labeling Mix (Sigma-Aldrich, 11277073910). After treatment with RNase-free DNase I (Sigma-Aldrich, 04716728001) for 15 min at 37°C, probes were hydrolyzed in hydrolysis buffer (40 mM $NaHCO_3$, 60 mM Na_2CO_3) at 65°C for 30 min.

Frozen section in situ hybridization: frozen slides were warmed for 20 min at room temperature and then 5 min at 50°C on a slide warmer. Sections were fixed in 4% PFA in PBS for 20 min at room temperature, washed x2 in PBS and treated with pre-warmed 10 μg/ml Proteinase K (Sigma-Aldrich, 03115828001) in PBS for 7 min at 37°C. Sections were then fixed in 4% PFA in PBS for 15 min at room temperature, washed x2 in PBS, acetylated in 0.25% acetic anhydrate in 0.1M Triethanolamine, pH 8.0, for 10 min, and washed again in PBS. Sections were then placed in pre-warmed hybridization buffer (50% formamide, 5x SSC buffer, 5 mM EDTA, 50 μg/ml yeast tRNA) for 3 h at 60°C in humidified chamber for prehybridization. Sections were then hybridized in 10 μg/ml probe/hybridization buffer overnight (12-16 h) at 60°C. The next day, sections were washed in 1x SSC for 10 min at 60°C, followed by 1.5x SSC for 10 min at 60°C, 2x SSC for 20 min at 37°C x2, and 0.2x SSC for 30 min at 60°C x2. Sections were then washed in KTBT (0.1 M Tris, pH 7.5, 0.15 M NaCl, 5 mM KCl, 0.1% Triton

X-100) at room temperature and blocked in KTBT + 20% sheep serum + 2% Blocking Reagent (Sigma-Aldrich, 11096176001) for 4 h. Blocking Reagent was dissolved in 100 mM Maleic acid, 150 mM NaCl, pH 7.5. Sections were then incubated in sheep anti-Digoxigenin-AP, Fab fragments (1:1000, Sigma-Aldrich, 11093274910) in KTBT + 20% sheep serum + 2% Blocking Reagent overnight at 4°C. Sections were then washed x3 in KTBT for 30 min at room temperature, and then washed x2 in NTMT (0.1 M Tris, pH 9.5, 0.1 M NaCl, 50 mM $MgCl_2$, 0.1% Tween 20) for 15 min. Sections were next incubated in NTMT + 1:200 NBT/BCIP Stock Solution (Sigma-Aldrich, 11681451001) in the dark at room temperature until color appeared. Sections were then washed in PBS, post-fixed in 4% PFA in PBS for 15 min and washed x2 in PBS. Finally, sections were dehydrated in 30% and then 70% methanol, 5 min each, followed by 100% methanol for 15 min. Sections were then rehydrated in 70% and 30% methanol and then PBS, 5 min each, and mounted in 95% glycerol.

Histology and Immunofluorescence

H&E staining was done by the Washington University Developmental Biology Histology Core. Immunofluorescence: frozen slides were warmed for 30 min at room temperature and washed in PBS before incubating in PBS + 0.5% Triton X-100 (PBST) for 1 h to permeabilize the tissue. Sections were then blocked using in PBST + 5% donkey serum for 1 h and then incubated in PBST + 1% donkey serum with the primary antibody overnight at 4°C in a humidified chamber. Sections were then washed x3 in PBS and incubated in PBS + 1% Triton X-100 with the secondary antibody. After wash in PBS x3, slides were mounted in VectaShield antifade mounting medium with DAPI (Vector Labs, H-1200).

Antibodies

Antibodies for immunofluorescence were used at the following concentrations:

- Rabbit anti-GFP (1:500; Life Technologies, A-11122)
- Chick anti-Beta galactosidase (1:500; Abcam, ab9361)
- Goat anti-Sox2 (1:200; Santa Cruz, sc-17320)
- Rabbit anti-Sox9 (1:500; Millipore, AB5535)
- Goat anti-OMP (1:1000; Wako Chemicals, 544-10001)
- Goat anti-Pde2a (1:100; Santa Cruz, sc-17227)
- Alexa Fluor conjugated secondary antibodies (1:500; Thermo Fisher)
- Sheep anti-Digoxigenin-AP, Fab fragments (1:1000, Sigma-Aldrich, 11093274910)

Cell proliferation assay

EdU (Thermo Fisher, E10187) was injected i.p. into pregnant dams at 100 µg per gram body weight. Except where noted, embryos were harvested at 1 h after injection. For 4 h EdU incorporation, 100 µg per gram body weight of EdU was injected at 4 h and 2 h before embryos were harvested. EdU was detected using the Click-iT Plus EdU Alexa Fluor 594 or 647 picolyl azide toolkit (Thermo Fisher, C10639, C10640) according to manufacturer's instructions.

Imaging

Brightfield microscopy was done using a Hamamatsu NanoZoomer slide scanning system with a 20x objective or on a Zeiss AxioPlan 2 with a 10x or 20x objective. Images were processed with the NanoZoomer Digital Pathology (NDP.view2) software or ImageJ (imagej.nih.gov).

Fluorescent microscopy was done using a Zeiss Axio Imager Z1 with Apotome 2, with z-stack step-size determined based on objective lens type (10x or 20x), as recommended by the ZEN software (around 1

μm). Fluorescent images shown are maximum projections. Most fluorescent images shown required stitching together, by hand, several images to capture the entire structure of interest. Some fluorescence microscopy was also done using a Zeiss Axio Imager Z2 with Apotome 2. In all cases, except where noted, *Fgf20*$^{GFP\text{-}Cre}$ expression was detected with an anti-GFP antibody. In all cases, mGFP, mTomato, tdTomato, and H2B-GFP expressions were detected by native fluorescence. Images were processed with ImageJ.

QUANTIFICATION AND STATISTICAL ANALYSIS

Measurements and cell quantification

Measurements and cell quantification (using the Cell Counter plugin by Kurt De Vos) were done using ImageJ.

For OE surface area measurements, length along the apical surface of the OE was measured in serial frontal sections starting just anterior to endoturbinate I and ending at the end of the nasal cavity. The measured length was then multiplied by the distance between sections to calculate surface area. OE was differentiated from respiratory epithelia based on histology (OE is pseudostratified); where ambiguous, epithelia <30 μm thick were not considered OE.

Fgf20$^{GFP\text{-}Cre}$ *lineage quantification*
OE surface area was measured as above, with the following specifics:

- E11.5: measurements were done on eleven to 14 sections per sample, starting anteriorly when the VNO was reached.
- E14.5: nine sections per sample, starting mid VNO, when n1 and n2 were reached.
- E17.5: eleven sections per sample, starting posterior to the VNO, when n2 was reached.
- P7: 14 sections per sample, starting posterior to the VNO, when n2 was reached.
- P30, nine to ten sections per sample, starting posterior to the VNO, when n2 was reached.

Linear Fgf20^{+} *and OMP*$^{+}$ *cell distribution plot*
OE of turbinate c1 was linearized in ImageJ at the level of OMP^{+} ORNs. The location of each *Fgf20*$^{+}$ and OMP^{+} cell was marked along this line. Plots from multiple samples were scaled to their average length and combined to represent an average/combined distribution across multiple samples. Plots were made in Canvas X (ACD Systems)

Phenotype analyses at P30

- Individual turbinate size: length was measured at the apical OE surface of each turbinate from two comparable sections at the anteroposterior middle of each turbinate, and then summed to estimate relative turbinate size. Outlines in Figure 3B' indicate measurements used to estimate turbinate size.
- Total surface area: OE surface area was measured as above, using 26-29 frontal sections, starting immediately posterior to the VNO for the OE, and 3-6 frontal sections spanning the entire septal organ anteroposteriorly, for the septal organ.

For the rest of this study (methods below), we focused on turbinate c1.

Phenotype analyses at E13.5 and E14.5

- OE thickness: average of three measurements made on one frontal section halfway through the turbinate. Measurements were at the turbinate tip/center and 50 μm on either side. Each measurement was the shortest distance from the epithelial-mesenchymal boundary to the apical surface of the OE.

- Mesenchyme thickness: as with OE thickness, average of three measurements at the turbinate tip/center and 50 μm on either side. Each measurement was the shortest distance from the epithelial-mesenchymal boundary to the nasal cavity wall.

Cell counts were made on comparable frontal sections halfway through the turbinate.

- Condensed mesenchymal cells were identified by high Sox9 staining, small soma, and dense packing of cells. A few cells outside of the condensations at E14.5 (closer to the epithelium) had high Sox9 expression, but were counted as diffuse mesenchymal cells. Condensed and diffuse cell numbers were normalized to the number of $Sox9^+$ chondrocytes in the adjacent nasal cavity wall to adjust for potential slight differences in angle of sectioning.
- Quantification of "OE adjacent cell" proliferation in the Fgf9-OA experiment: average c1 diffuse mesenchyme thickness in control embryos was measured to be 69 μm. In Fgf9-OA embryos, the c1 OE was outlined at the basal side; this outline was then moved 69 μm away from the basal side of the OE. Cells between this line and the OE were considered "OE adjacent cells." The average normalized number of "OE adjacent cells" quantified was 1.2 ± 0.1 in Fgf9-OA embryos, the same as the normalized number of diffuse cells in control (1.2 ± 0.2).
- BC number was normalized to OE basal surface length. OMP^+ cell number was normalized to OE apical surface length. *Fgf20*$^+$ cell counts were normalized to OE area on a section.

Phenotype analyses at E17.5 and P0

- Turbinate cartilage size: a curved line was drawn to the contour of the lateral nasal cavity wall dorsal and ventral to c1; the cartilage projection medial to this line was considered the turbinate. Cartilaginous area of c1 was measured in 5 to 7 serial frontal sections spanning the entire turbinate anteroposteriorly. The measured area was then multiplied by the distance between sections to calculate volume.
- Turbinate OE surface area: length of the turbinate was measured along the epithelial-mesenchymal boundary in 5 to 7 serial frontal sections and multiplied by the distance between sections. Inflection points in the OE curvature at "neck" regions were used to differentiate between turbinate OE (OE overlying the turbinate) and OE overlying the nasal cavity wall. For reference, see dashed line in Figures S3H, 6C, and S6C. In cases where the turbinate was completely absent (βFF-CKO, shape 3), what was considered turbinate OE was estimated based on the height (dorsoventral length) of the turbinate in less severe βFF-CKO littermates (see Figure 6C, dashed line). Note the "neck" OE regions of c1 are further apart in βFF-CKO mice (turbinate "neck" cartilage is thicker); this was taken into consideration in the estimate.
- Mesenchyme thickness: three measurements at the turbinate tip/center and 100 μm on either side, on 3 sections 96 μm apart for a total of 9 measurements (which were then averaged). Each measurement was the shortest distance from the epithelial-mesenchymal boundary to the turbinate cartilage.
- OE thickness: same as mesenchyme thickness. Each measurement was the shortest distance from the epithelial-mesenchymal boundary to the apical surface of the OE.
- $Sox2^+$ and OMP^+ cell count: on comparable sections at the anteroposterior middle of the turbinate. BC number was normalized to OE basal surface length. Sus cell and ORN numbers were normalized to OE apical surface length.
- Mesenchyme EdU-incorporating cell count: "neck" region mesenchyme was defined as mesenchyme adjacent to FEP cell area, both dorsal and ventral to c1, combined. "Tip" region was a similarly sized area at the tip of c1.
- Chondrocyte EdU-incorporating cell count: all chondrocytes of c1 ("neck" and "tip") on a frontal section halfway through the turbinate were counted.

In situ hybridization analyses

In situ hybridization for *Dusp6* was evaluated, blinded to genotype, by alkaline phosphatase color reaction intensity in the c1 mesenchyme. 2-3 serial sections per sample from *Fgf20*-KO (n = 7 control, 7 *Fgf20*-KO), Fgf9-OA (n = 4 control, 4 Fgf9-OA), and βFF-CKO (n = 4 control, 6 βFF-CKO) E14.5 embryos were examined. For *Fgf20*-KO samples, the genotypes of 13 out of 14 total samples were scored correctly based on *Dusp6* expression intensity (one control sample was wrongly scored as *Fgf20*-KO). Figures 3H, S4G, and S5C show representative images of each genotype.

Statistics and plotting

All figures were made in Canvas X. Data analysis was performed using the Python programming language (python.org) in Jupyter Notebook (jupyter.org) with the following libraries: Pandas (pandas.pydata.org), NumPy (numpy.org) and SciPy (scipy.org). Plotting was done using the Matplotlib library (matplotlib.org). Statistics (t-test and one-way ANOVA) were performed using the SciPy module Stats; Tukey's HSD was performed using the Statsmodels package (statsmodels.org).

Data from βFF-CKO mice were plotted in different colors to visualize differences in phenotype severity (shapes 1, 2, and 3). However, data from all shapes were combined for statistical analysis. Comparisons of two means in βFF-CKO experiments were performed using two-tailed, unpaired Welch's (unequal variance) t-test, since βFF-CKO mice exhibited variability in phenotype while controls did not. All other comparisons of two means were performed using two-tailed, unpaired Student's t-test. For comparisons of more than two means, one-way ANOVA was used; for significant results at $\alpha = 0.05$, Tukey's HSD was performed for post-hoc pair-wise analysis.

All statistical details can be found in the figures and figure legends. In all cases, sample size (n) represents the number of animals. Data are represented as mean ± standard deviation (SD).

SUPPLEMENTAL INFORMATION TITLES AND LEGENDS

Figure S1. Related to Figure 1.

(A-G) H&E staining in frontal sections through the nasal cavity.
(A) Nasal pit (NP) at E10.5.
(B) Turbinates n1 and n2 at E12.5. n3 appears at this stage and can be found in more posterior sections (data not shown). * indicates site of future c1 development. VNO, vomeronasal organ.
(C) Turbinates n1, c1, and n2 at E14.5. n1 and n2 are connected at this section. c2, n3, and n4 appear at this stage and can be found in more posterior sections (data not shown).
(C') Magnification of the boxed region in (C). c1 appears as a mesenchymal condensation (M) between the OE and the nasal cavity wall (N).
(D-F) All six turbinates in anterior (D), mid (E), and posterior (F) sections at E17.5.
(E') Magnification of the boxed region in (E). Condensed mesenchymal cells have differentiated into chondrocytes. N, nasal cavity wall; T, turbinate cartilage; M, mesenchyme.
(G) All six turbinates at P7.
(G') Magnification of the boxed region in (G). Cartilage have been mostly replaced by eosinophilic ossified bone. * indicates remaining hypertrophic chondrocytes. N, nasal cavity wall; T, ossified turbinate; M, mesenchyme.
(H) Diagram of a frontal section through the nasal cavity at perinatal stages, showing three layers of tissue: OE, mesenchyme (mes), and cartilage. Inset: zoom showing "neck" and "tip" regions of c1.
(I) H&E staining in anterior (1), mid-anterior (2), mid-posterior (3), and posterior (4) frontal sections through the mouse nasal cavity at P30. Individual turbinates (n1, c1, n2, c2, n3, n4) are outlined. OB, olfactory bulb.
(I') Diagram of a mid-sagittal adult mouse nasal cavity showing locations of the four sections in (I).
S, nasal septum. D, dorsal; M, medial. Scale bars, 100 μm (A-C, C', E', G'), 500 μm (D-G), 1 mm (H).

Figure S2. Related to Figure 2.

(A) *Fgf20*$^{GFP\text{-}Cre}$ expression and EdU incorporation in *Fgf20*$^{GFP\text{-}Cre/+}$ c1 OE at E17.5. OE overlying the "neck" and "tip" regions of the developing turbinate are outlined.
(B) Quantification of proliferating cells in c1 OE overlying "neck" and "tip" regions per 1000 μm^2 of OE.
(C,D) *Fgf20*$^{GFP\text{-}Cre}$ and OMP expression in anterior (C) and posterior (D) sections at E17.5. RE, respiratory epithelium. Arrowheads indicate negatively-curved "neck" OE.
(E) Linear plot of OMP$^+$ ORN and *Fgf20*$^+$ cell distribution along c1 OE (dashed outline in (C)) at E17.5. Length: 1.27 mm.
(F) Pde2a expression in c1 dorsal "neck" or cul-de-sac region at P30.
(G) *Fgf20*$^{GFP\text{-}Cre}$ and (lack of) Pde2a expression in c1 dorsal "neck" region at E17.5.
(H) *Fgf20*$^{GFP\text{-}Cre}$; *ROSA*^{mTmG} lineage (mG) in the vomeronasal organ (VNO, outlined).
(I) *Fgf20*$^{GFP\text{-}Cre}$; *ROSA*^{mTmG} lineage (mG) in the septal organ (SO, outlined).
Dashed line, epithelial-mesenchymal boundary. DAPI, nuclei. Scale bars, 500 μm (C, H), 100 μm (A, F, G). Error bars, mean ± SD.

Figure S3. Related to Figure 3

(A,B) H&E staining in anterior (A) and posterior (B) sections through the nasal cavity in control (*Fgf20*$^{GFP\text{-}Cre/+}$) and *Fgf20*-KO (*Fgf20*$^{GFP\text{-}Cre/\beta gal}$) mice at P0. S, nasal septum.
(A') Magnification of boxed region in (A). N, nasal cavity wall; T, turbinate cartilage; M, mesenchyme.
(C-F) Quantification of c1 cartilage volume (C), OE surface area (D), mesenchyme thickness (E), and OE thickness (F) at P0. n = 7 control, 8 *Fgf20*-KO, Student's t-test.
(G) *Fgf20*$^{GFP\text{-}Cre}$ and Sox2 expression in c1 at P0. BC, basal cells; Sus, sustentacular cells.

(H) OMP expression in c1 at P0.
(I) Quantification of c1 OMP^+ ORNs, Sus cells, and $Sox2^+$ BCs per 100 μm OE at P0. n = 4, Student's t-test.
(J) EdU incorporation in c1 OE $Sox2^+$ cells at E14.5. M, mesenchyme.
(K-M) Quantification of c1 OE thickness (K), $Sox2^+$ BCs per 100 μm (L), and percent of EdU-incorporating $Sox2^+$ BCs (M) at E14.5. n = 7, Student's t-test.

Dashed line, epithelial-mesenchymal boundary. DAPI, nuclei. Scale bars, 500 μm (A), 100 μm (A', G, H, J). Error bars, mean ± SD.

Figure S4. Related to Figure 3
(A-E) EdU incorporation in control (*Fgf20*$^{GFP\text{-}Cre/+}$) and *Fgf20*-KO (*Fgf20*$^{GFP\text{-}Cre/\beta gal}$) mice at E17.5.
(A) *Fgf20*$^{GFP\text{-}Cre}$ expression and 1 h EdU incorporation in c1 at E17.5. N, nasal cavity wall; T, turbinate cartilage; M, mesenchyme.
(A') Magnification of boxed region in (A). M, mesenchyme. Dashed line, epithelial-mesenchymal boundary. Solid line, cartilage-mesenchyme boundary.
(B-E) Quantification of 1 h (n = 6) and 4 h (n = 3 control, 4 *Fgf20*-KO) EdU incorporation in c1 "neck" region mesenchymal cells (B), "tip" region mesenchymal cells (C), "neck" and "tip" chondrocytes (D), and FEP cells (E) at E17.5. Student's t-test.
(F-L) EdU incorporation and *Dusp6* in situ hybridization in control (*Fgf20*$^{GFP\text{-}Cre/+}$; *ROSA*^{rtTA}) and Fgf9-OA (*Fgf20*$^{GFP\text{-}Cre/+}$; *ROSA*^{rtTA}; TRE-Fgf9-IRES-eGfp) mice at E14.5.
(F) EdU incorporation in c1 condensed and diffuse mesenchymal cells at E14.5. Dashed outline, c1 mesenchyme (M), including both condensed ($Sox9^{hi}$) and diffuse cells. N, nasal cavity wall. Brackets, "OE adjacent cells" within 69 μm below OE.
(G) In situ hybridization at E14.5 showing c1 mesenchymal *Dusp6* expression in control and increased expression in Fgf9-OA embryos (arrows). Data is representative of 4 control and 4 Fgf9-OA embryos. N, nasal cavity wall.
(H-L) Quantification of c1 normalized condensed cell number (H), normalized diffuse cell number (I), ratio of condensed cells to diffuse cells (J), and percent of EdU-incorporating condensed cells (K) and EdU-incorporating diffuse cells (L) at E14.5. n = 4 control and 6 Fgf9-OA, Student's t-test.
DAPI, nuclei. Scale bars, 100 μm. Error bars, mean ± SD.

Figure S5. Related to Figure 5
(A) *Fgf20*$^{GFP\text{-}Cre}$ and Sox2 expression in control (*Fgf20*$^{GFP\text{-}Cre/+}$; *βCat*$^{fl(ex2\text{-}6)/+}$), βFF-CKO (*Fgf20*$^{GFP\text{-}Cre/+}$; *βCat*$^{fl(ex2\text{-}6)/fl(ex2\text{-}6)}$), and βDF-CKO (*Fgf20*$^{GFP\text{-}Cre/+}$; *βCat*$^{DM/fl(ex2\text{-}6)}$) mice at P0, with two βFF-CKO phenotype examples (shapes 2 and 3). S, nasal septum. Inset, 2x magnification of the boxed region; arrows indicate presence of FEP cells (*Fgf20* and Sox2 double-positive in control; Sox2 single-positive in βFF-CKO, shape 2).
(B) Left: H&E staining in control, βFF-CKO, and βDF-CKO mice at P30. S, nasal septum. Right: 10x magnification of boxed regions showing OMP expression on an adjacent frontal section from the same sample. Region a, magnification of c1 "tip" OE; region b, magnification of c1 "neck" OE. Arrowhead indicates area with extremely thin or absent OE, as indicated by lack of OMP expression. Ax, axon bundles. Dashed line, epithelial-mesenchymal boundary.
(C) In situ hybridization at E14.5 showing c1 mesenchymal *Dusp6* expression in control and loss of in βFF-CKO embryos (arrows). Data is representative of 4 control and 6 βFF-CKO embryos. N, nasal cavity wall.
(D) H&E staining in control (*Fgf20*$^{GFP\text{-}Cre/+}$; *βCat*$^{fl(ex2\text{-}6)/+}$) and βDF-CKO (*Fgf20*$^{GFP\text{-}Cre/+}$; *βCat*$^{DM/fl(ex2\text{-}6)}$) mice at P0. S, nasal septum.

(D') Magnification of boxed region in (D). N, nasal cavity wall; T, turbinate cartilage; M, mesenchyme. Inset, 2x magnification of the OE at the turbinate tip. Dashed line, epithelial-mesenchymal boundary.

(E-G) Quantification of c1 cartilage volume (E, $p < 0.001$, one-way ANOVA), surface area (F, $p < 0.001$, one-way ANOVA), and mesenchyme thickness (G, $p = 0.04$, one-way ANOVA) of *Fgf20*$^{GFP\text{-}Cre/+}$; *βCat*$^{+/+}$ (n = 7), *Fgf20*$^{GFP\text{-}Cre/+}$; *βCat*$^{DM/+}$ (n = 5), *Fgf20*$^{GFP\text{-}Cre/+}$; *βCat*$^{fl(ex2\text{-}6)/+}$ (n = 5), and *Fgf20*$^{GFP\text{-}Cre/+}$; *βCat*$^{DM/fl(ex2\text{-}6)}$ (n = 7) mice at P0. * indicates statistically significant at $\alpha = 0.05$ by Tukey's HSD.

DAPI, nuclei. Scale bars, 1 mm (B), 500 μm (A, D), 100 μm (C, D'). Error bars, mean ± SD.

Figure S6. Related to Figure 6

(A) Sox2 expression in c1 of control (*Fgf20*$^{GFP\text{-}Cre/+}$; *βCat*$^{fl(ex2\text{-}6)/+}$) and βDF-CKO (*Fgf20*$^{GFP\text{-}Cre/+}$; *βCat*$^{DM/fl(ex2\text{-}6)}$) mice at P0. Arrows indicate presence of FEP cells in control mice. Arrowheads indicate absence of FEP cells in βDF-CKO mice. BC, basal cells; Sus, sustentacular cells.

(B) Quantification of c1 OE thickness in *Fgf20*$^{GFP\text{-}Cre/+}$; *βCat*$^{+/+}$ (n = 7), *Fgf20*$^{GFP\text{-}Cre/+}$; *βCat*$^{DM/+}$ (n = 5), *Fgf20*$^{GFP\text{-}Cre/+}$; *βCat*$^{fl(ex2\text{-}6)/+}$ (n = 5), and *Fgf20*$^{GFP\text{-}Cre/+}$; *βCat*$^{DM/fl(ex2\text{-}6)}$ (n = 7) mice at P0. $p < 0.001$, one-way ANOVA. * indicates statistically significant at $\alpha = 0.05$ by Tukey's HSD.

(C) OMP expression in c1 at P0.

(D) Quantification of c1 OMP$^+$ ORNs (n = 4), Sus cells (n = 4 control, 5 βDF-CKO), and Sox2$^+$ BCs (n = 4 control, 5 βDF-CKO) per 100 μm OE at P0. Student's t-test.

(E) EdU incorporation in c1 OE Sox2$^+$ cells at E17.5. Arrow indicates presence of FEP cells. T, turbinate cartilage; M, mesenchyme.

(F-H) Quantification of c1 OE thickness (F), Sox2$^+$ BCs per 100 μm OE (G), and percent of EdU-incorporating Sox2$^+$ BCs (H) at E17.5. n = 3, Student's t-test.

(I) *Fgf20*$^{GFP\text{-}Cre}$ and OMP expression in c1 at E17.5, with linear plot of OMP$^+$ ORN and *Fgf20*$^+$ cell distribution along the c1 OE (dashed outline). Distribution plot length: 1.27 mm, control; 0.787 mm, βDF-CKO (average of n = 3). Arrows indicate *Fgf20* expression. Arrowheads indicate c1 "neck" region OE. N, "neck"; T "tip".

Dashed line, epithelial-mesenchymal boundary. DAPI, nuclei. Scale bars, 100 μm. Error bars, mean ± SD.

Figure S7. Related to Figure 7

(A) *Fgf20*$^{GFP\text{-}Cre}$ expression without anti-GFP antibody staining in c1 in control (*Fgf20*$^{GFP\text{-}Cre/+}$; *βCat*$^{+/+}$) and βEX3-OA (*Fgf20*$^{GFP\text{-}Cre/+}$; *βCat*$^{fl(ex3)/+}$) mice at E17.5. N, nasal cavity wall; T, turbinate cartilage; M, mesenchyme. Arrowheads indicate faint *Fgf20*$^{GFP\text{-}Cre}$ expression in control. Arrows indicate duct structures in the mesenchyme. Inset, 3x magnification of boxed region. Note: in all other figures except S7A, GFP-Cre expression was detected with an anti-GFP antibody (including S7B, S7C, and S7E).

(B) *Fgf20*$^{GFP\text{-}Cre}$ expression and EdU incorporation in c1 at E17.5. Dashed outline, epithelial-mesenchymal boundary in control, FEP cell clumps in βEX3-OA. Solid line, cartilage-mesenchyme boundary. N, nasal cavity wall; T, turbinate cartilage; M, mesenchyme.

(C) *Fgf20*$^{GFP\text{-}Cre}$ and Sox2 expression in dorsomedial n2 at E17.5. BC, basal cells; Sus, sustentacular cells.

(D) Sox9 and OMP expression in dorsomedial n2 at E17.5. Note: high Sox9 expression was also found in Bowman's gland and duct cells, which can be seen in the mesenchymal layer and OE, respectively (Packard et al., 2011).

(E) *Fgf20*$^{GFP\text{-}Cre}$ expression and EdU incorporation in c1 at E13.5. M, mesenchyme. Arrowheads indicate a dense clump of FEP cells.

(F-H) Quantification of c1 OE thickness (F), *Fgf20*$^+$ cells per 100 μm^2 of OE (G), and percent of EdU-incorporating *Fgf20*$^+$ cells (H) at E13.5. n = 4, Student's t-test.

DAPI, nuclei. Dashed line, epithelial-mesenchymal boundary. Scale bars, 100 μm. Error bars, mean ± SD.

KEY RESOURCES TABLE

REAGENT or RESOURCE	SOURCE	IDENTIFIER
Antibodies		
Rabbit anti-GFP	Thermo Fisher	Cat# A-11122; RRID:AB_221569
Chick anti-Beta galactosidase	Abcam	Cat# ab9361; RRID:AB_307210
Goat anti-Sox2	Santa Cruz Biotech	Cat# sc-17320; RRID:AB_2286684
Rabbit anti-Sox9	Millipore	Cat# AB5535; RRID:AB_2239761
Goat anti-OMP	Wako Chemicals	Cat# 544-10001; RRID:AB_664696
Goat anti-Pde2a	Santa Cruz Biotech	Cat# sc-17227; RRID:AB_653928
Donkey anti-Rabbit IgG (H+L), Alexa Fluor 488	Thermo Fisher	Cat# A-21206; RRID:AB_2535792
Donkey anti-Goat IgG (H+L); Alexa Fluor 555	Thermo Fisher	Cat# A-21432; RRID:AB_2535853
Goat anti-Rabbit IgG (H+L); Alexa Fluor 555	Thermo Fisher	Cat# A-21428; RRID:AB_2535849
Goat anti-Chicken IgY (H+L); Alexa Fluor 555	Thermo Fisher	Cat# A-21437; RRID:AB_2535858
Sheep anti-Digoxigenin-AP, Fab fragments	Sigma-Aldrich	Cat# 11093274910; RRID:AB_514497
Chemicals, Peptides, and Recombinant Proteins		
Dox Diet, Grain-Based Doxycycline, 200 mg/kg	Bio-Serv	Cat# S3888
Critical Commercial Assays		
VectaShield antifade mounting medium with DAPI	Vector Labs	Cat# H-1200
Click-iT Plus EdU Alexa Fluor 594 picolyl azide toolkit	Thermo Fisher	Cat# C10639
Click-iT Plus EdU Alexa Fluor 647 picolyl azide toolkit	Thermo Fisher	Cat# C10640
Experimental Models: Organisms/Strains		
Mouse: *Fgf20*$^{GFP\text{-}Cre}$: B6.129-*Fgf20*$^{tm2.1(cre/EGFP)Dor}$/J	Huh et al., 2015	MGI:5751785
Mouse: *Fgf20*$^{\beta gal}$: B6.129-*Fgf20*$^{tm1.1Dor}$/J	Huh et al., 2012	RRID:MGI:5425887
Mouse: *ROSA*^{mTmG}: B6.129-*Gt(ROSA)26Sor*$^{tm4(ACTB\text{-}tdTomato,\text{-}EGFP)Luo}$/J	Muzumdar et al., 2007	RRID:IMSR_JAX:007576
Mouse: *ROSA*^{tdTomato}: B6.129-*Gt(ROSA)26Sor*$^{tm9(CAG\text{-}tdTomato)Hze}$/J	Madisen et al., 2010	RRID:IMSR_JAX:007905
Mouse: *ROSA*^{rtTA}: B6.129-*Gt(ROSA)26Sor*$^{tm1(rtTA,EGFP)Nagy}$/J	Belteki et al., 2005	RRID:IMSR_JAX:005670
Mouse: TRE-Fgf9-IRES-eGfp: B6.129-Tg(tetO-Fgf9,-EGFP)#Dor/J	White et al., 2006	MGI:5538516
Mouse: Tcf/Lef:H2b-Gfp: B6.129-Tg(TCF/Lef1-HIST1H2BB/EGFP)61Hadj/J	Ferrer-Vaquer et al., 2010	RRID:IMSR_JAX:013752
Mouse: *βCat*$^{fl(ex2\text{-}6)}$: B6.129-*Ctnnb1*^{tm2Kem}/J	Brault et al., 2001	RRID:IMSR_JAX:004152
Mouse: *βCat*^{DM}: B6.129-*Ctnnb1*^{tm3Kba}/J	Valenta et al., 2011	MGI:5308947
Mouse: *βCat*$^{fl(ex3)}$: B6.129-*Ctnnb1*^{tm1Mmt}/J	Harada et al., 1999	MGI:1858008
Recombinant DNA		
Plasmid: pBSKS-Dusp6	Gift of Dr. Suzanne Mansour (Li et al., 2007)	N/A

Software and Algorithms		
ZEN	Zeiss	https://www.zeiss.com/microscopy/us/downloads/zen.html
NanoZoomer Digital Pathology (NDP.view2)	Hamamatsu	https://www.hamamatsu.com/jp/en/U12388-01.html
Canvas X	ACD Systems	http://www.canvasgfx.com/
ImageJ	National Institutes of Health	https://imagej.nih.gov/ij/
Cell Counter plugin for ImageJ	Kurt De Vos	https://imagej.nih.gov/ij/plugins/cell-counter.html
Python	Guido van Rossum and Python developers	https://www.python.org/
Pandas	Pandas core team	https://pandas.pydata.org/
NumPy	NumPy developers	http://www.numpy.org/
SciPy	SciPy developers	https://www.scipy.org/
Matplotlib	John Hunter and contributors	https://matplotlib.org/
Statsmodels	Josef Perktold, Skipper Seabold, Jonathan Taylor, and statsmodels developers.	https://www.statsmodels.org/stable/index.html

Yang et al., Figure 1

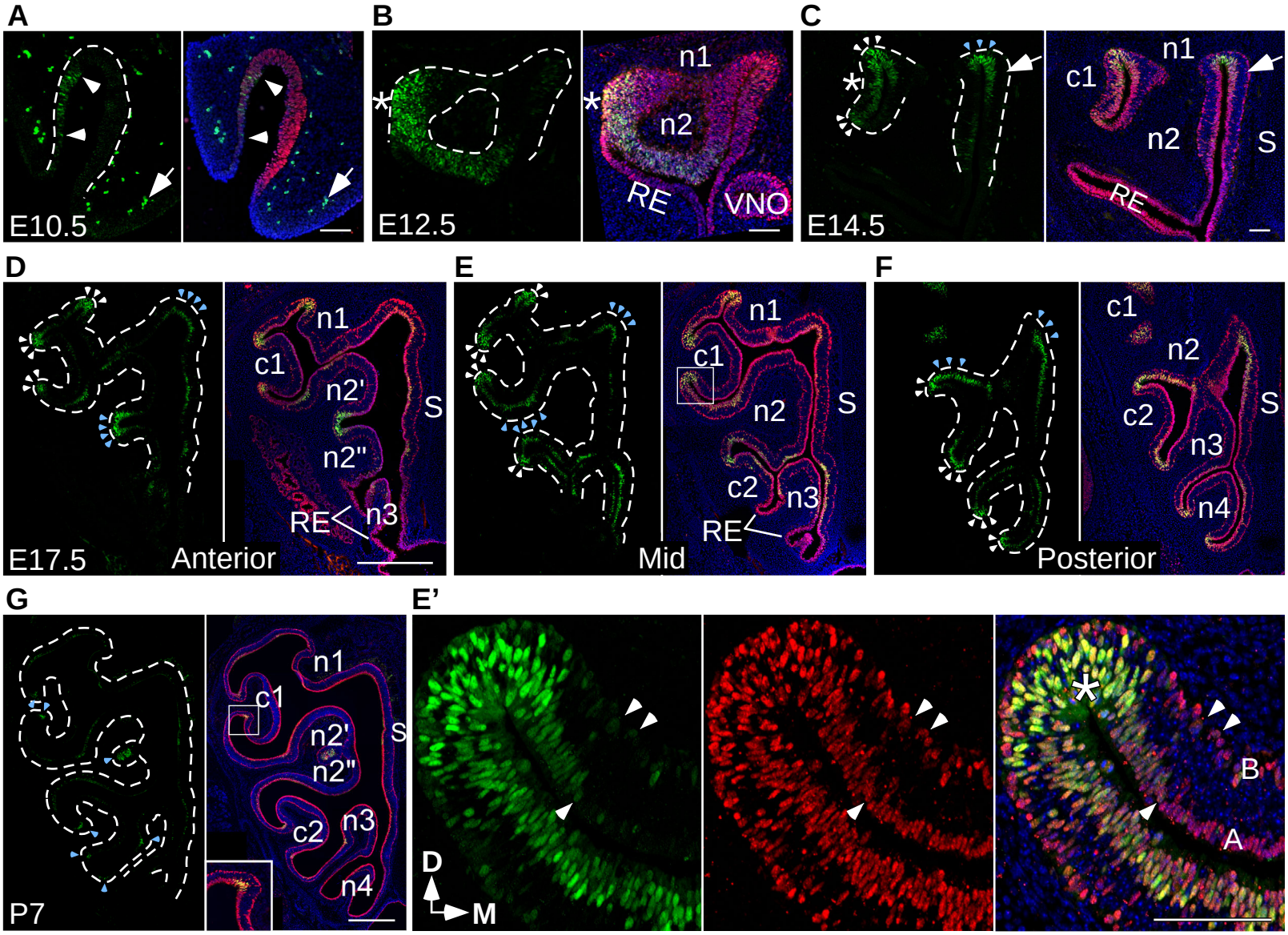

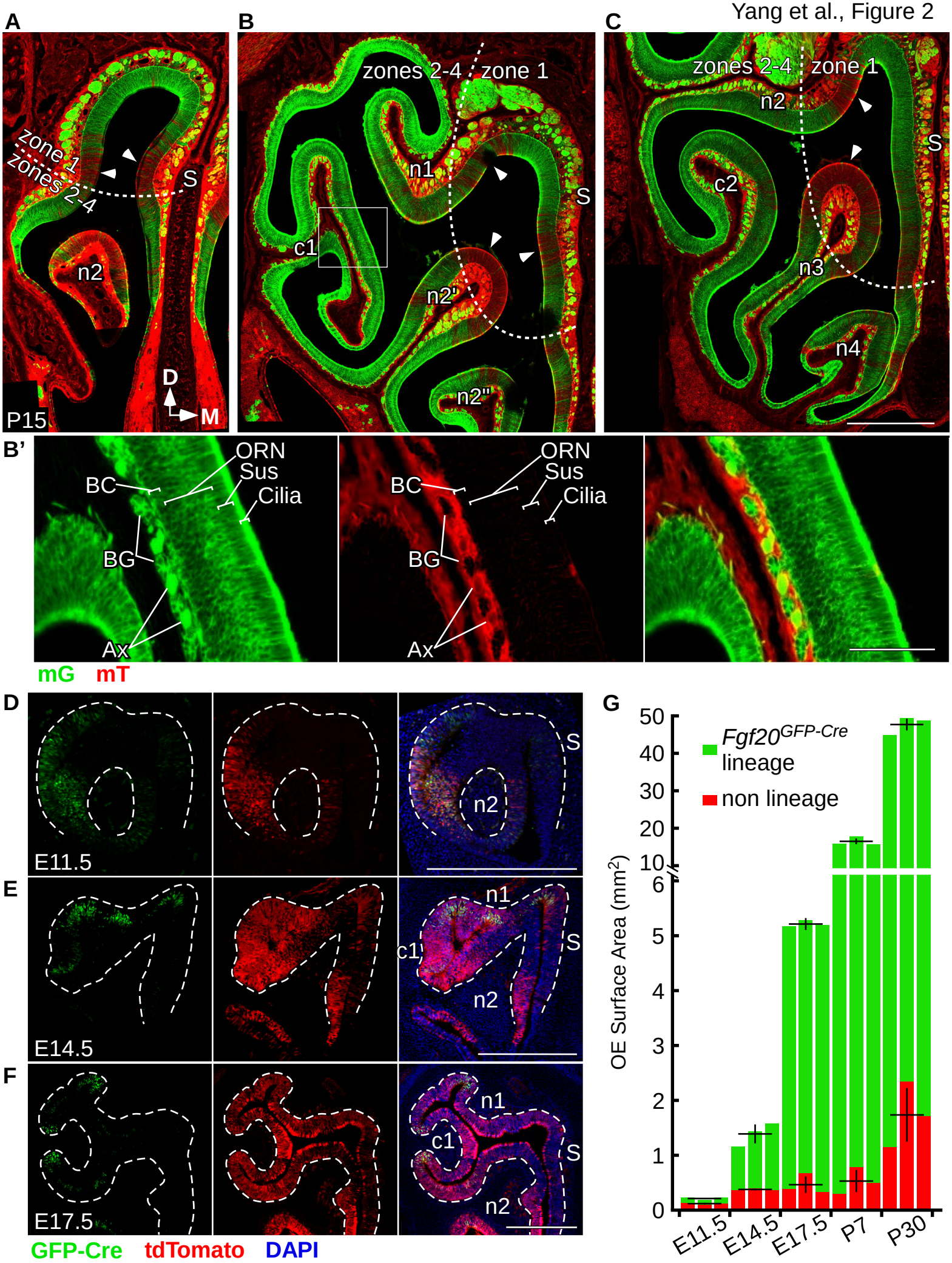
A
zone 1
zones 2-4
S
n2
P15
D
M
B
zones 2-4
zone 1
n1
S
c1
n2'
n2"
C
zones 2-4
zone 1
n2
S
c2
n3
n4
B'
ORN
Sus
BC
Cilia
BG
Ax
mG
mT
D
E11.5
S
n2
E
E14.5
n1
c1
S
n2
F
E17.5
n1
c1
S
n2
GFP-Cre
tdTomato
DAPI
G
Fgf20GFP-Cre lineage
non lineage
OE Surface Area (mm2)
50
40
30
20
10
6
5
4
3
2
1
0
E11.5
E14.5
E17.5
P7
P30

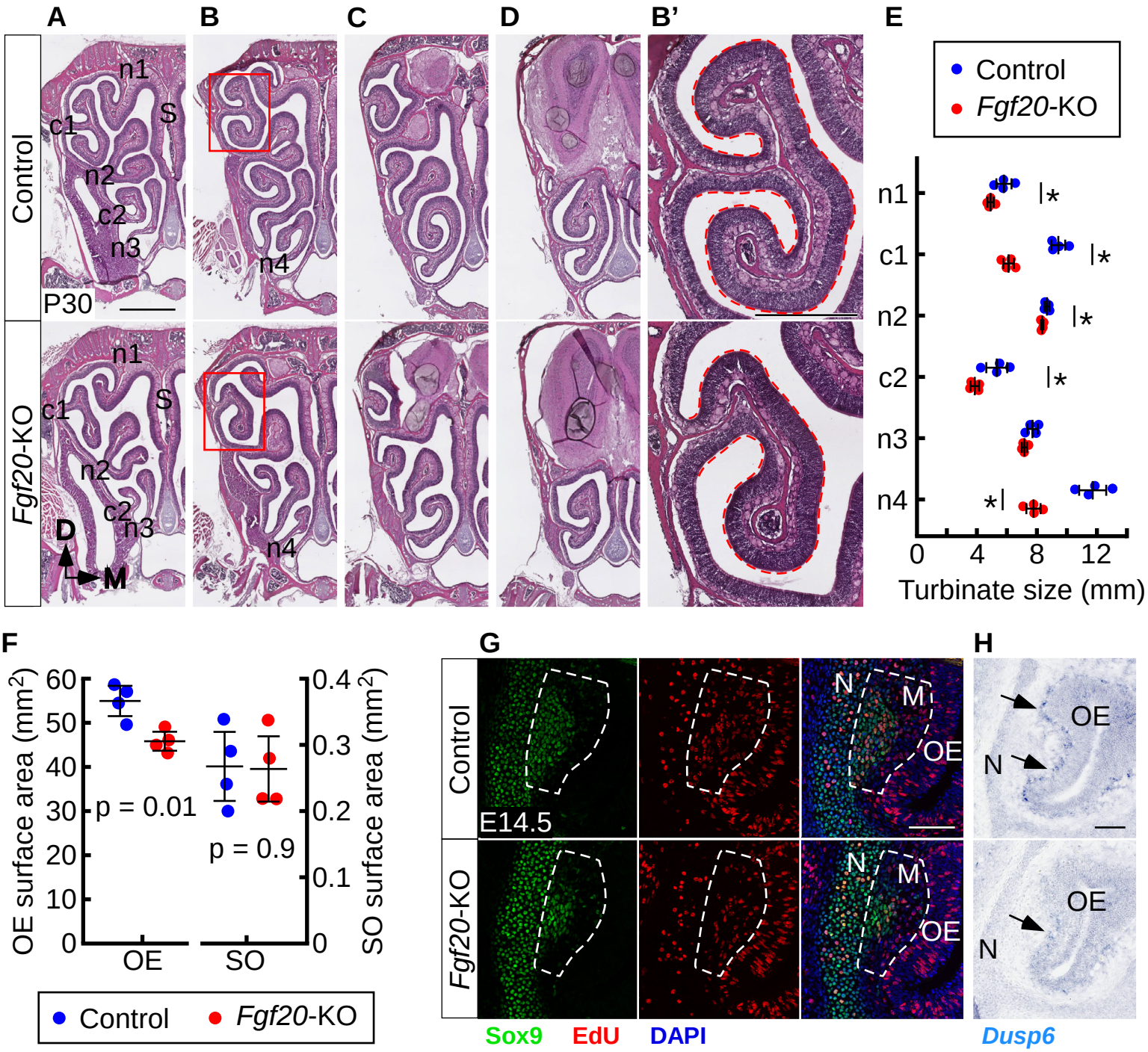
A
B
C
D
B'
E
Control
Fgf20-KO
n1
c1
S
n2
c2
n3
n4
P30
D
M
Control
Fgf20-KO
n1
c1
n2
c2
n3
n4
0
4
8
12
Turbinate size (mm)
F
OE surface area (mm²)
SO surface area (mm²)
p = 0.01
p = 0.9
OE
SO
Control
Fgf20-KO
G
H
Control
Fgf20-KO
E14.5
N
M
OE
Sox9
EdU
DAPI
Dusp6
I
Condensed cells (normalized)
p = 0.1
J
Diffuse cells (normalized)
p = 0.8
K
Condensed/ diffuse cell ratio
p = 0.05
L
EdU+ condensed cells (%)
p = 0.007
M
EdU+ diffuse cells (%)
p = 0.06

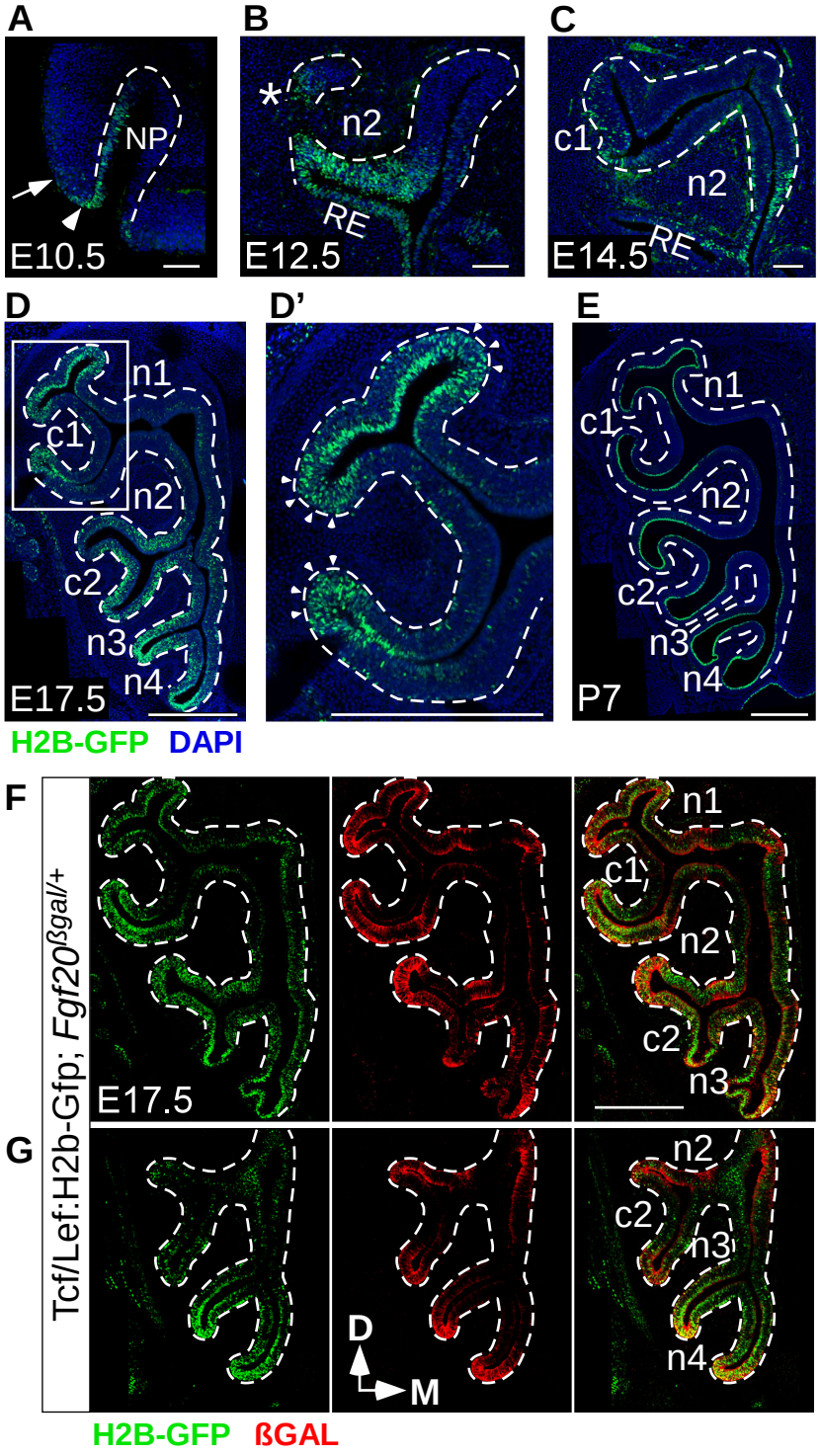
A
B
C
NP
E10.5
n2
RE
E12.5
c1
n2
RE
E14.5
D
D'
E
n1
c1
n2
c2
n3
n4
E17.5
n1
c1
n2
c2
n3
n4
P7
H2B-GFP DAPI
F
G
Tcf/Lef:H2b-Gfp; Fgf20ßgal/+
E17.5
n1
c1
n2
c2
n3
n2
c2
n3
n4
D
M
H2B-GFP ßGAL

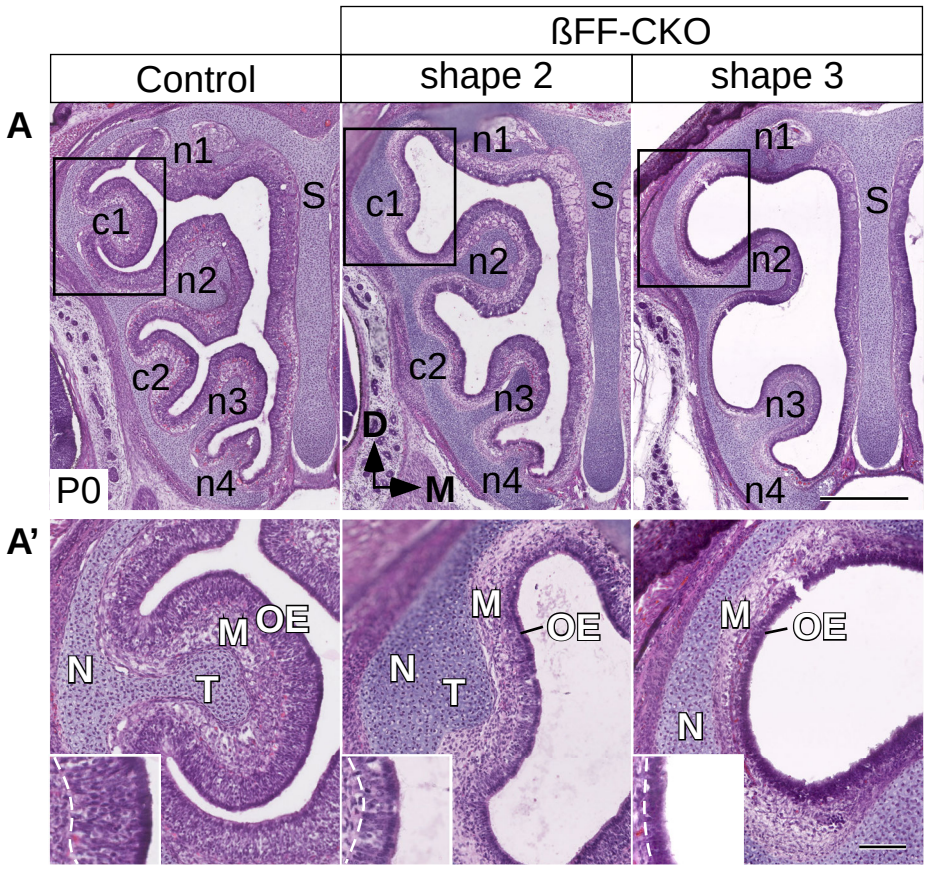
ßFF-CKO
Control
shape 2
shape 3
A
n1
c1
S
n2
c2
n3
n4
D
M
P0
A'
M
OE
N
T

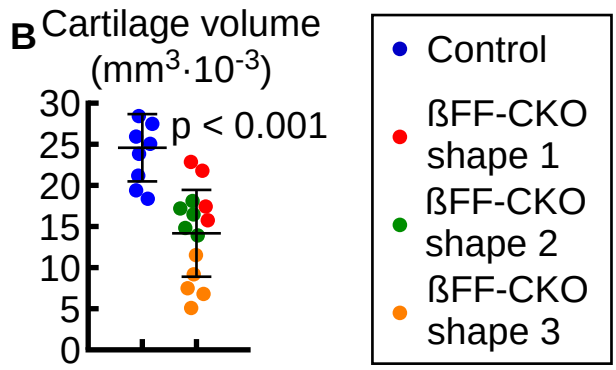
B
Cartilage volume
(mm3·10-3)
p < 0.001
Control
ßFF-CKO shape 1
ßFF-CKO shape 2
ßFF-CKO shape 3

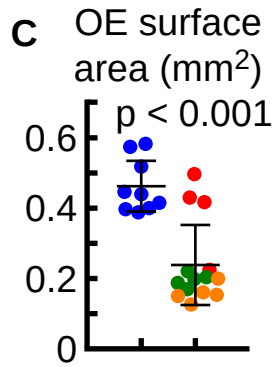
C
OE surface area (mm2)
p < 0.001

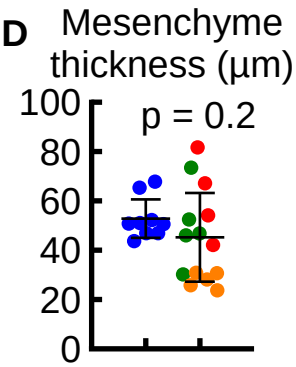
D
Mesenchyme thickness (µm)
p = 0.2

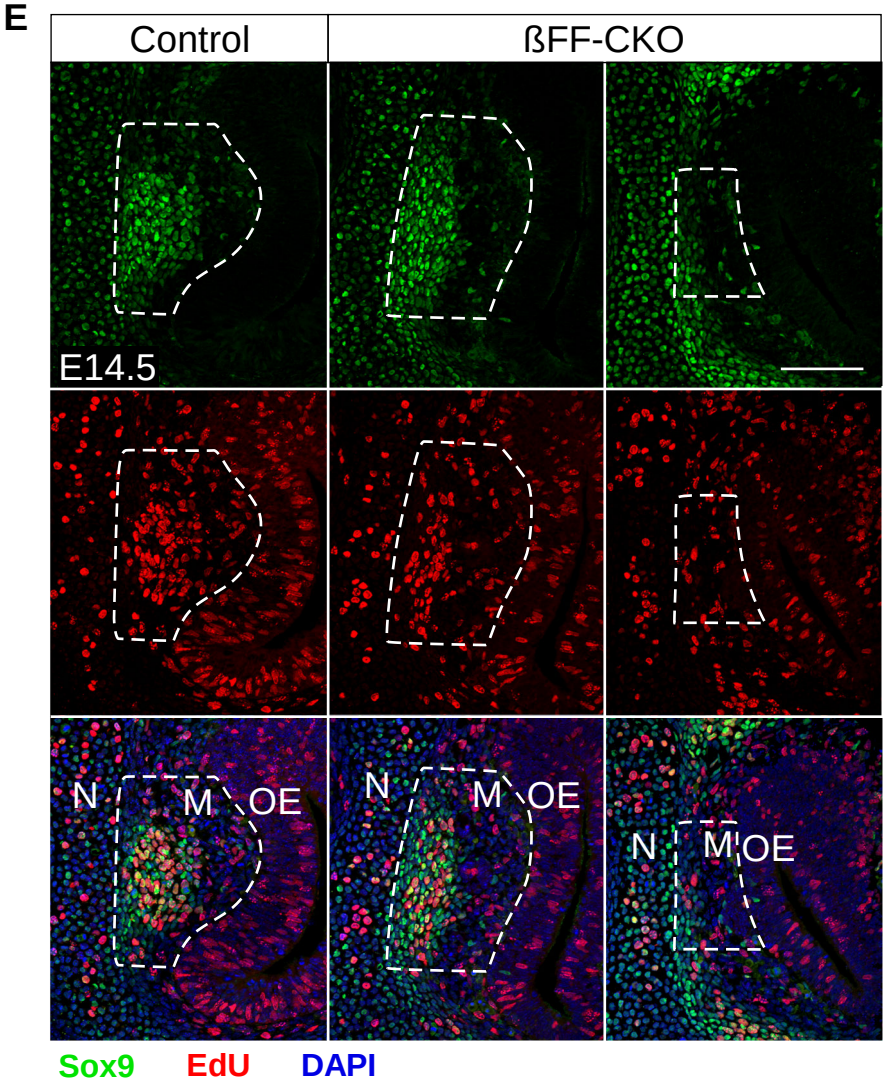
E
Control
ßFF-CKO
E14.5
N
M
OE
Sox9
EdU
DAPI

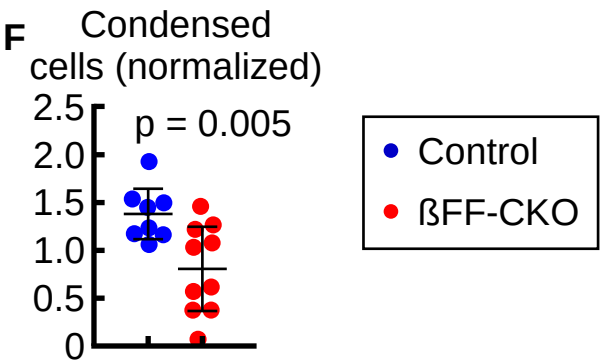
F
Condensed cells (normalized)
p = 0.005
Control
ßFF-CKO

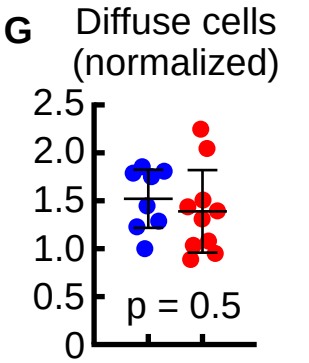
G
Diffuse cells (normalized)
p = 0.5

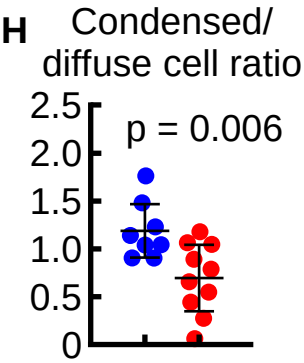
H
Condensed/ diffuse cell ratio
p = 0.006

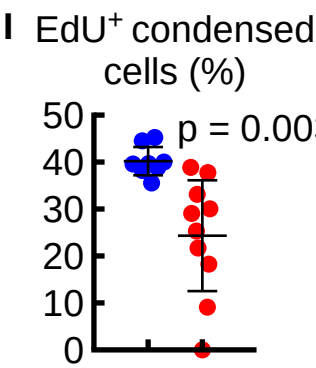
I
EdU+ condensed cells (%)
p = 0.003

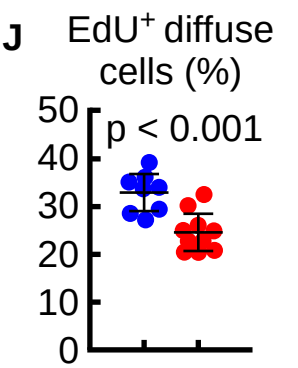
J
EdU+ diffuse cells (%)
p < 0.001

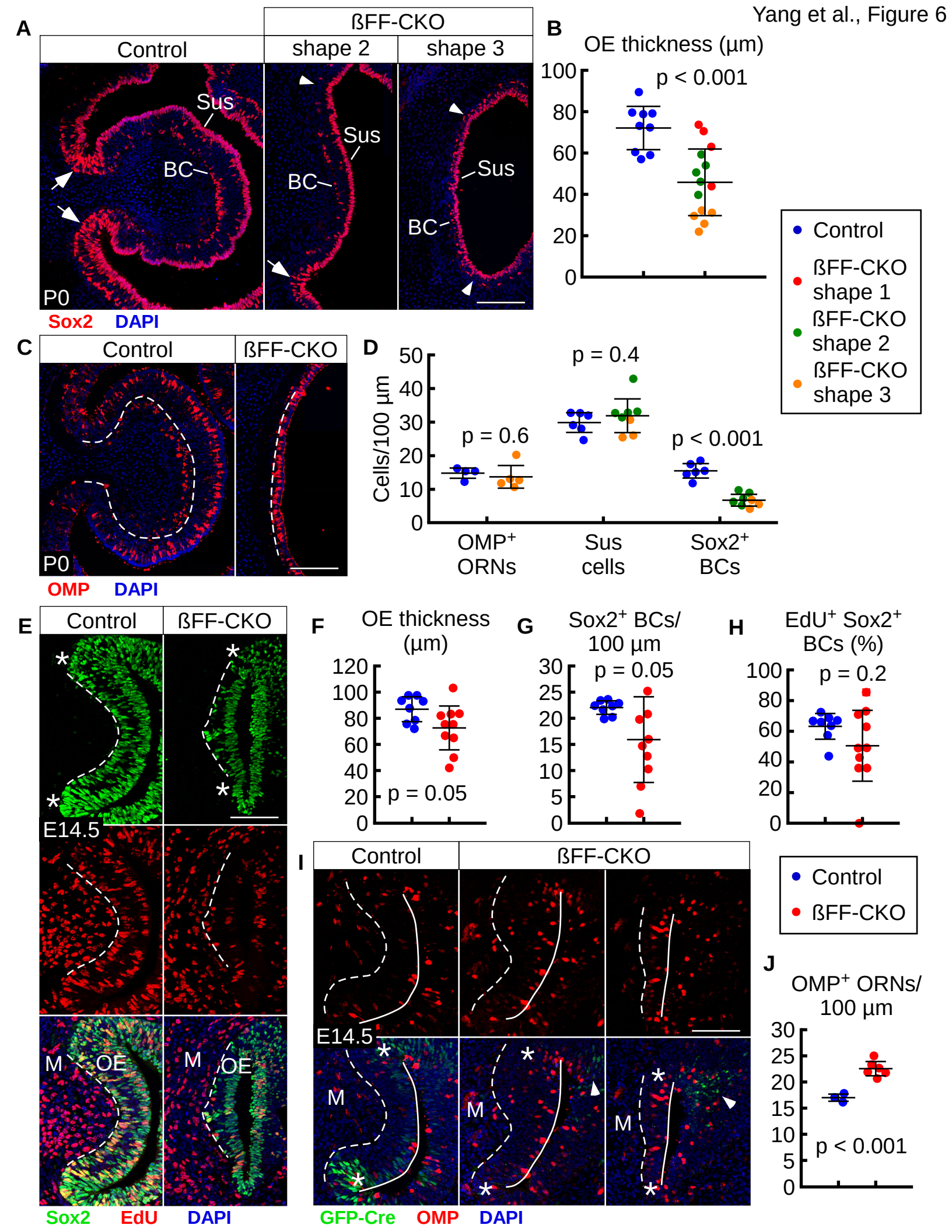
A
Control
ßFF-CKO
shape 2
shape 3
Sus
BC
P0
Sox2 DAPI
B
OE thickness (µm)
p < 0.001
Control
ßFF-CKO shape 1
ßFF-CKO shape 2
ßFF-CKO shape 3
C
Control
ßFF-CKO
P0
OMP DAPI
D
Cells/100 µm
p = 0.6
p = 0.4
p < 0.001
OMP+ ORNs
Sus cells
Sox2+ BCs
E
Control
ßFF-CKO
E14.5
M
OE
Sox2 EdU DAPI
F
OE thickness (µm)
p = 0.05
G
Sox2+ BCs/ 100 µm
p = 0.05
H
EdU+ Sox2+ BCs (%)
p = 0.2
I
Control
ßFF-CKO
E14.5
M
GFP-Cre OMP DAPI
J
OMP+ ORNs/ 100 µm
p < 0.001

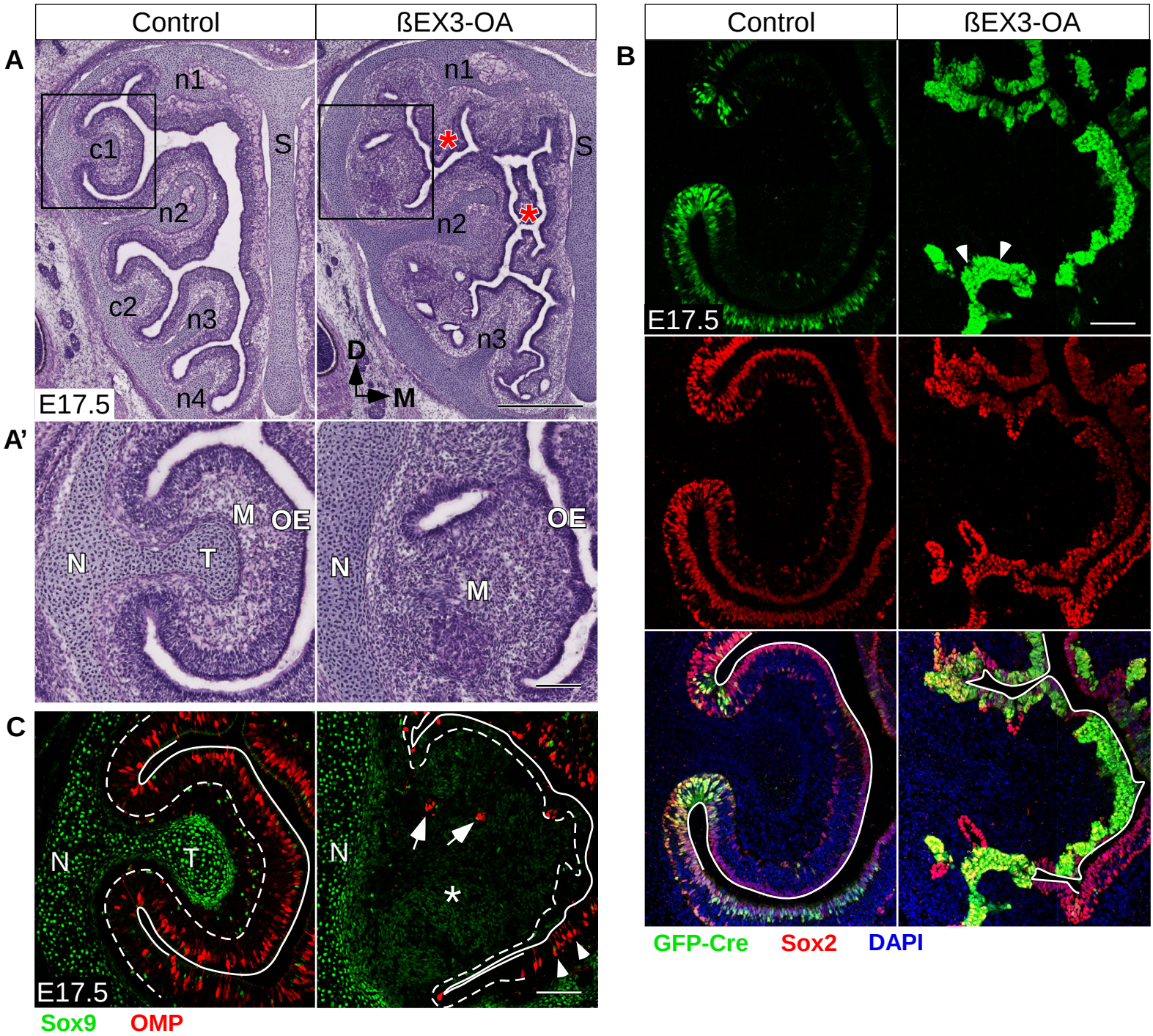
Control
ßEX3-OA
A
n1
c1
S
n2
c2
n3
n4
E17.5
D
M
A'
M
OE
N
T
B
E17.5
GFP-Cre
Sox2
DAPI
C
N
T
E17.5
Sox9
OMP
D
Control
ßEX3-OA
E13.5
Sox9
EdU
DAPI
E
Mesenchyme thickness (µm)
200
160
120
80
40
0
p = 0.07
F
EdU+ mesenchymal cells (%)
40
30
20
10
0
p = 0.004
Control
ßEX3-OA

Yang et al., Figure S1

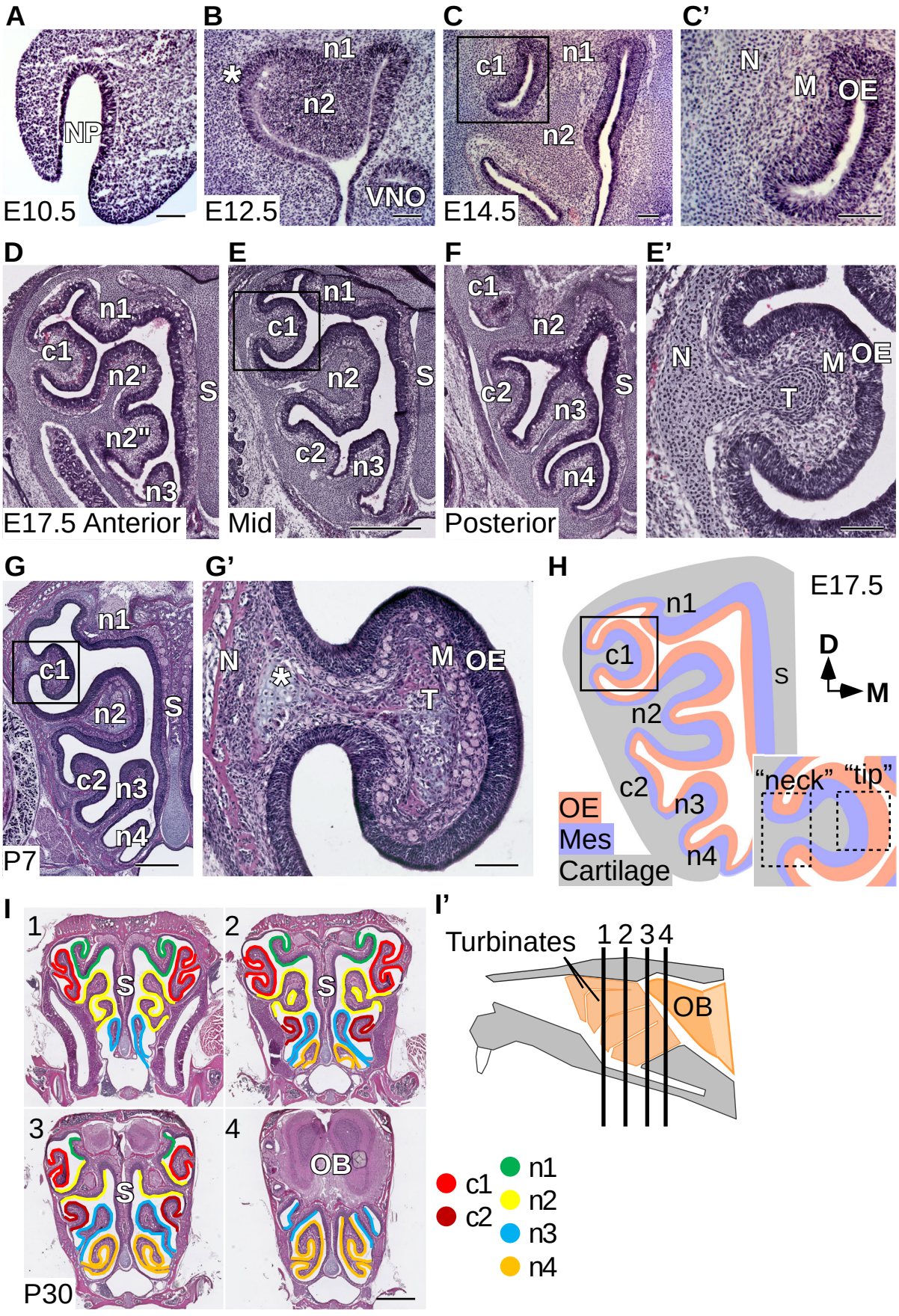

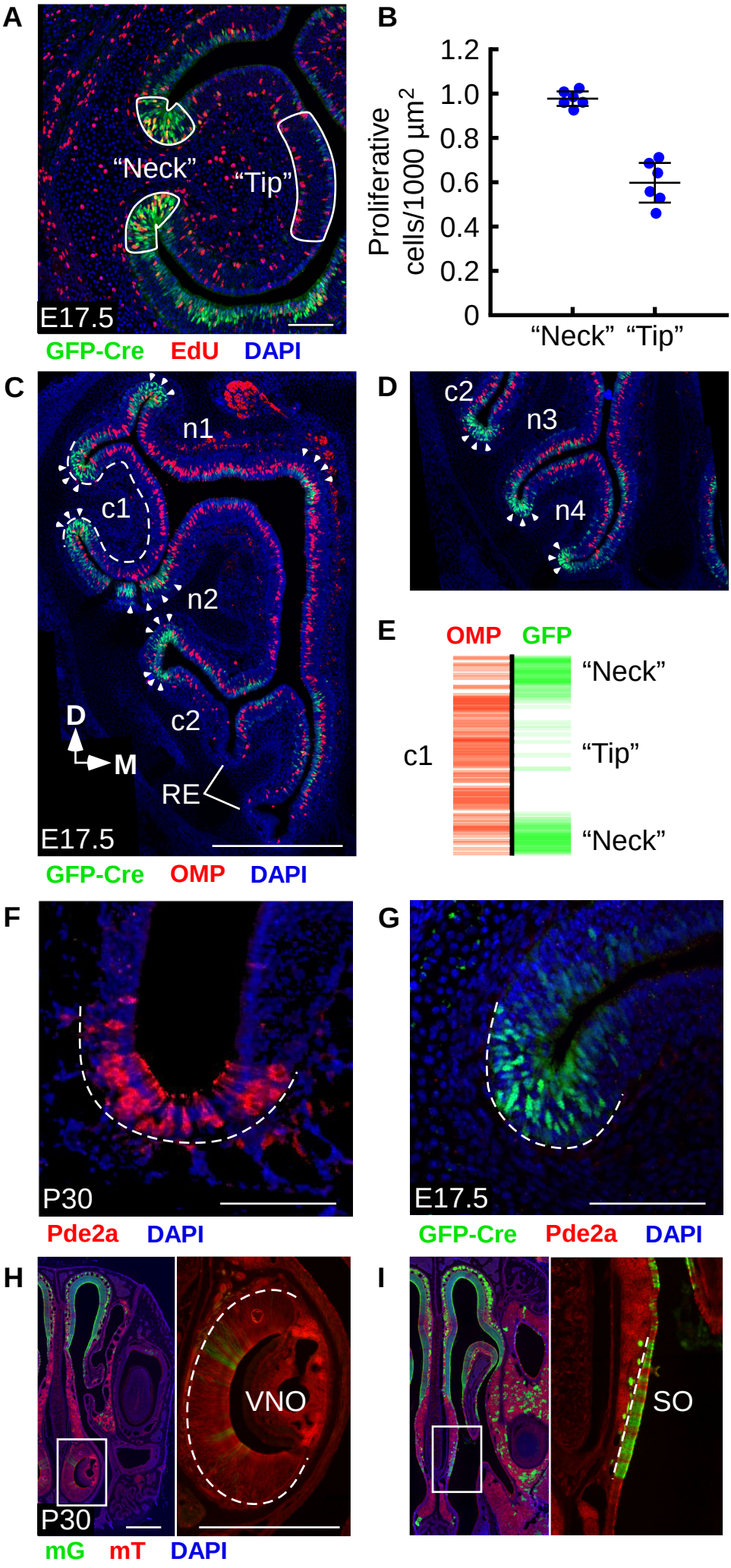
A
"Neck"
"Tip"
E17.5
GFP-Cre EdU DAPI
B
Proliferative cells/1000 μm²
1.2
1.0
0.8
0.6
0.4
0.2
0
"Neck" "Tip"
C
n1
c1
n2
c2
D
M
RE
E17.5
GFP-Cre OMP DAPI
D
c2
n3
n4
E
OMP GFP
c1
"Neck"
"Tip"
"Neck"
F
P30
Pde2a DAPI
G
E17.5
GFP-Cre Pde2a DAPI
H
VNO
P30
mG mT DAPI
I
SO

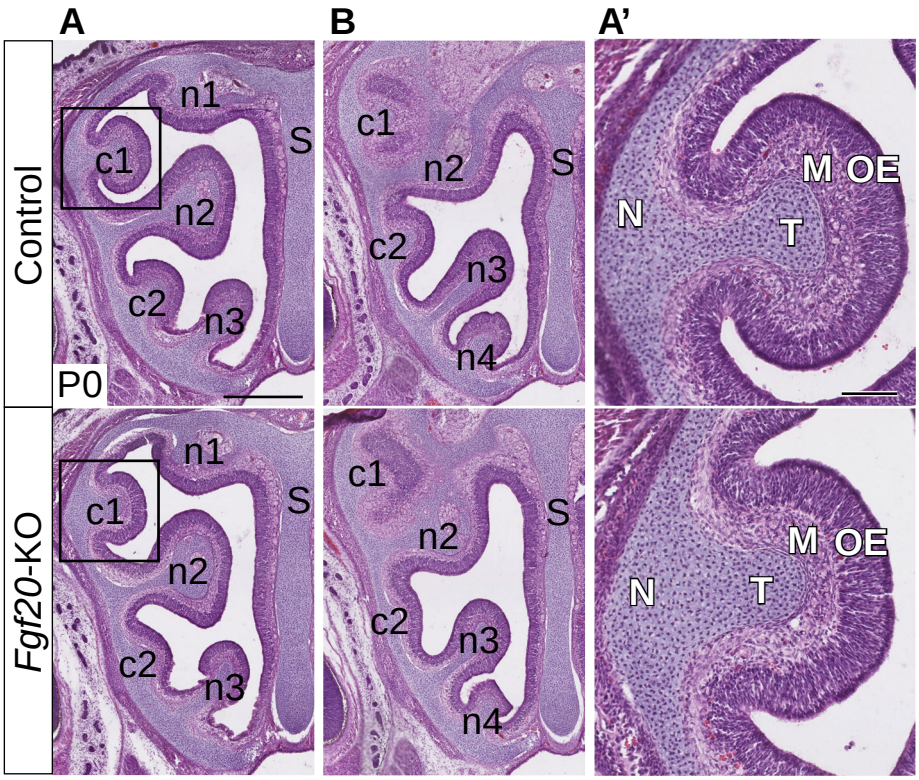
A
B
A'
Control
Fgf20-KO
P0
n1
c1
n2
c2
n3
n4
S
M
OE
N
T

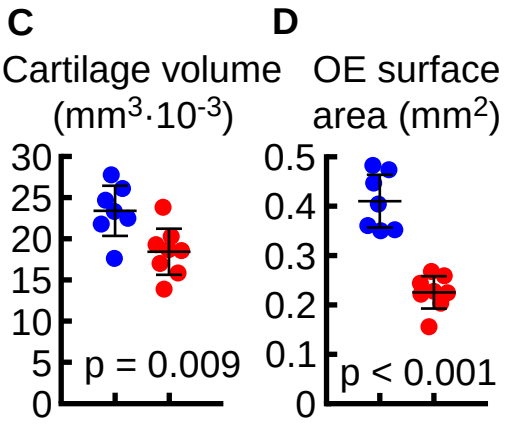
C
Cartilage volume
(mm3·10-3)
p = 0.009
D
OE surface
area (mm2)
p < 0.001

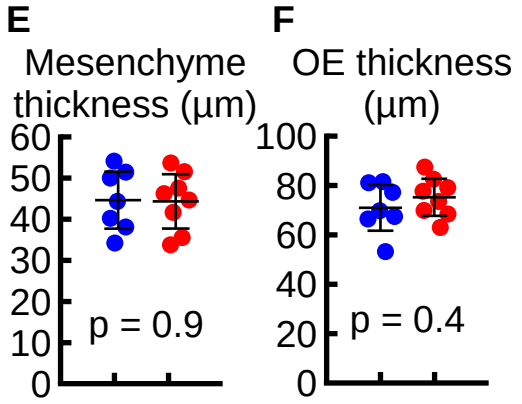
E
Mesenchyme
thickness (μm)
p = 0.9
F
OE thickness
(μm)
p = 0.4

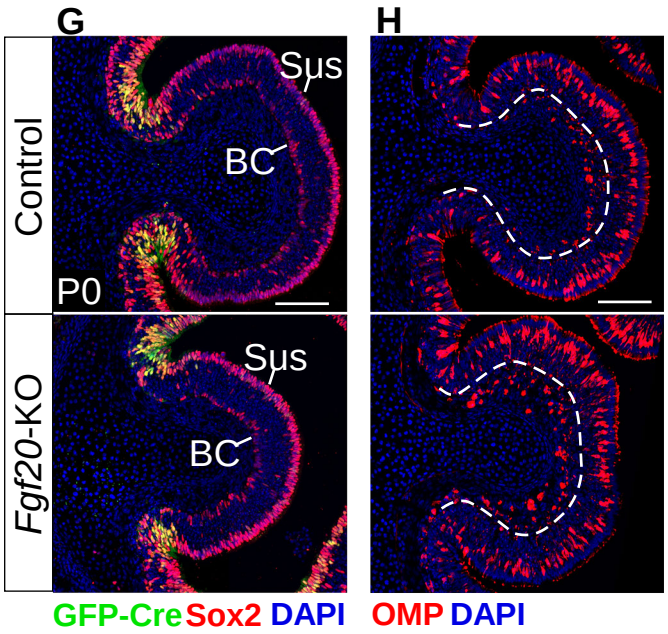
G
H
Control
Fgf20-KO
P0
Sus
BC
GFP-Cre Sox2 DAPI
OMP DAPI

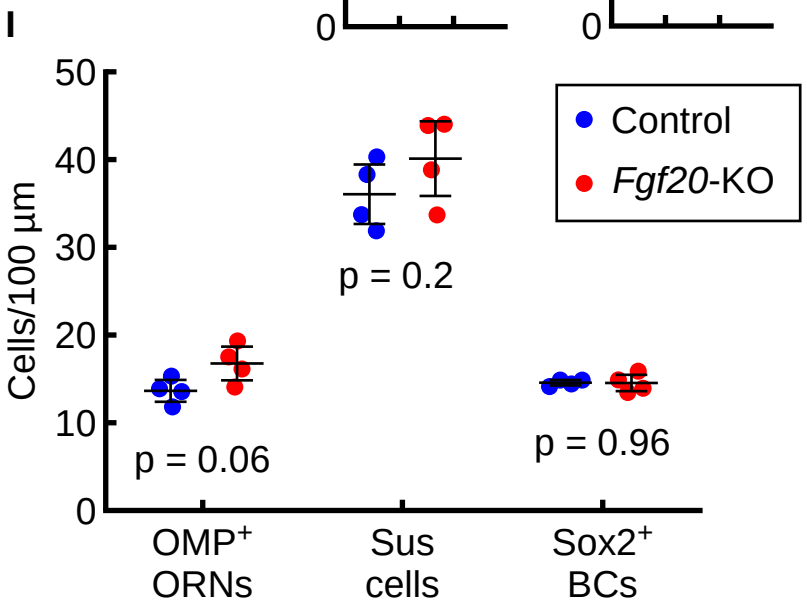
I
Cells/100 μm
Control
Fgf20-KO
p = 0.06
p = 0.2
p = 0.96
OMP+
ORNs
Sus
cells
Sox2+
BCs

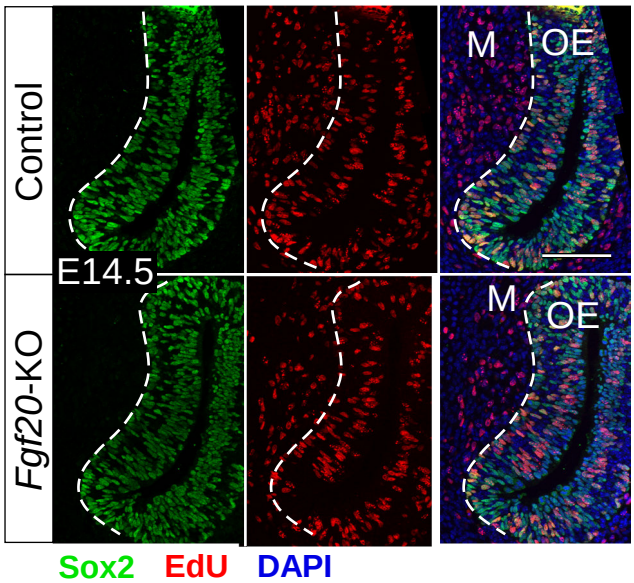
J
Control
Fgf20-KO
E14.5
M
OE
Sox2 EdU DAPI

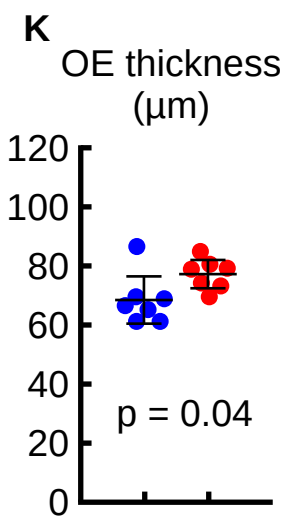
K
OE thickness
(μm)
p = 0.04

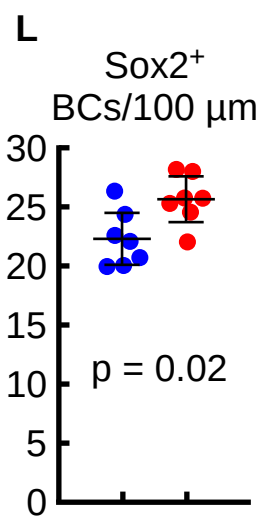
L
Sox2+
BCs/100 μm
p = 0.02

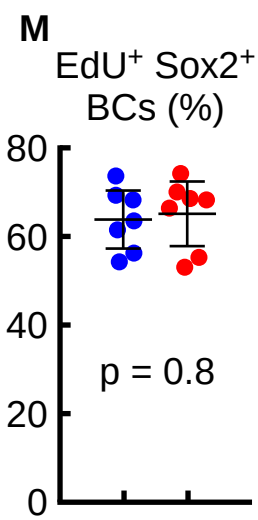
M
EdU+ Sox2+
BCs (%)
p = 0.8

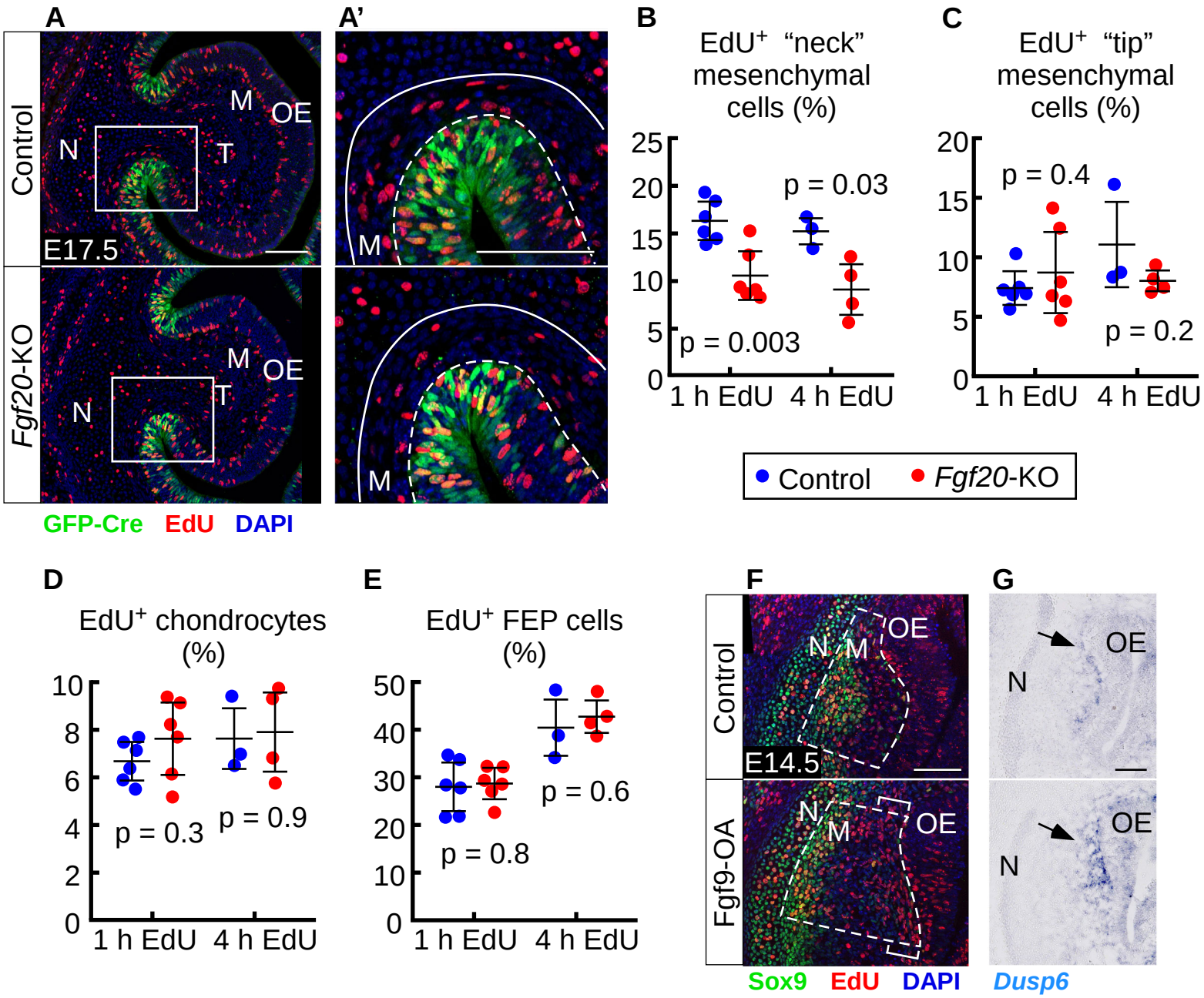
A
A'
B
C
Control
Fgf20-KO
M
OE
N
T
E17.5
EdU+ "neck" mesenchymal cells (%)
p = 0.03
p = 0.003
1 h EdU
4 h EdU
EdU+ "tip" mesenchymal cells (%)
p = 0.4
p = 0.2
Control
Fgf20-KO
GFP-Cre
EdU
DAPI
D
E
F
G
EdU+ chondrocytes (%)
p = 0.3
p = 0.9
EdU+ FEP cells (%)
p = 0.8
p = 0.6
Fgf9-OA
E14.5
Sox9
Dusp6

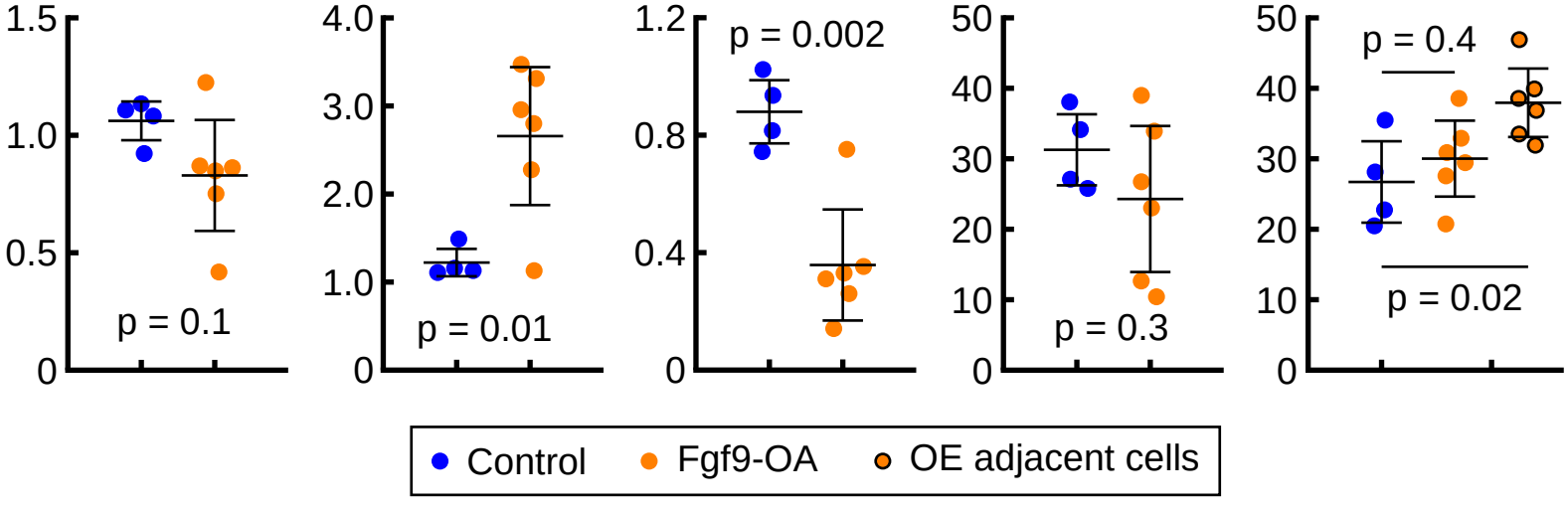
H
I
J
K
L
Condensed cells (normalized)
p = 0.1
Diffuse cells (normalized)
p = 0.01
Condensed/ diffuse cell ratio
p = 0.002
EdU+ condensed cells (%)
p = 0.3
EdU+ diffuse cells (%)
p = 0.4
p = 0.02
Control
Fgf9-OA
OE adjacent cells

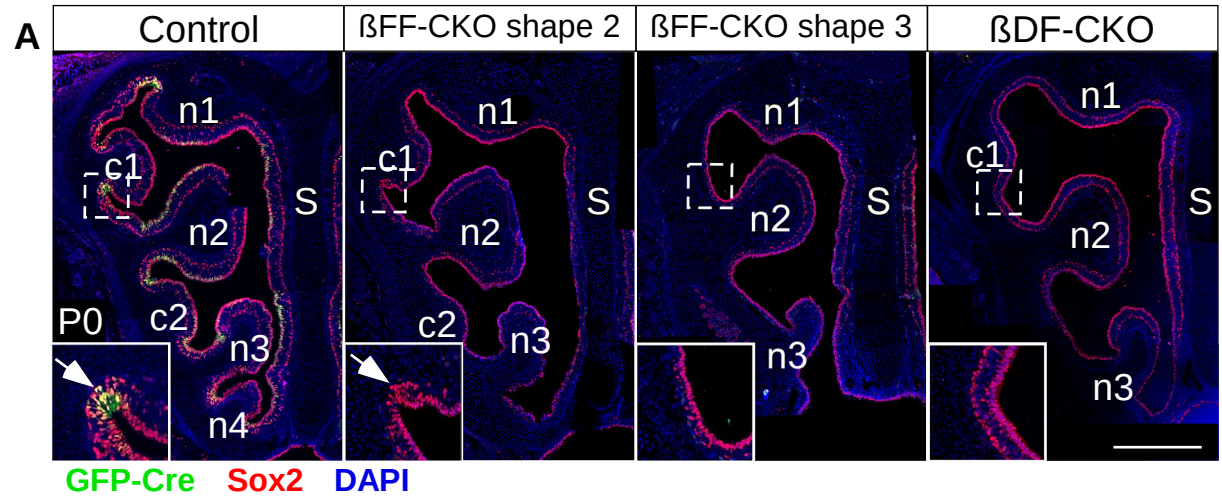
A
Control
ßFF-CKO shape 2
ßFF-CKO shape 3
ßDF-CKO
n1
c1
S
n2
c2
n3
n4
P0
GFP-Cre Sox2 DAPI

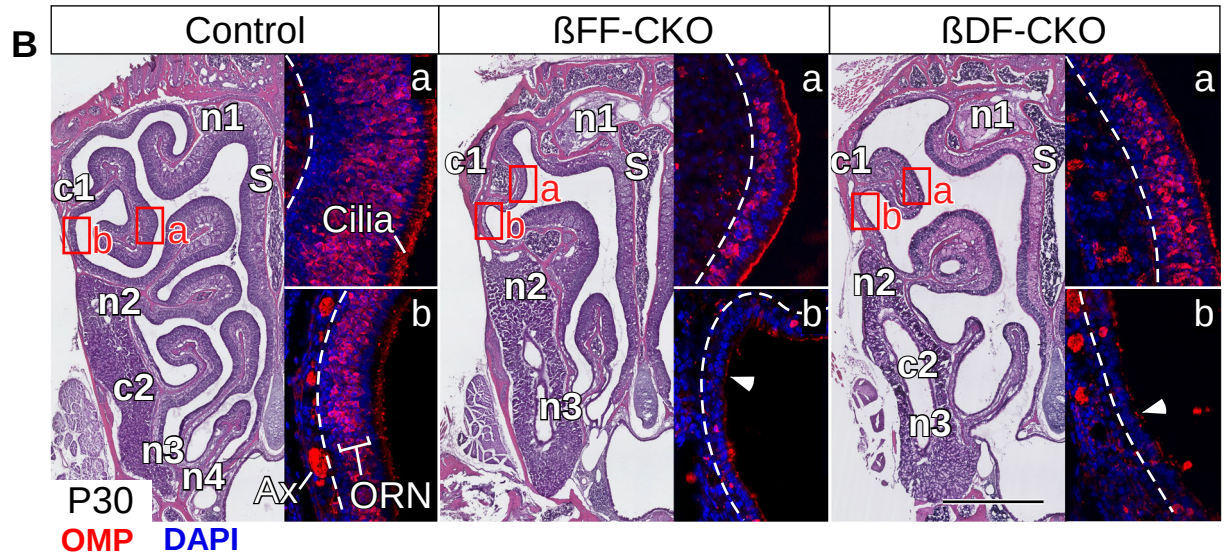
B
Control
ßFF-CKO
ßDF-CKO
a
b
Cilia
ORN
Ax
P30
OMP DAPI

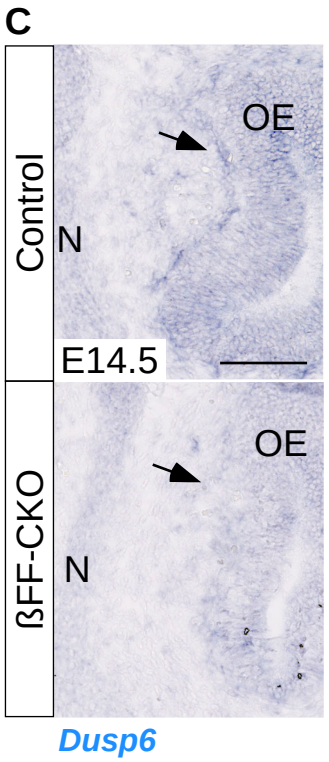
C
Control
ßFF-CKO
OE
N
E14.5
Dusp6

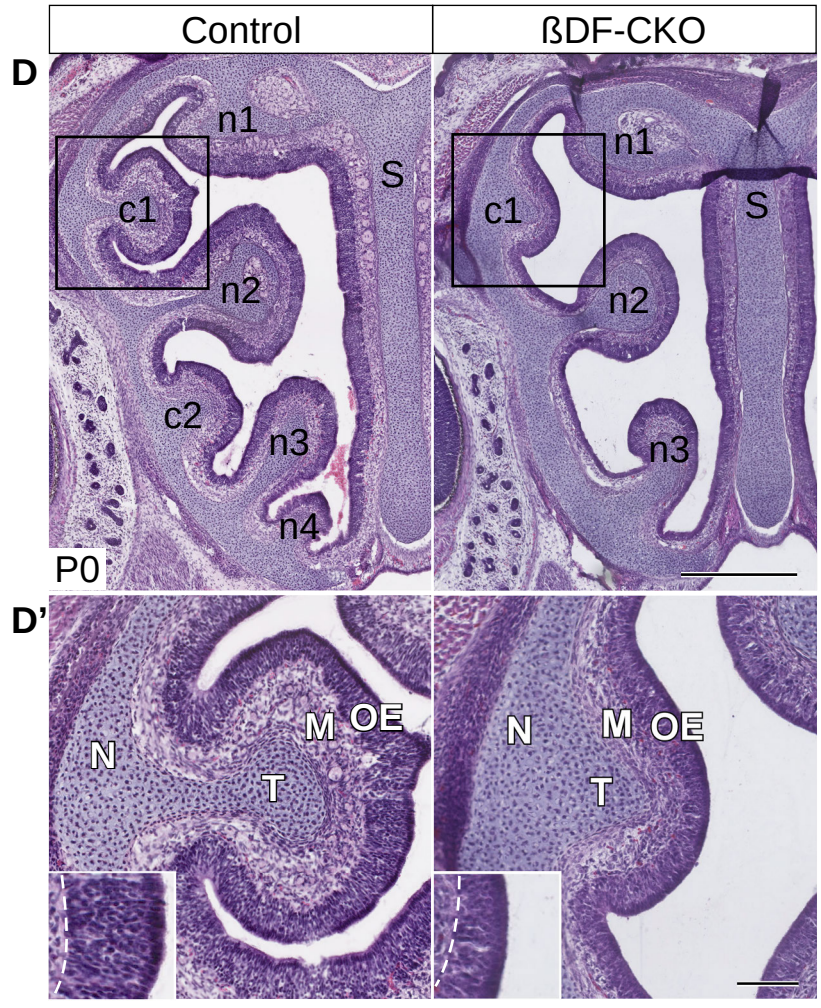
D
Control
ßDF-CKO
P0
D'
M
T

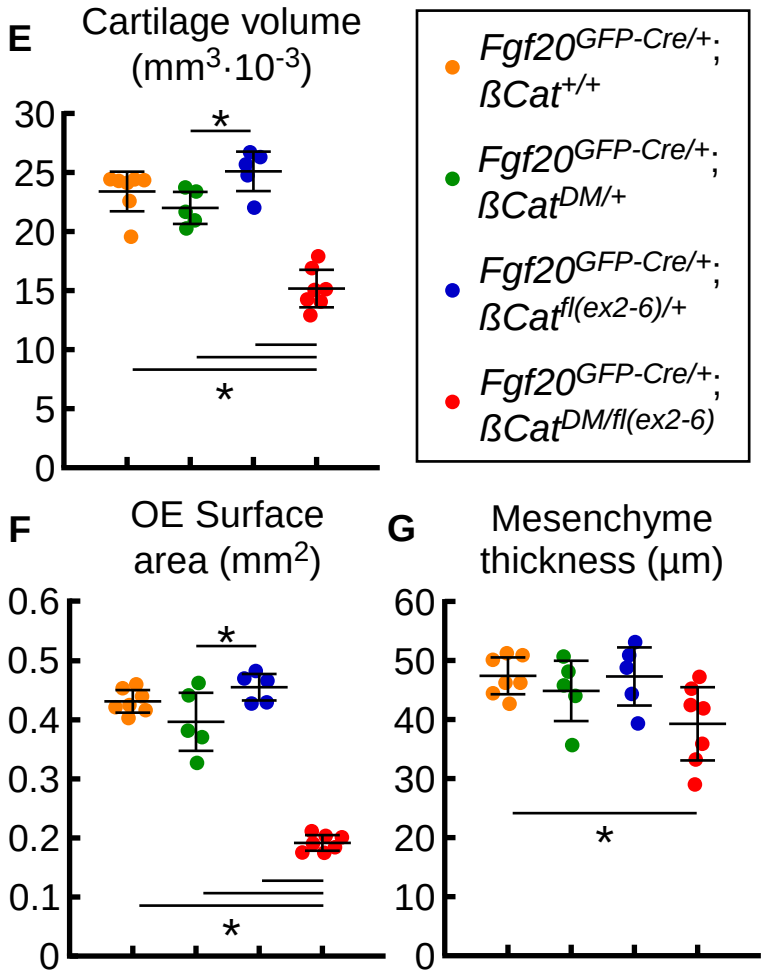
E
Cartilage volume (mm3·10-3)
F
OE Surface area (mm2)
G
Mesenchyme thickness (µm)
Fgf20GFP-Cre/+; ßCat+/+
Fgf20GFP-Cre/+; ßCatDM/+
Fgf20GFP-Cre/+; ßCatfl(ex2-6)/+
Fgf20GFP-Cre/+; ßCatDM/fl(ex2-6)

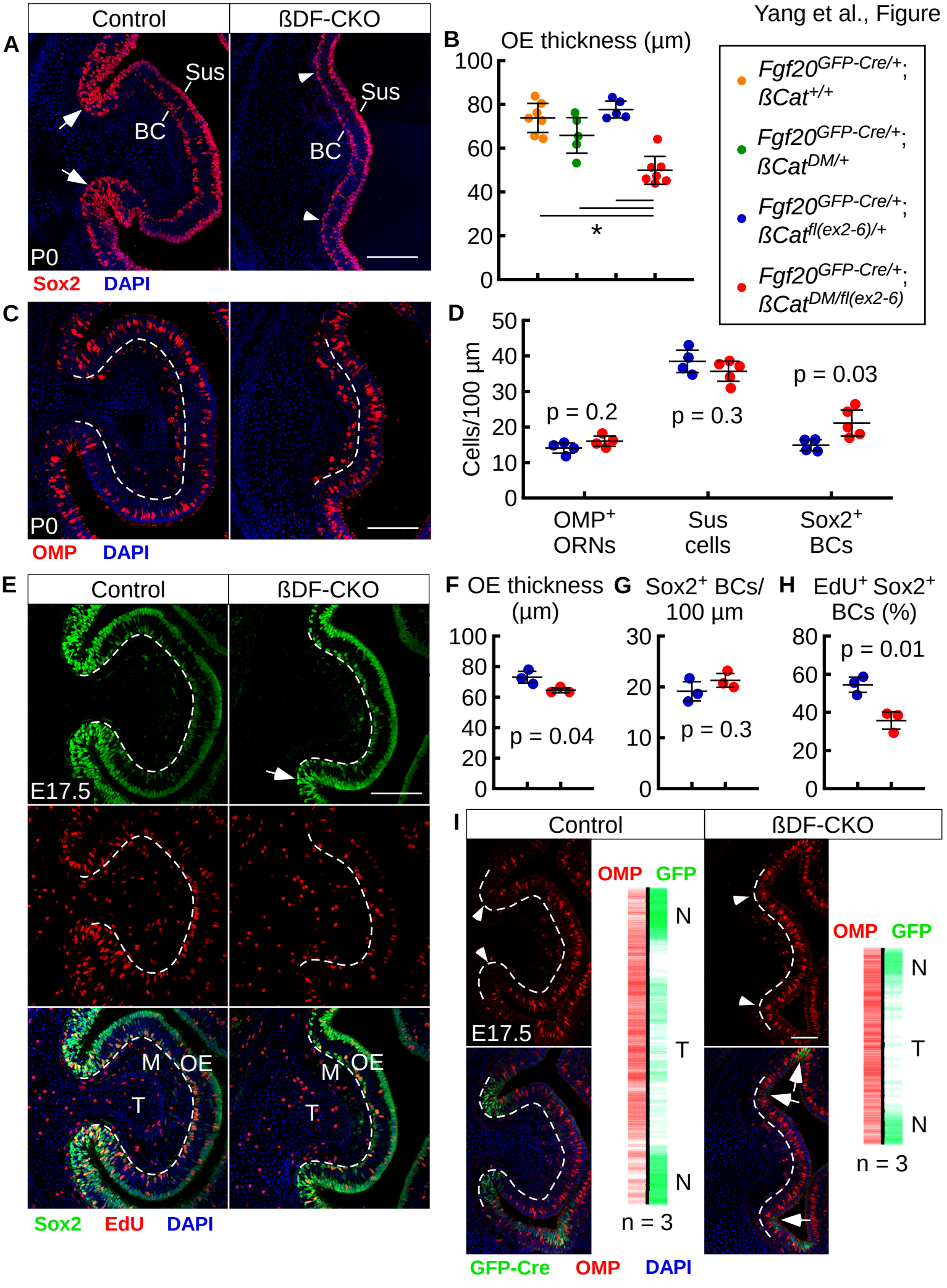
A
Control
ßDF-CKO
Sus
BC
P0
Sox2 DAPI
B
OE thickness (µm)
100
80
60
40
20
0
*
Fgf20GFP-Cre/+; ßCat+/+
Fgf20GFP-Cre/+; ßCatDM/+
Fgf20GFP-Cre/+; ßCatfl(ex2-6)/+
Fgf20GFP-Cre/+; ßCatDM/fl(ex2-6)
C
P0
OMP DAPI
D
Cells/100 µm
50
40
30
20
10
0
p = 0.2
p = 0.3
p = 0.03
OMP+ ORNs
Sus cells
Sox2+ BCs
E
Control
ßDF-CKO
E17.5
M
OE
T
Sox2 EdU DAPI
F OE thickness (µm)
100
80
60
40
20
0
p = 0.04
G Sox2+ BCs/ 100 µm
30
20
10
0
p = 0.3
H EdU+ Sox2+ BCs (%)
80
60
40
20
0
p = 0.01
I
Control
ßDF-CKO
E17.5
OMP GFP
N
T
N
n = 3
OMP GFP
N
T
N
n = 3
GFP-Cre OMP DAPI

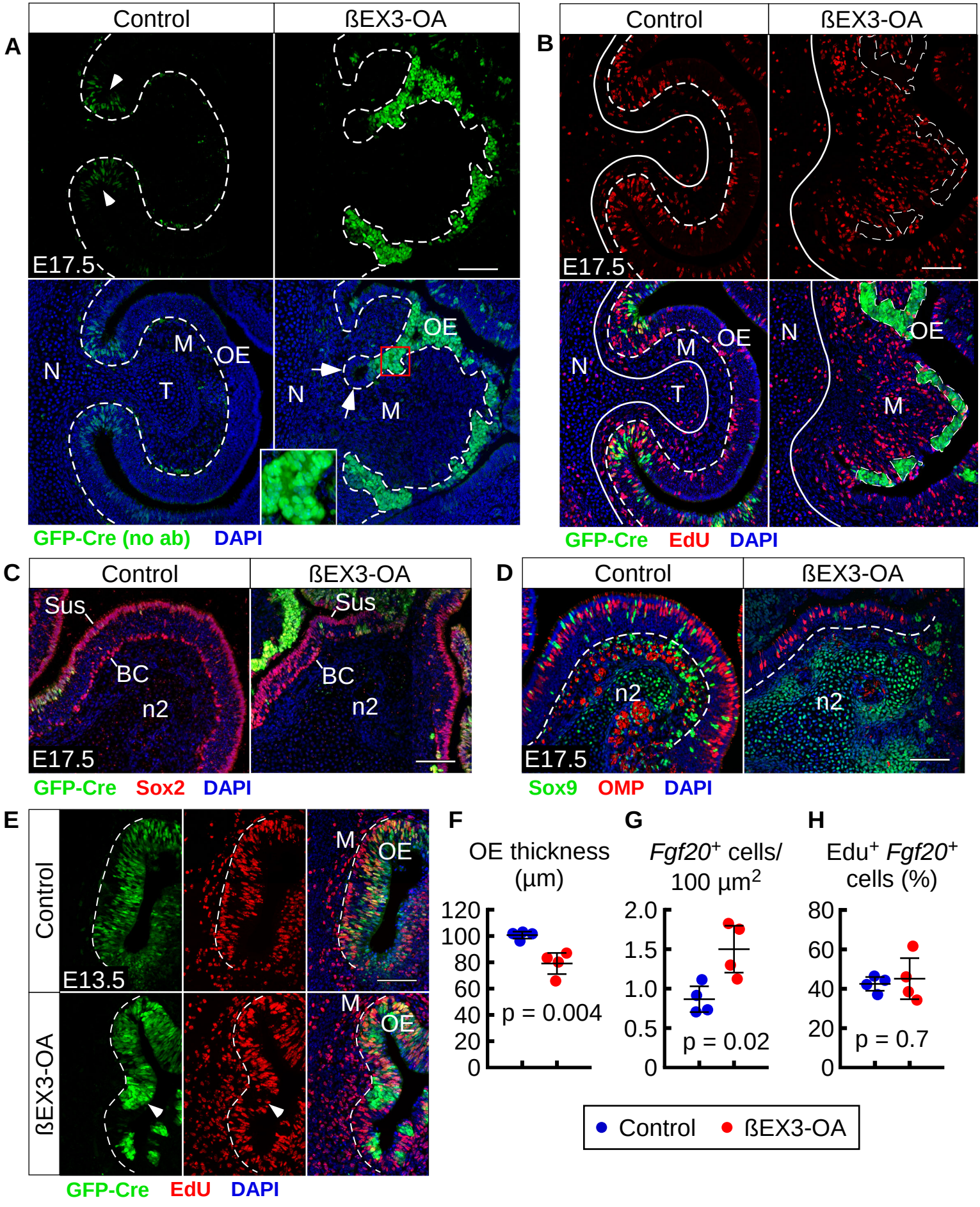
A
Control
ßEX3-OA
E17.5
N
M
OE
T
GFP-Cre (no ab)
DAPI
B
Control
ßEX3-OA
E17.5
N
M
OE
T
GFP-Cre
EdU
DAPI
C
Control
ßEX3-OA
Sus
BC
n2
E17.5
GFP-Cre
Sox2
DAPI
D
Control
ßEX3-OA
n2
E17.5
Sox9
OMP
DAPI
E
Control
ßEX3-OA
E13.5
M
OE
GFP-Cre
EdU
DAPI
F
OE thickness (µm)
120
100
80
60
40
20
0
p = 0.004
G
Fgf20+ cells/ 100 µm2
2.0
1.5
1.0
0.5
0
p = 0.02
H
Edu+ Fgf20+ cells (%)
80
60
40
20
0
p = 0.7
Control
ßEX3-OA